REPORT DOCUMENTATION PAGE

AFRL-SR-BL-TR-02-

0030

1. AGENCY USE ONLY *(Leave blank)*	2. REPORT DATE	3. REPORT TYPE AND DATES COVERED
	8 January 2002	Final 15 Mar 99 - 15 Dec 01

4. TITLE AND SUBTITLE
Comparison of turbulence over Japan and New Mexico from MST radar observations

5. FUNDING NUMBERS
F49620-99-C-0016

6. AUTHOR(S)
Gregory D. Nastrom

7. PERFORMING ORGANIZATION NAME(S) AND ADDRESS(ES)
Nastrom Consulting, LLC
125 Benton Oaks Drive
Sauk Rapids, MN 56379

8. PERFORMING ORGANIZATION REPORT NUMBER

9. SPONSORING/MONITORING AGENCY NAME(S) AND ADDRESS(ES)
Air Force Office of Scientific Research (AFOSR/NM)
801 North Randolph, Rm 732
Arlington, VA 22203-1977

10. SPONSORING/MONITORING AGENCY REPORT NUMBER

11. SUPPLEMENTARY NOTES

20020206 100

12a. DISTRIBUTION AVAILABILITY STATEMENT
Approved for public release, distribution unlimited

12b. DISTRIBUTION CODE

13. ABSTRACT *(Maximum 200 words)*

Observations from Mesosphere-Stratosphere-Troposphere (MST) radars at White Sands, New Mexico, Vandenburg, California, and Shigaraki, Japan, are used to study the relationships between the intensity of refractivity turbulence and large-scale weather conditions. (a) The gravity wave intensity seen by satellites (GPS/MET) agrees with that seen by the radar at White Sands. (b) The gravity wave source mechanisms are different at White Sands and Japan, although the wave energies are about the same magnitude. (c) The intensity of refractivity turbulence in the stratosphere, above 18 km, is not changed by the presence of thunderstorms in the troposphere. (d) The diurnal changes in the intensity of refractivity turbulence and in the spectral width are very small during all seasons at both White Sands and Japan. (e) The intensity of refractivity turbulence in the stratosphere is highly correlated with relative vorticity. Since the correlation is improved when distance from the tropopause is used as the vertical coordinate and when the data are normalized by local atmospheric density, the model developed is thus a combined conceptual/ physical/statistical model. (f) A case study at Vandenburg shows that turbulence and wave intensities increase during the passage of a cyclone in the presence of a strong surface inversion. (g) Case studies in Japan show that turbulence intensities in the lower stratosphere are often more closely related to the intensity of gravity waves than to in situ wind speed and large-scale wind vertical shear.

14. SUBJECT TERMS	15. NUMBER OF PAGES
Refractivity turbulence, Atmospheric turbulence, Doppler radar	51
	16. PRICE CODE

17. SECURITY CLASSIFICATION OF REPORT	18. SECURITY CLASSIFICATION OF THIS PAGE	19. SECURITY CLASSIFICATION OF ABSTRACT	20. LIMITATION OF ABSTRACT

I. Project objectives.

The following objectives were originally proposed, and the course of progress during this research effort has been remarkably closely focused toward these general goals, considering that research efforts must be flexible to allow for unexpected developments and opportunities. Examples of communications reporting on results for each objective are given in brackets.

(a) Working with the MU radar group of Kyoto University, describe the salient features of variations of C_n^2 and ε at the MU and WS VHF radars with height, time of day, season, background winds and other weather conditions. [II(e), III(a.7)]
(b) Compare the intensities of gravity wave activity at MU and WS and their relationship to variables of the large-scale flow such as jet stream intensity, wind shear, season, and time-of-day. [III(a.6)]
(c) Compare the intensity of gravity wave activity from radar measurements with those from other measurement platforms, such as GPS/MET satellite, to generate an algorithm for extrapolating results seen at radar sites to remote regions of the world. [II(a)]
(d) Develop conceptual, physical, or statistical models of the variations of C_n^2 or ε as functions of atmospheric variables of the large-scale flow that are routinely available such as static stability, jet stream features (horizontal proximity, vertical wind shear, maximum speed, ageostrophic wind speed indicators, jet height, tropopause discontinuity, among others), season and time of day. [II(h)]
(e) Using the above models, test their effectiveness by using predictions of the large-scale flow from routinely available numerical weather prediction models to predict levels of C_n^2 or ε at MU or WS.
(f) Make case studies of the intensity of observed and derived turbulence variables during these periods to draw conclusions regarding relevant physical processes and relationships to mean winds, stability, and background weather conditions. [II(i), III(a.14)]

II. Publications

(a) Nastrom, G.D., A. R. Hansen, T. Tsuda, M. Nishida, and R. Ware, 2000: A comparison of gravity wave energy observed by VHF radar and GPS/MET over central North America. J. Geophys. Res., 105, 4685-4687.

(b) Hansen, A. R., G.D. Nastrom , Eaton, F.D, 2001: Seasonal variation of gravity wave activity at 5 – 20 km observed with the VHF radar at White Sands Missile Range, New Mexico, J. Geophys. Res., 106, 17171-17183.

(c) Nastrom, G.D., and T.E. VanZandt, 2001: The Seasonal Variability of the Observed Vertical Wavenumber Spectra of Wind and Temperature and the Effects of Prewhitening, J. Geophys. Res., 106, 14369-14375.

(d) Nastrom, G.D., and F.D. Eaton, 2001: Persistent layers of enhanced C_N^2 in the lower stratosphere from VHF radar observations. Radio Science, 36, 137-149.

(e) Nastrom, G.D., and T. Tsuda, 2001: Anisotropy of Doppler spectral parameters in the VHF radar observations at MU and White Sands, Ann. Geophys., 19, 883-888.

(f) Hansen, A.R., G.D.Nastrom, J. A. Otkin, and F.D.Eaton, 2002: MST radar observations of gravity waves and turbulence near thunderstorms, J. Appl. Meteor., in press.

(g) VanZandt , T.E., G.D. Nastrom, J. Furumoto, T. Tsuda, and W.L.Clark, 2002: A Dual-Beamwidth Method for observing atmospheric turbulence intensity with radar, Geophys. Res. Lettr., submitted.

(h) Nastrom, G.D., and F. D. Eaton, 2002: A case study of wave and turbulence changes from MST radar observations at Vandenburg AFB during cyclone passage. J. Appl. Meteor., in preparation.

(i) Nastrom, G.D., A.R. Hansen, and F.D. Eaton, 2002: MST radar observations of gravity waves and turbulence near jet streams, J. Appl. Meteor., in preparation.

III. Interactions

(a) Participation/presentations:

(1) Eaton, F.D., G.D. Nastrom, A.R. Hansen, and W. Brown, 1999. Variability of slant-path turbulence parameters and inner scale effects. SPIE 12th Annual International Symposium on Aerospace, 13-17 April, Orlando, FL, preprints.

(2) Eaton, F.D., G.D. Nastrom, B. Masson, I. Hahn, K. McCrae, S. R. Novlin, and T. Berkopec, 1999. Radar and aircraft observations of a layer of strong refractivity turbulence. SPIE 12th Annual International Symposium on Aerospace, 13-17 April, Orlando, FL, preprints.

(3) Hansen, A. R., G.D. Nastrom, Eaton, F.D, 1999: The annual cycle of gravity wave activity at 5-20 km from VHF radar observations at White Sands Missile Range, New Mexico, Preprints, 29th Conference on Radar Meteorology, AMS, Montreal, 12-16 July, 509-512.

(4) Nastrom, G.D., 1999: Measurements of eddy dissipation rate and inner and outer scales of turbulence from MST radar. Invited, NCAR Workshop on meter-scale turbulence, Boulder, August 9-11.

(5) Hansen, A. R., G.D. Nastrom, Eaton, F.D, 2000: Seasonal variation of gravity wave activity at 5 – 20 km observed with the VHF radar at White Sands Missile Range, New Mexico. Proceedings, 9th International Workshop on Technical and Scientific Aspects of MST Radar, Toulouse, March 13-17.

(6) Nastrom, G.D., and T.Tsuda, 2000: Comparisons of turbulence intensity and its variability over New Mexico and Japan, Proceedings, 9th International Workshop on Technical and Scientific Aspects of MST Radar, Toulouse, March 13-17.

(7) Nastrom, G.D., and T.Tsuda, 2000: Anisotropy of Doppler spectral parameters in the MU and White Sands VHF radar observations, Proceedings, 9th International Workshop on Technical and Scientific Aspects of MST Radar, Toulouse, March 13-17.

(8) Nastrom, G.D., J. Furumoto, T.E. VanZandt, and T. Tsuda, 2000: A Dual-Beamwidth Method for observing atmospheric turbulence intensity with radar, Fifth International Symposium on Tropospheric Profiling: Needs and Technologies. Adelaide, December 4-8.

(9) Nastrom, G.D., 2000: Comparisons of turbulence over Japan and New Mexico using radar observations, ABL-AFOSR Atmospheric Workshop, Kirtland AFB, July 26-28.

(10) VanZandt, T.E., W. L. Clark, J. Furumoto, T. Tsuda, and G. D. Nastrom, 2001: A Dual-Beamwidth Radar Method for Measuring the Turbulent Velocity Variance, URSI 2001, Boulder, January.

(11) Nastrom, G.D., J. Furumoto, T. Tsuda, T.E. VanZandt, C. Love, and W.L.Clark, 2001: A Dual-Beamwidth Method for observing atmospheric turbulence intensity with radar, IAMAS 2001, Innsbruck, July 10-18.

(12) Nastrom, G.D., A. R. Hansen, J. Otkin, and F.D. Eaton, 2001: MST radar observations of gravity waves and turbulence near thunderstorms. IAMAS 2001, Innsbruck, July 10-18.

(13) Nastrom, G.D., F. D. Eaton, and A. R. Hansen, 2002: Some sources of gravity waves as seen from MST radar observations. International Symposium on Equatorial Processes Including Coupling, Kyoto, Japan, March 18-22, Submitted.

(14) Nastrom, G. D., F. D. Eaton, and E. Boll, 2002: A case study of atmospheric conditions at 2-19 km over Vandenburg AFB during passage of a cyclone. 10th Conference on Aviation, Range, and Aerospace Meteorology, Portland, May 13-16, Submitted.

(b) Consultative and advisory functions

At the request of Dr. E. M. Dewan of AFRL/VSBM, Hanscom AFB, MA, informal review comments were given on a journal article on gravity waves that he is preparing. Also, graphs of data from another project on gravity waves and turbulence were provided to Dr. Dewan at his request.. Also at the request of Dr. E. M. Dewan of AFRL/VSBM, Hanscom AFB, MA, a brief effort was made to evaluate a prediction of his gravity wave model. As this task will require considerable time it will be held until further time becomes available.

IV. Other results

(a) C_n^2 and synoptic-scale vorticity.

See Appendix A.

(b) Results from the Vandenburg AFB MST radar.

See Appendix B.

(c) Case studies of waves and turbulence at the MU MST radar.

See Appendix C.

V. Summary of accomplishments/new findings.

(a) The demonstration that the gravity wave intensity seen by satellites (GPS/MET) agrees with that seen by the radar at White Sands. This agreement establishes confidence in the GPS/MET values; since the satellite data are global this result provides a means of studying the global distribution of gravity wave intensity.

(b) The demonstration that gravity wave source mechanisms are different at WS and MU although the wave energies are about the same magnitude.

(c) The demonstration that C_n^2 in the stratosphere, above 18 km, is not changed by the presence of thunderstorms in the troposphere.

(d) The demonstration that the diurnal changes in C_n^2 and spectral width above the mid-troposphere are very small during all seasons at both WS and MU.

(e) The demonstration that C_n^2 in the stratosphere at both WS and MU is very highly correlated with relative vorticity. The correlation is improved when distance from the tropopause is used as the vertical coordinate and when the C_n^2 is normalized by local atmospheric density. The model developed is thus a combined conceptual/ physical/statistical model.

(f) The demonstration in the case study at Vandenburg AFB that turbulence (C_n^2 and specific turbulent kinetic energy) and waves increase during the passage of a cyclone are generated only by upper tropospheric effects because upwelling effects from the planetary boundary layer are cut off by a strong surface inversion.

(g) The demonstration in the case studies at MU that turbulence intensities in the lower stratosphere are often more closely related to the intensity of gravity waves than to in situ wind speed and large-scale wind vertical shear.

VI. Personnel.

The following persons were supported during this effort.

Dr. Gregory D. Nastrom, PI

Dr. Anthony R. Hansen, (Augsburg College), Contractor

Appendix A. C_n^2 and the Synoptic-Scale Vorticity

To determine if a linkage exists between the intensity of mesoscale turbulence and synoptic-scale features in the mid latitude atmosphere, a study was undertaken to compare radar turbulence measurements with analyzed synoptic scale wind fields. The radar data used in this study consisted of the uncalibrated back-scattered power measured at the MU radar in Japan from 1991-1996 and C_n^2 measurements taken at the WSMR radar during the same period. The analysis period was confined to the cold season months when mean wind speeds in the upper troposphere were relatively high at both stations. Months used for study at MU were October through April of each year and at WSMR the months used were November through April of each year. Analysis of synoptic-scale meteorological fields was accomplished through the use of NCAR/NCEP reanalysis data for the same periods. This report will concentrate on comparisons involving analyzed winds at 300 mb and 500 mb. The analyzed winds were used to compute wind shears and relative vorticity of the synoptic scale flow. The objective is to establish what relationship exists between variations in the synoptic-scale winds and the locally measured turbulence in the vicinity of the tropopause.

Consider first the results obtained using the MU data. Winds for the grid points surrounding the MU radar site were extracted from the NCAR/NCEP reanalysis and the relative vorticity, ζ, for the location directly above the radar was computed. The reanalysis data were available at 6 hour intervals. The resulting relative vorticity values were compared to the hourly means of the uncalibrated, back-scattered power measurements from MU. (The uncalibrated, back-scattered power is used as a proxy for C_n^2.) Vorticity values were considered constant within 3 hours of a reanalysis time for the purposes of computing correlations with the hourly back-scattered power measurements. In addition, to remove the possibility that any resulting correlation was the result merely of vertical displacements of the tropopause resulting from the passage of synoptic-scale waves or jet streaks, the measured back-scattered power profiles were adjusted vertically to a tropopause relative co-ordinate system. To establish the tropopause height above MU, routine radiosonde measurements from the nearby stations of Wajima (37.22N 136.54E) and Shiono-misaki (33.27N, 135.46E) were used. Tropopause heights based upon the WMO definition were computed from the soundings at 12 hourly intervals and tropopause heights for MU were interpolated in space and time from these results. Thus, for each hourly mean radar measurement, a tropopause height was determined and the radar power profile was adjusted, based up the mean profile from the dataset, to a tropopause relative vertical co-ordinate. These values were then correlated with the MU vorticity values determined from the reanalysis.

In addition, a factor to normalize the radar data to remove possible dependence of the backscatter power values on the air density was employed. Measurements of the air pressure and temperature at the level of the WMO-definition tropopause for MU were computed from the radiosonde data. From these a factor to normalize these results from the air density at the tropopause for each hour to the air density at 14 km was employed. This factor

$$N = (\rho_{trop}/\rho_{14\,km})^2$$

is designed to remove any possible dependence in the results on mere density differences between the tropopause level on one day versus another. A selection of results is presented below.

Fig. A-1 illustrates the comparison of all hourly power and vorticity pairs for MU, using the relative vorticity at 300 mb at an altitude 1.2 km below the local tropopause. The relationship at this altitude was relatively strong. At higher altitudes, particularly above the tropopause, similar results also appeared in that the regression curves between the relative vorticity and the departure of the back-scattered power from its mean are nearly identical, but the correlations between the regression line fit to the data and the data is lower at altitudes above the tropopause. Inspection of this figure clearly indicates a relationship between increasing cyclonic vorticity and increasing back-scattered power (and therefore increased levels of turbulence). The correlation of r=0.41 between this data sample and the plotted linear regression fit to the data is quite impressive considering the noise level in the underlying data. To reduce the noise level in this plot, the data pairs were binned within ranges of relative vorticity and means computed. These results are presented in Fig. A-2. Error bars in this figure correspond to estimates of the standard error in the mean of the data plotted. The resulting correlation of a linear regression fit to the averaged data is quite high.

Corresponding results at 500 mb for MU are similar to those at 300 mb but fit of the regression lines to the data are not as strong. Fig. A-3 illustrates the same results as Fig. A-2 except that the vorticity at 500 mb was used.

The same procedure was followed for the WSMR radar data. Reanalysis data corresponding to the location of WSMR were extracted and vorticity values computed. The measured C_n^2 values from the WSMR radar were also adjusted vertically to produce tropopause relative co-ordinates. The WSMR tropopause was determined from radiosonde measurements from nearby El Paso, TX (ELP). In addition, the same density normalizing factor, N, was used to remove any dependence of the results on mere altitude differences between the tropopause-relative vertical co-ordinate at one hour versus that at another hour.

The results for WSMR, also at 1.2 km below the tropopause between the normalized C_n^2 and the relative vorticity at 500 mb is given in Fig. A-4. A very similar relationship to that found at MU is also apparent in this independent data sample. That is, normalized C_n^2 values increase with increasingly cyclonic relative vorticity in the synoptic-scale flow. For anticyclonic conditions, the C_n^2 values are relatively lower. For cyclonic conditions, C_n^2 values are higher. Results based purely on the lateral shear of the synoptic scale flow lead to essentially the same results (not shown). The results at WSMR show a better fit to the regression curve at 500 mb than do the corresponding results at MU.

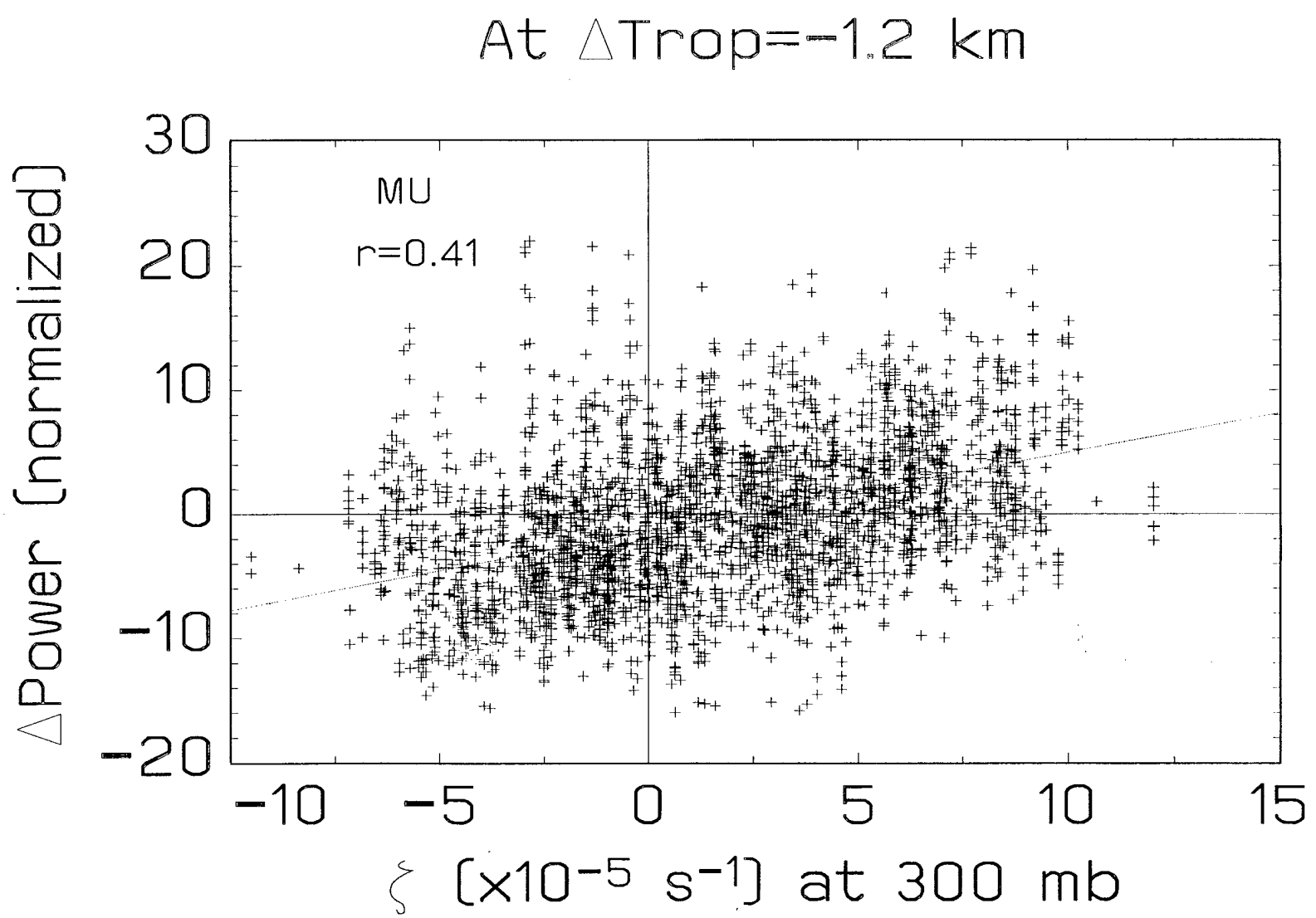
At △Trop=-1.2 km
MU
r=0.41
△Power (normalized)
30
20
10
0
-10
-20
-10
-5
0
5
10
15
ζ (x10⁻⁵ s⁻¹) at 300 mb

mu_shear\muthirdb.g Tue Jan 08 15:56:21 2002

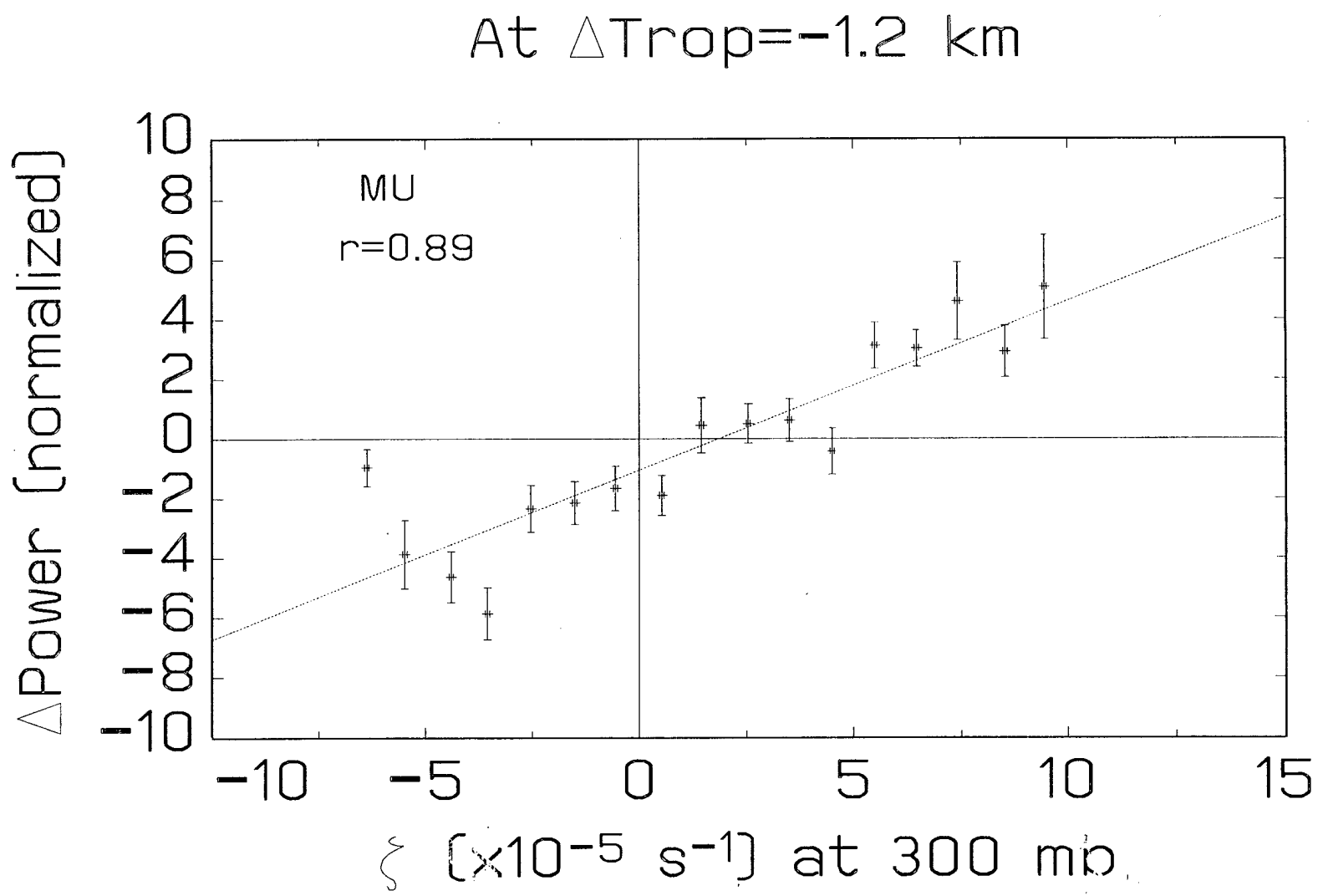

mu_shear\muthirdb.g Tue Jan 08 16:00:27 2002

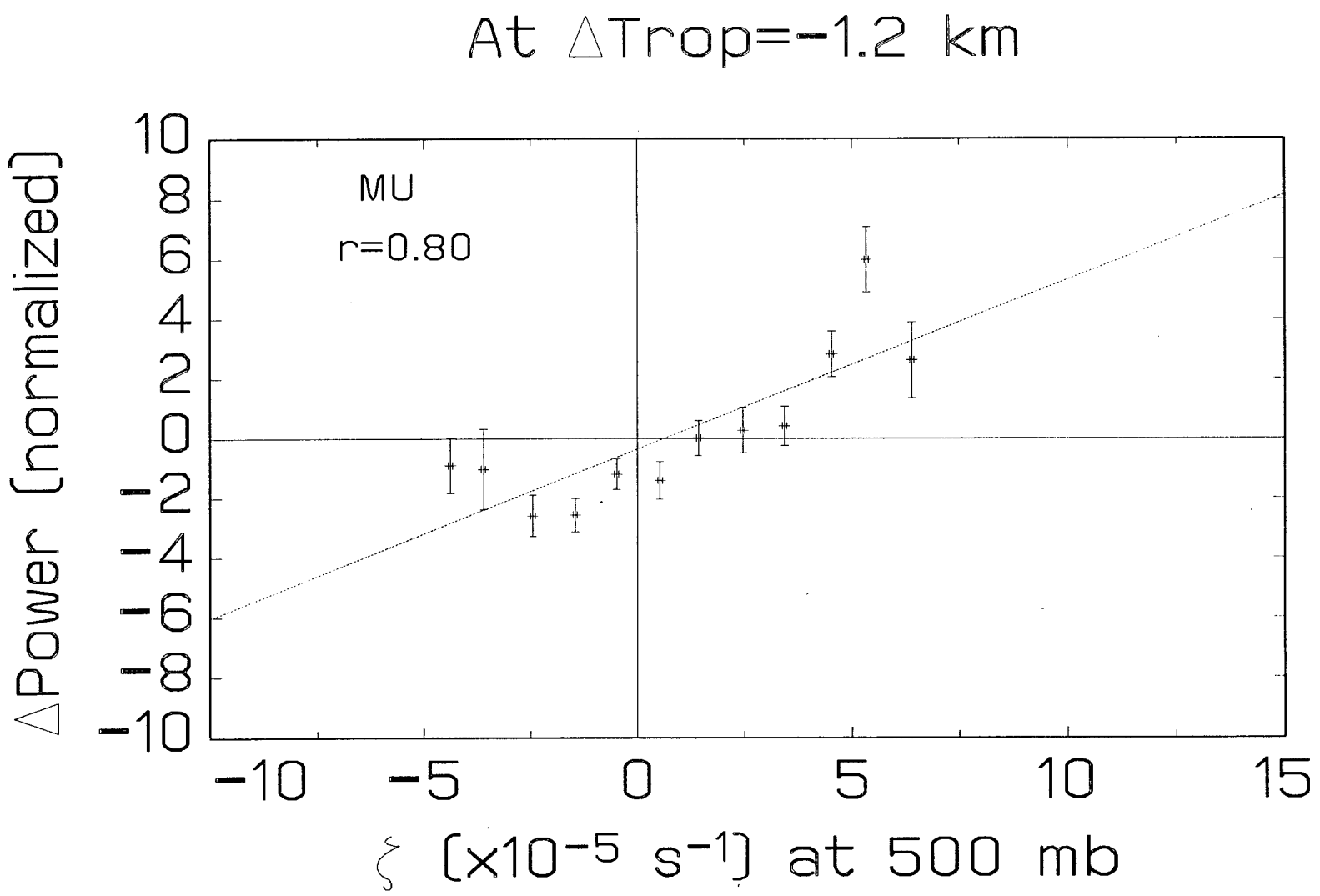

jason\shear\rethrd3s.g Tue Jan 08 15:58:46 2002

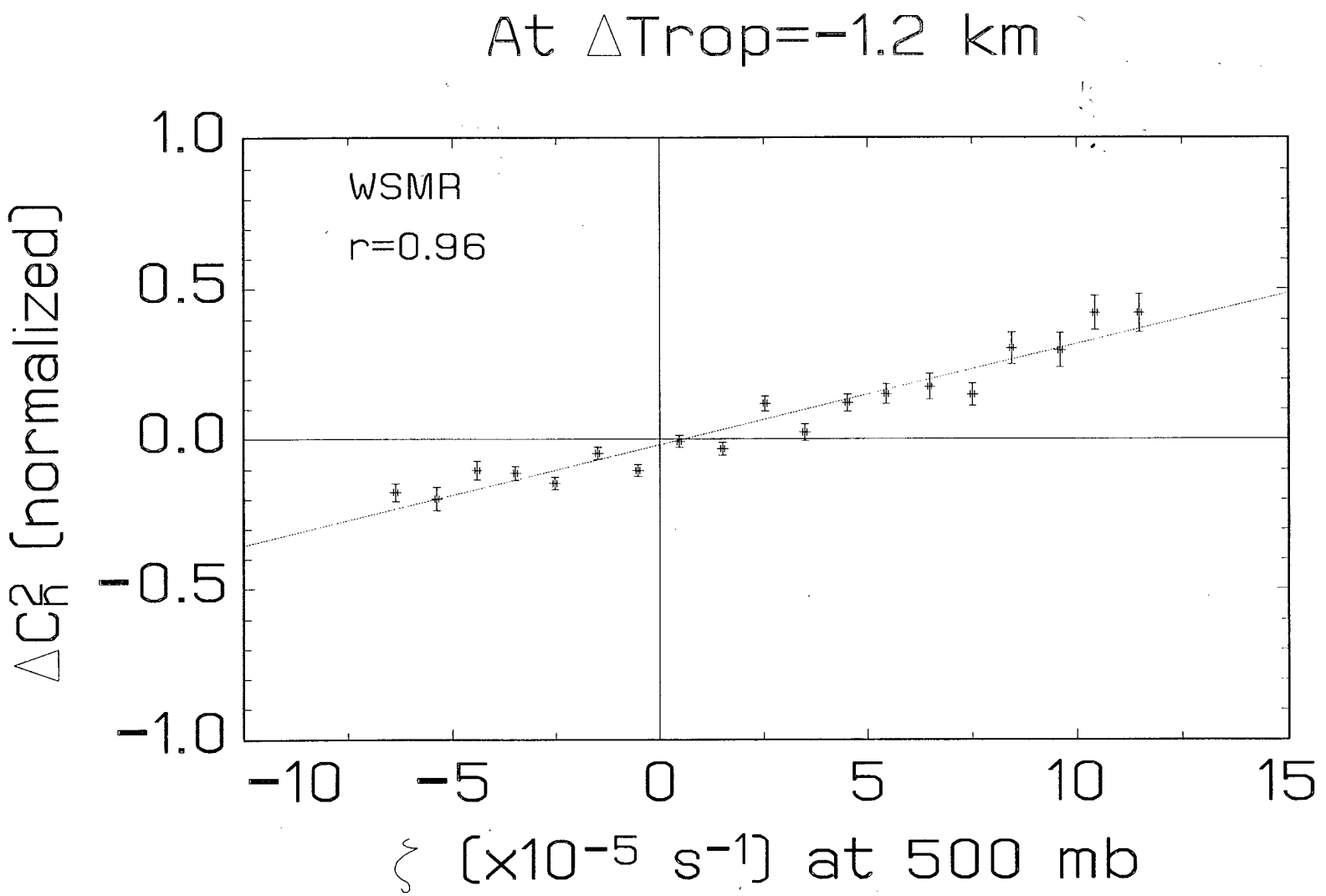

Appendix B. Results from the Vandenburg AFB MST radar

A case study of atmospheric conditions at 2-19 km over Vandenburg AFB during passage of a cyclone

I. Introduction.

The purpose of this report is to describe a case study of winds and turbulence over Vandenburg AFB, CA, during 7/20/20Z to 7/27/23Z July 2001. During this period the 50 MHz radar at Vandenburg AFB was operated continuously. Vertical profiles of the wind speed, backscattered power (reported as signal-to-noise ratio, SNR, and calibrated as the refractivity turbulence structure constant, C_n^2), and the Doppler spectral width (HPHW, in ms^{-1}) were obtained at 3-minute intervals on the three beams (vertical and 15 degrees from the zenith at azimuths 225 and 315 degrees). The VBG radar is similar in size (half-power beamwidth 3.2 degrees) and power (208 kW peak) to that operated at White Sands Missile Range during the 1990s. The radar data are augmented by rawinsonde ascents and surface weather observations at Vandenburg AFB and by routine weather map analyses.

II. Data Quality

A. Initial data inspection. At first glance the vertical profiles of the observations look reasonable. For example, Fig. 1 shows the individual profiles of log C_n^2, SNR (in dB), velocity (ms^{-1}), and log spectral width for each beam (beams vertical, 315°, and 225° in rows upper, center, and lower, respectively) for the hour 7/21/00Z. The number of profiles available (16 or 20) is given above the C_n^2 plot for each beam. A vigorous quality control algorithm was used; briefly, C_n^2, velocity, and width were not used if SNR<-12 dB or if velocity or C_n^2 failed temporal consistency checks or if the vertical shear of horizontal wind exceeded realistic limits. Note that the apparent layered structure of C_n^2 is persistent throughout the hour. Also, many of the small-scale features of the horizontal velocity profiles are persistent (horizontal velocities were estimated by multiplying the radial velocities by csc 15°; i.e., the effects of vertical velocities were assumed to be negligible). Although the relative variability of the width profiles at a given height is larger than that of C_n^2 and wind, the general shape appears constant throughout the hour. Inspection of corresponding plots from the other hours (not shown) gives similar results. Thus, the data appear reasonable; for convenience, hourly medians of the individual observations at each level will be used below. Any minor adjustments, such as re-calibration of the C_n^2 values, will not change the present conclusions.

B. Sensitivity limits. Note in Fig. 1 that the left-hand side of the oblique-beam C_n^2 profiles appear to be "clipped", that is, there seems to be a lower limit of sensitivity that slopes upward toward the right. This feature is confirmed in Fig. 2. Fig. 2 shows the hourly-median profiles for all 172 hours in the lower panels. The upper panels show the profile of the median of the 172 hourly values (solid) and the profiles of the maximum

and minimum value at each level. Also plotted in Fig. 2 are the sensitivity limits (called the "minimum detectable" limit by Green et al., 1979). The minimum detectable level is computed by multiplying the reported C_n^2 by the ratio $SNR_{min}/SNR_{reported}$, where SNR_{min} was taken to be –12 dB. The "clipped" left edge of the C_n^2 profiles obviously arises from the effects of sensitivity limits. Also, note that the minimum detectable signal curve has a knee of uncertain origin at about 3.5 km; thus, we should not use C_n^2 values below 3.5 km.

C. Anisotropy. Fig. 3 compares the median profiles of C_n^2 and Width from the oblique beams. Right hand panels show the ratios of Beam 225 to Beam 315. The values of C_n^2 from Beam 225 are larger (from 0 to 2 dB) in the troposphere, and above about 14 km the values are indistinguishable. In view of the very small differences at high altitude, where tilting of specular layers might be quite small, this result suggests that the two beams are well-calibrated with respect to each other. Regarding width, the values for Beam 315 are very slightly larger above 4 km. However, note that the plotted values are observed widths and that corrections for beam-, shear-, and wave-broadening effects must be applied to these (e.g., Nastrom and Eaton, 1997). In summary, the two oblique beams appear to give similar results.

III. Radar Observations

A. Radar wind observations. Fig. 4 (upper panels) shows the hourly medians of zonal and meridional wind speeds (ms^{-1}). For reference, hour 100 is 7/25/00Z. The color contours are at 10 ms^{-1} intervals; for zonal wind the zero line is that between light blue and dark blue and for meridional wind it is that between blue and green. The salient features of zonal wind are the westward winds below about 6 km from hours 90-150, the waxing and waning of the jet near 13 km with strongest pulse near hour 90, and the quasi-periodic oscillations above 16 km with downward phase progression with time. The main features of meridional wind are the strong burst of southward winds near 9 km at hour 100 and the quasi-periodic oscillation above 16 km. Corresponding wind speed and wind direction charts are given in the lower panels where each of the features mentioned above can easily be found.

The quasi-periodic wind behavior above 16 km is interesting; however, it will be seen in Figs. 5 and 6 below that it does not seem to have a large influence on SNR or C_n^2. Since this report concerns C_n^2, the periodic oscillation will not be discussed further.

B. Radar SNR. Fig. 5 shows the time-height plots of SNR in dB. Those for Beam 315 (225) are in the upper (lower) panel. The left-hand panel shows the entire range 2-21 km. Very large SNR values are seen in the troposphere, below about 6 km. At higher altitudes the main feature is an enhancement of SNR at about 8-16 km from about hour 70-112 (about 7/23/18Z to 7/25/12Z). This enhancement is seen in more detail in the right-hand panels which show only the region above 10 km.

C. Radar C_n^2. Fig. 6 is similar to Fig. 5, except it shows log C_n^2. The logarithm is used hereafter, but will be referred to as just C_n^2, because past studies have shown the logarithm of C_n^2 is normally distributed. The main features in Fig. 6 are the very rapid

decrease of C_n^2 above about 6 km and the apparent enhancement of C_n^2 up to about 16 km during approximately hours 70-112. Due to the large range of C_n^2 values in the left-hand panels of Fig. 6 it is difficult to tell how low this feature extends. To help see the extent of the enhancement, Fig. 7 shows plots of the perturbations of C_n^2, defined as the hourly values minus the median of all hourly values at each level. Profiles of the medians are given in the upper panel for convenience (Beam 315 is the solid line). Note that the enhancement in Fig. 7 (especially for Beam 225) extends from about hour 70-112 (about 7/23/18Z to 7/25/12Z) and that it extends from below 4 km (the minimum level of reliable C_n^2 values) to about 15 km.

D. Turbulent Kinetic Energy (TKE). The upper panels of Fig. 8 show the radar spectral width plotted as the turbulent kinetic energy density, σ_t^2 (m^2s^{-2}). These values have been corrected for beam-, shear-, and wave-broadening effects following Nastrom and Eaton (1997). The main feature is the general enhancement of σ_t^2 from about hour 70-112. This time period correlates very well with the enhancement times noted for SNR and C_n^2, although the relative intensity of the enhancement of σ_t^2 is smaller than that for SNR or C_n^2.

E. Standard deviation of vertical velocity. The lower-right panel of Fig. 8 shows the hourly standard deviations of vertical velocity, σ_w (ms^{-1}). The values are generally very small, less than about 0.1 ms^{-1}, except between about hours 80 and 110 at about 9-14 km when values exceed 0.25 ms^{-1}.

IV. Case study results

A. Synoptic weather patterns. Fig. 9 shows the 500 mb maps at 12Z daily for 7/20-7/27 2001. The flow over Vandenburg AFB was from the southwest through 7/22. On 7/23 a sharp trough began to influence conditions over southern California as winds at VBG became westerly. The trough deepened and formed into a closed low centered just north of VBG on 7/24. By 7/25 the low had filled a little and its center had moved several hundred km east of VBG. By 7/26 the remaining weak trough was over Arizona with the flow over VBG much weaker. Flow was back to southwest on 7/27.

Rawinsonde observations from VBG for 23/00Z-27/12Z are given in Fig. 10 (the launch was made from South Vandenburg on 25/00Z, a site about 10 km south of VBG). The temperature soundings show a strong inversion over VBG throughout this period with the top of the inversion several thousand feet above the surface. Surface weather observations from VBG (not shown) indicate continuous low cloud coverage with occasional fog throughout this period. All local hills were well below the top of the inversion, and winds in the lower levels were consistently relatively light, 10 knots or less, throughout this period. Thus, it appears that the upper levels were isolated from the boundary layer.

Note that the winds from the radar (Fig. 3) agree very well with the geostrophic flow pattern (Fig. 9) and the winds from the rawinsondes (Fig. 10). This agreement gives further confidence in the radar observations.

At first glance, the strong wind changes in the upper troposphere seen in Fig. 4, as well as the enhancements in SNR, C_n^2, σ_t^2, and σ_w in Figs. 5-8, will be attributed to the

passage of the upper level cyclonic circulation feature. Due to the strong low level inversion and light low level winds, it seems unlikely that boundary layer effects (such as flow over rough terrain or low level convection) were the source of the enhancements in SNR, C_n^2, σ_t^2, and σ_w seen in Figs. 5-8.

B. Correlation patterns. Fig. 11 shows time series of the median C_n^2, σ_t^2, and σ_w over all levels in the layer 10-15 km in the left-hand panels. The right-hand panels show plots of the same data, scaled to have a range of unity. The upper (center) panel compares C_n^2 with σ_t^2 (σ_w) and the lower panel compares σ_t^2 and σ_w. There is high correlation of C_n^2 with σ_t^2 (0.87). The correlation of C_n^2 with σ_w is also fairly high (0.60), and note that σ_t^2 and σ_w are fairly well-correlated (0.59).

The high correlation coefficient for C_n^2 with σ_t^2 (0.87) is important because it implies that a large part of the variability in C_n^2 is due to turbulence changes. In general, local values of C_n^2 depend on both the intensity of turbulence through the outer scale of turbulence, L_o, and the mean gradient of refractive index (M)

$$C_n^2 = a^2 \alpha' L_o^{4/3} M^2 \qquad (1)$$

where a^2 is a constant and α' is the ratio of eddy diffusivities, usually taken as constant (see Gage, 1990, for a review). L_o is is related to the eddy dissipation rate, ε, and the wind shear, du/dz, by $L_o=(\varepsilon/\gamma)^{1/2}|du/dz|^{-3/2}$ where γ is usually taken as constant. M is related to the stability ($d\ln\theta/dz$) and specific humidity (q) as

$$M = -77x10^{-6}\frac{p}{T}\left(\frac{d\ln\theta}{dz} + \frac{15500q}{T}\frac{d\ln\theta}{dz} - \frac{7800}{T}\frac{dq}{dz}\right) \qquad (2)$$

In the presence of high humidity and humidity gradients M and hence C_n^2 depends strongly upon humidity (Tsuda et al., 1988). However, the rawinsonde reports during this period (Fig. 10) show that humidity levels were low and uniform with time above about 700 mb (about 3 km). The rawinsonde reports further show that the stability was uniform with time. Nastrom and Eaton (2001) show that in the absence of humidity the volume averaged C_n^2 is proportional only to turbulence intensity and stability, and since the stability changes here were small the changes in C_n^2 with time were due to changes in turbulence intensity. The high correlation of C_n^2 with σ_t^2 seen in Fig. 11 supports this suggestion.

C. Source of turbulence. Fig. 12 compares time series of the hourly median C_n^2 at 10-15 km with those of wind speed and vertical wind shear over 300 m intervals. (For reference, time series of the median C_n^2 and median wind speed and direction over 1 km intervals at 10-15 km are given in Fig. 13. Note in Fig. 13 that the wind speed and direction are very similar at all levels 10-13 km and are different at 14-15 km.) Returning to Fig. 12, note that the correlation between C_n^2 and wind shear (0.80) is much greater than that between C_n^2 and wind speed (0.49), suggesting that the turbulence is generated by a local dynamic instability and that this instability is not necessarily related to wind speed. That is, since C_n^2 is not closely related to wind speed (wind speed is an indicator of the large-scale flow), the turbulence may be due to instabilities in small-scale

flow features such as gravity waves (this suggestion is supported by the correlation of C_n^2 and σ_w in Fig. 11 since σ_w is generally regarded as an indicator of gravity wave intensity).

Possible sources of gravity waves include geostrophic adjustment processes and shear instabilities along the edges of the jet stream. Since the flow is cyclonic it seems unlikely that inertial instability processes are important, and since the planetary boundary layer is capped by a strong inversion with weak low-level flow it seems unlikely that upwelling of waves from the low levels is important.

In another Appendix of this report it is shown that C_n^2 at White Sands Missile Range and returned power at MU in Japan are well-correlated with vorticity. Fig. 14 shows the time series of geostrophic vorticity at 200 mb over VBG computed using the height field shown on routine weather maps. The main feature is a spike in vorticity centered at 25/00Z; this time corresponds to hour 100 in Figs. 4-7 and thus is about at the center of the period of enhanced C_n^2. This case study provides further evidence for the usefulness of vorticity as a predictor of C_n^2.

References

Gage, K.S., 1990: Radar observations of the free atmosphere: Structure and dynamics. In Radar in Meteorology, Chapt. 28a, Ed. David Atlas, Am. Meteor. Soc., Boston.

Green, J.L., K.S. Gage, and T.E. VanZandt, 1979: Atmospheric measurements by VHF pulsed Doppler radar. IEEE Trans. Geosci. Electon., GE-17, No. 4, 262-280.

Nastrom, G.D., and F.D. Eaton, 1997: Turbulence eddy dissipation rates from radar observations at 5-20 km at White Sands Missile Range, New Mexico. J. Geophys. Res., 102, 19495-19506.

Nastrom, G.D., and F.D. Eaton, 2001: Persistent layers of enhanced C_n^2 in the lower stratosphere from VHF radar observations. Radio Sci., 36, 137-149.

Tsuda, T., P.T. May, T. Sato, S. Kato, and S. Fukao, 1988: Simultaneous observations of reflection echoes and refractive index gradient in the troposphere and lower stratosphere. Radio Sci., 23, 655-665.

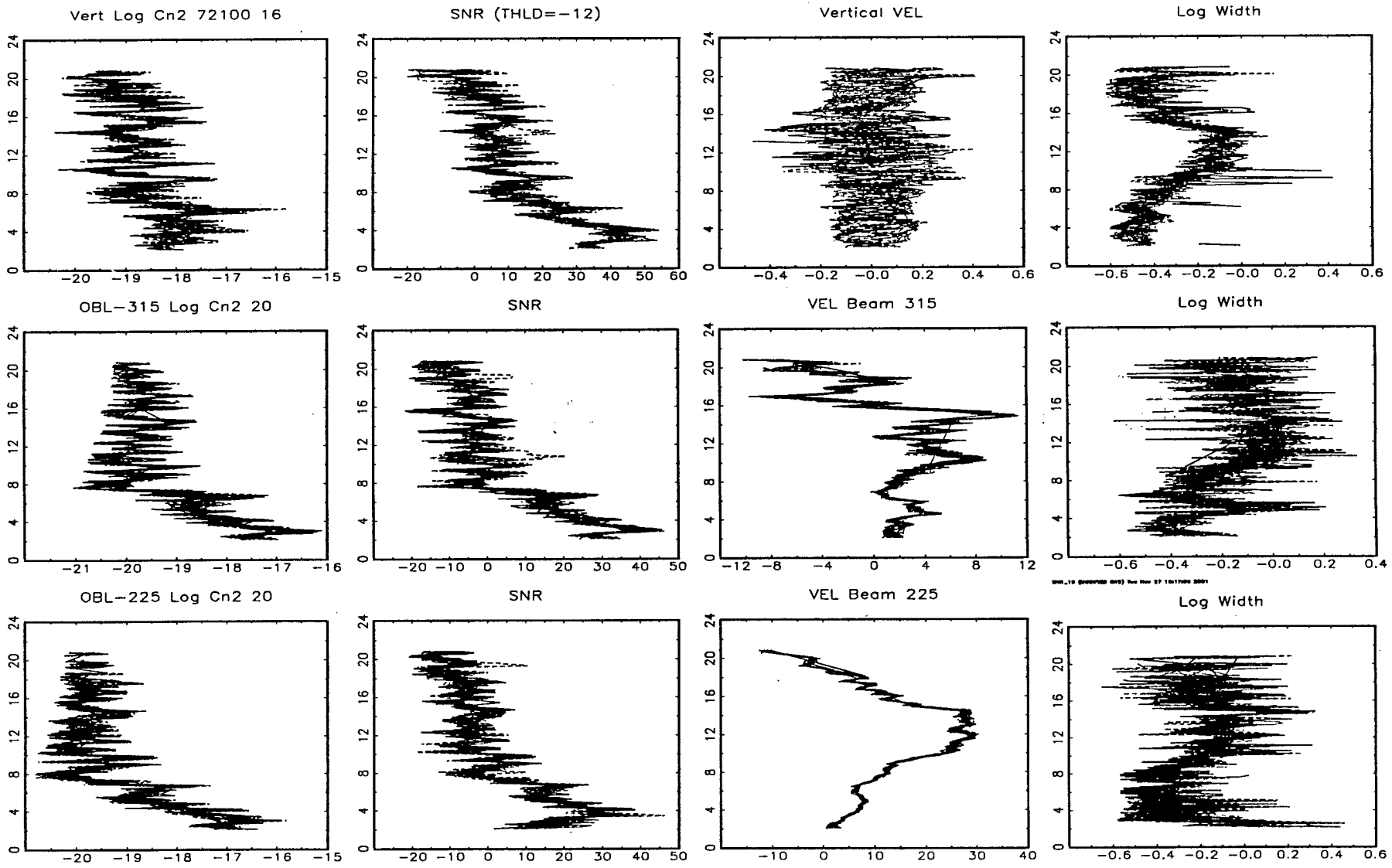
Vert Log Cn2 72100 16
SNR (THLD=-12)
Vertical VEL
Log Width
OBL-315 Log Cn2 20
SNR
VEL Beam 315
Log Width
OBL-225 Log Cn2 20
SNR
VEL Beam 225
Log Width

C:\gouse\HOURS_CN2 (MODIFIED CN2) Wed Nov 28 09:39:18 2001

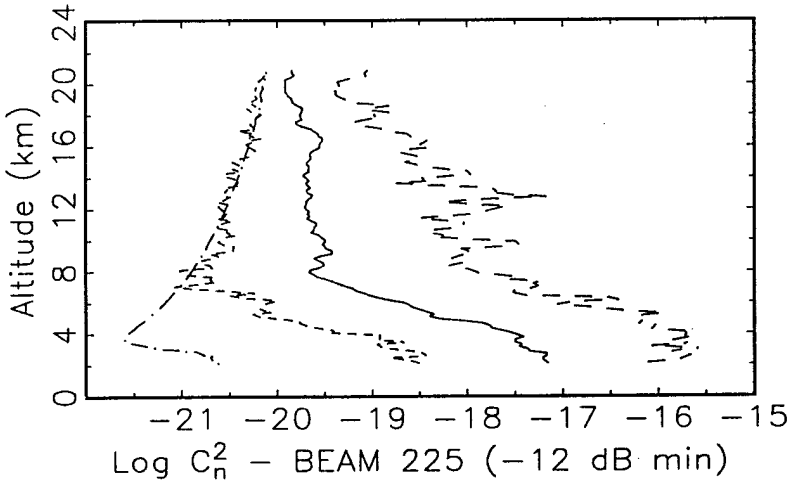

Wed Nov 28 09:39:19 2001

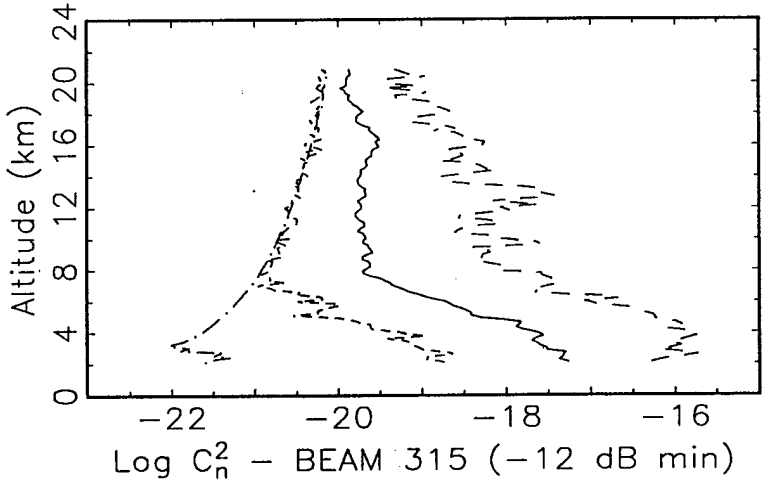

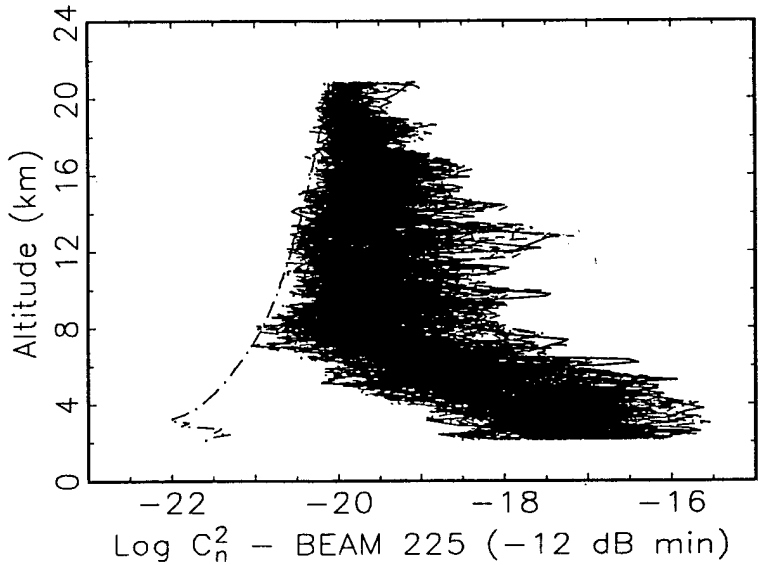

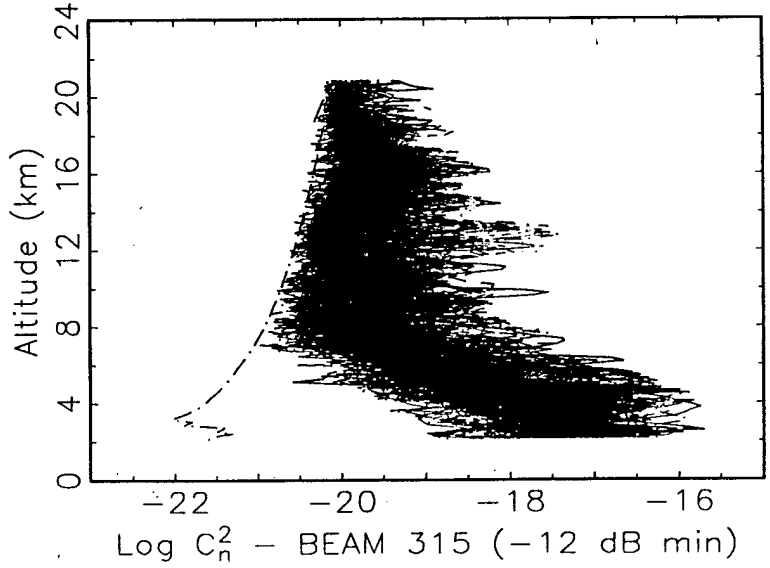

2

C:\gauss\HOURS_CN2 (MODIFIED CN2) Wed Nov 28 10:47:03 2001

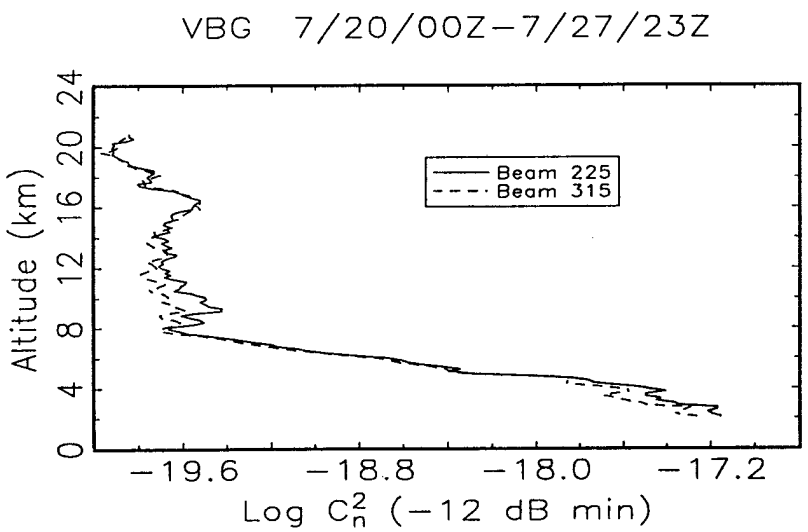

C:\gauss\HOURS_CN2 (MODIFIED CN2) Wed Nov 28 10:47:03 2001

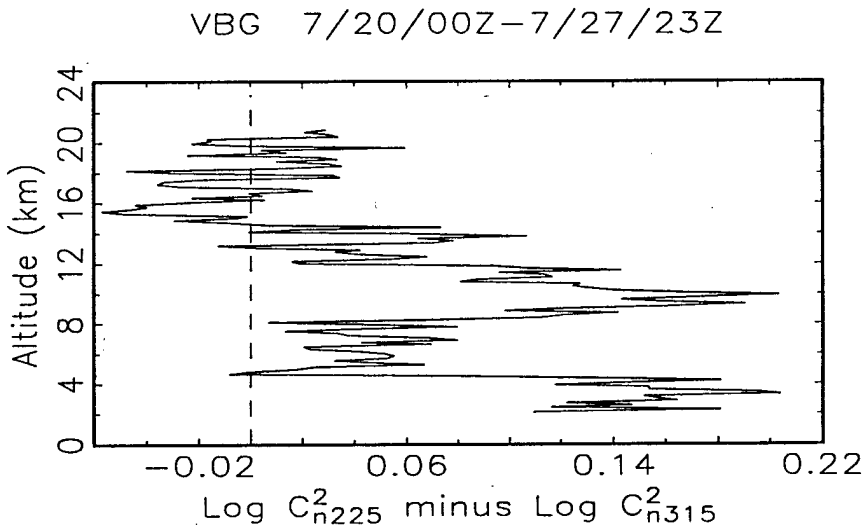

Wed Nov 28 10:47:04 2001

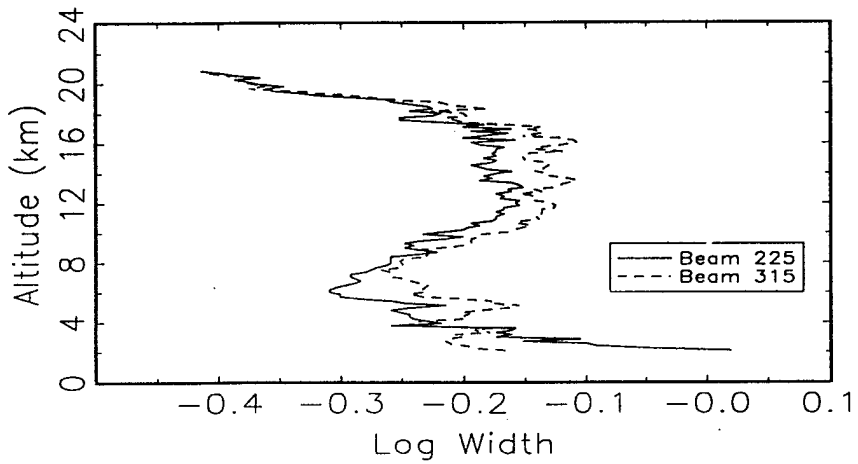

Wed Nov 28 10:47:04 2001

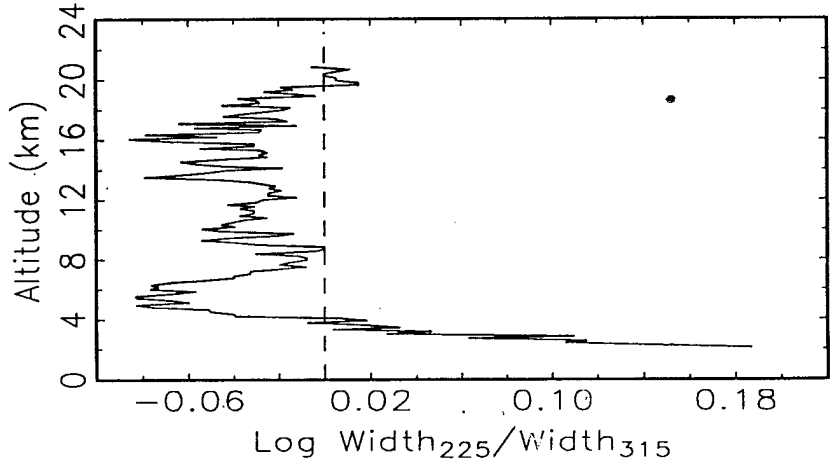

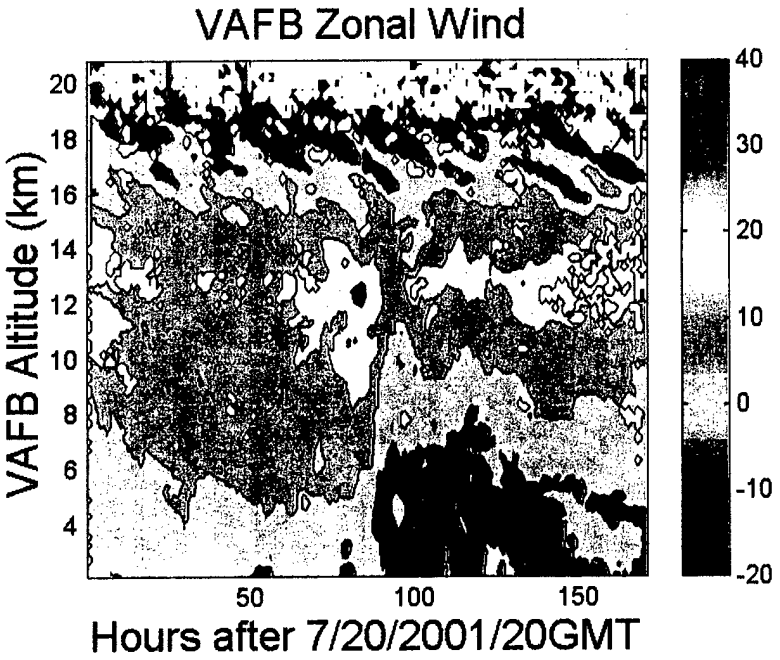
VAFB Zonal Wind
VAFB Altitude (km)
20
18
16
14
12
10
8
6
4
50
100
150
Hours after 7/20/2001/20GMT
40
30
20
10
0
-10
-20

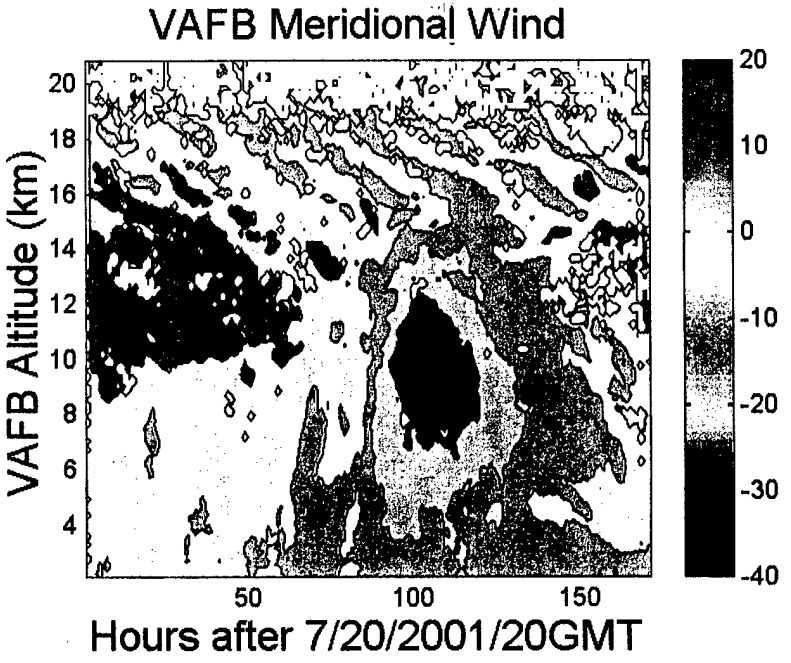
VAFB Meridional Wind
VAFB Altitude (km)
20
18
16
14
12
10
8
6
4
50
100
150
Hours after 7/20/2001/20GMT
20
10
0
-10
-20
-30
-40

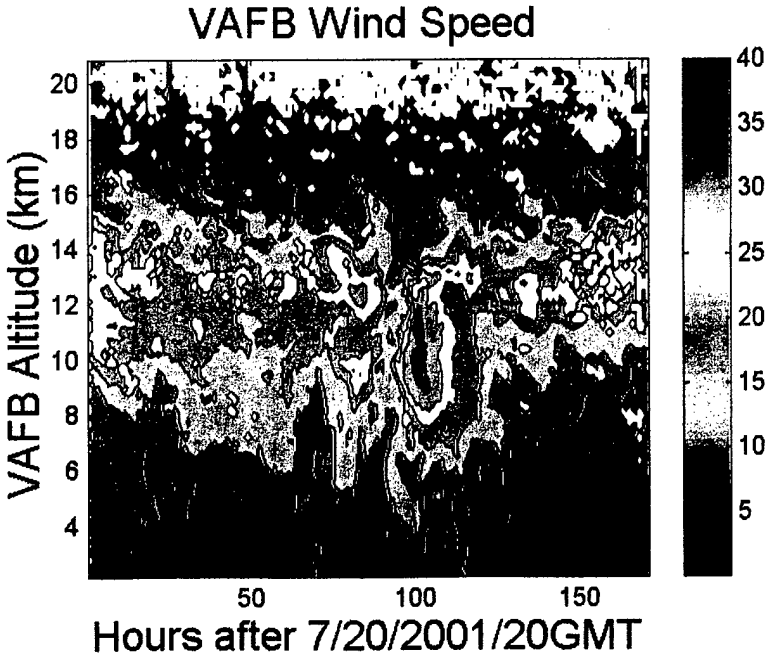
VAFB Wind Speed
VAFB Altitude (km)
20
18
16
14
12
10
8
6
4
50
100
150
Hours after 7/20/2001/20GMT
40
35
30
25
20
15
10
5

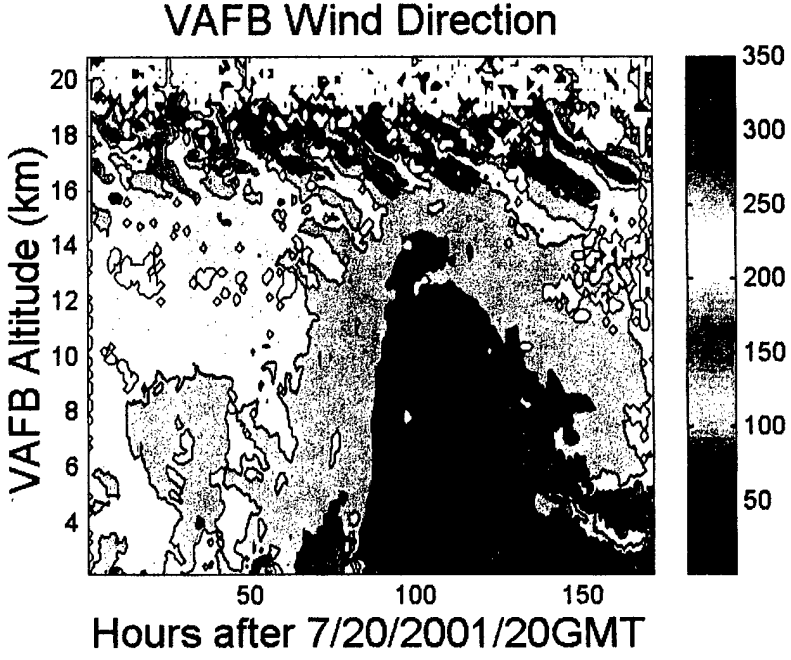
VAFB Wind Direction
VAFB Altitude (km)
20
18
16
14
12
10
8
6
4
50
100
150
Hours after 7/20/2001/20GMT
350
300
250
200
150
100
50

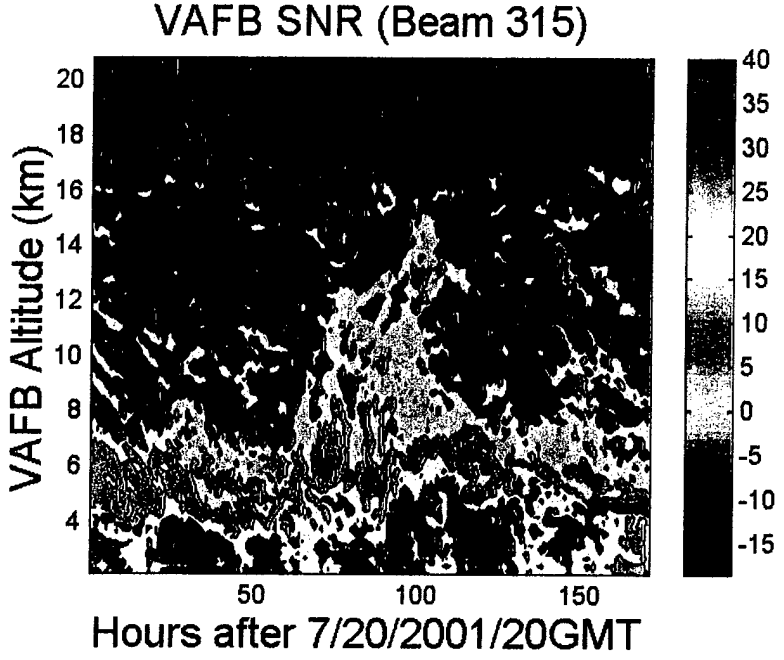
VAFB SNR (Beam 315)
VAFB Altitude (km)
20
18
16
14
12
10
8
6
4
50
100
150
Hours after 7/20/2001/20GMT
40
35
30
25
20
15
10
5
0
-5
-10
-15

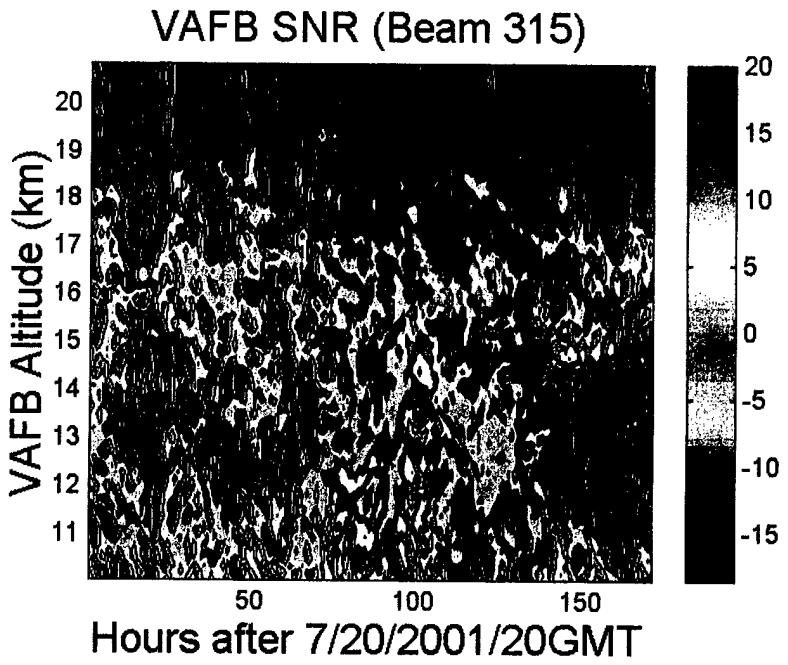
VAFB SNR (Beam 315)
VAFB Altitude (km)
20
19
18
17
16
15
14
13
12
11
50
100
150
Hours after 7/20/2001/20GMT
20
15
10
5
0
-5
-10
-15

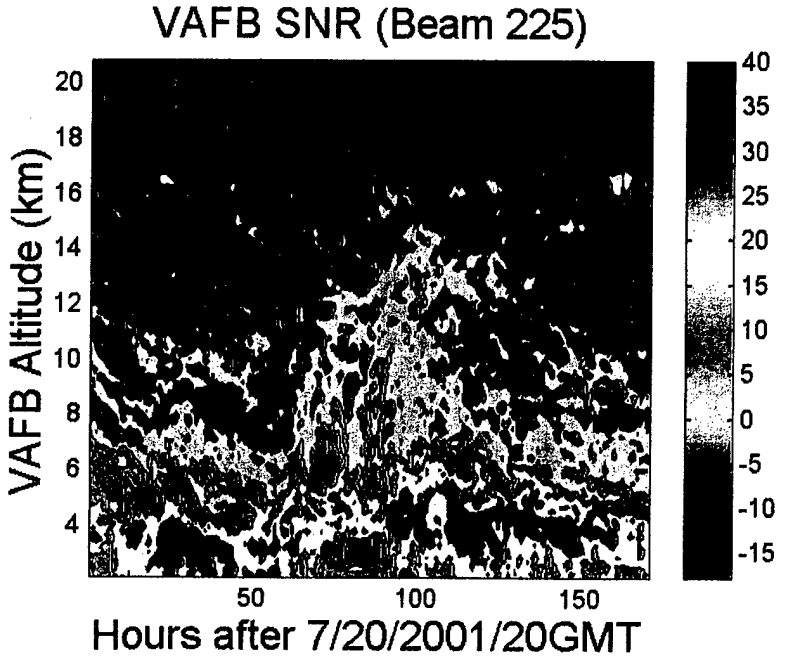
VAFB SNR (Beam 225)
VAFB Altitude (km)
20
18
16
14
12
10
8
6
4
50
100
150
Hours after 7/20/2001/20GMT
40
35
30
25
20
15
10
5
0
-5
-10
-15

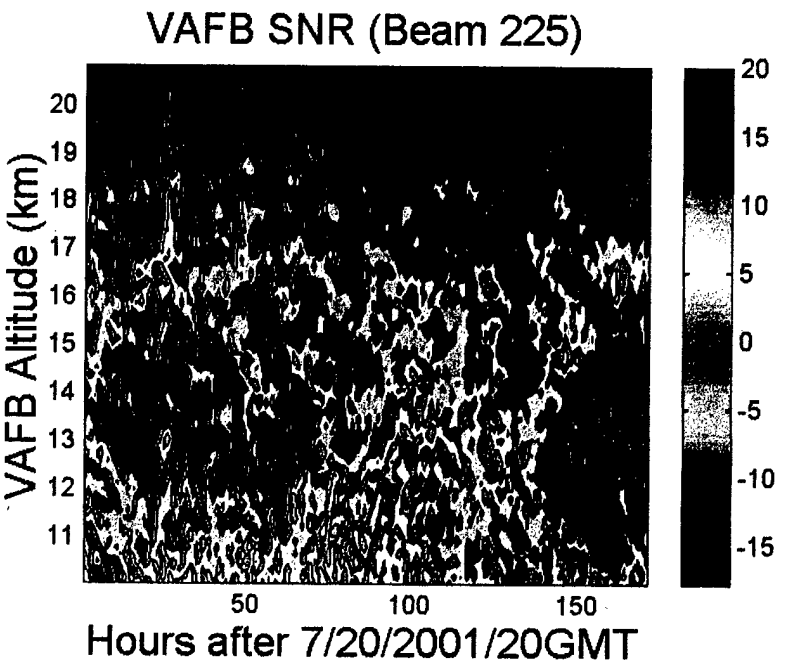
VAFB SNR (Beam 225)
VAFB Altitude (km)
20
19
18
17
16
15
14
13
12
11
50
100
150
Hours after 7/20/2001/20GMT
20
15
10
5
0
-5
-10
-15

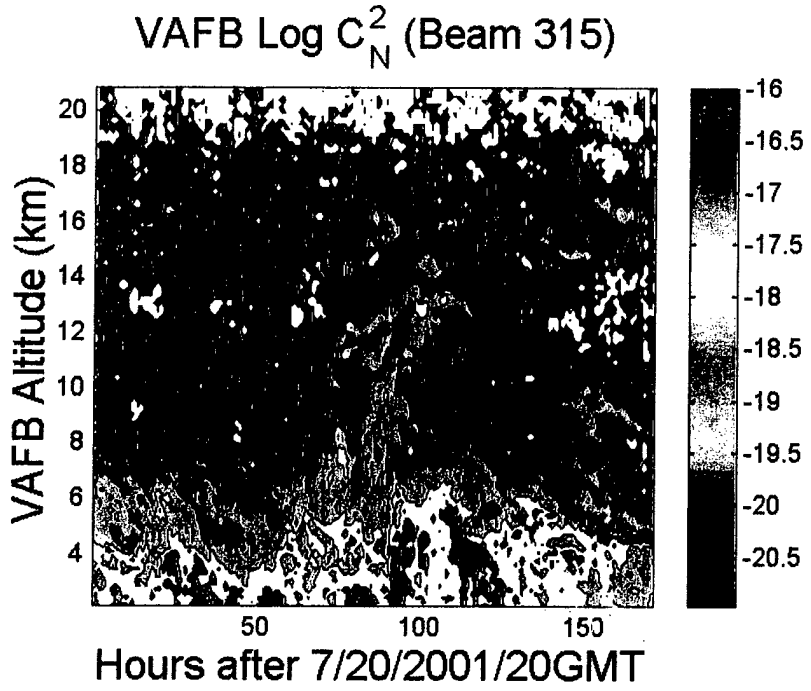
VAFB Log C_N^2 (Beam 315)
VAFB Altitude (km)
20
18
16
14
12
10
8
6
4
50
100
150
Hours after 7/20/2001/20GMT
-16
-16.5
-17
-17.5
-18
-18.5
-19
-19.5
-20
-20.5

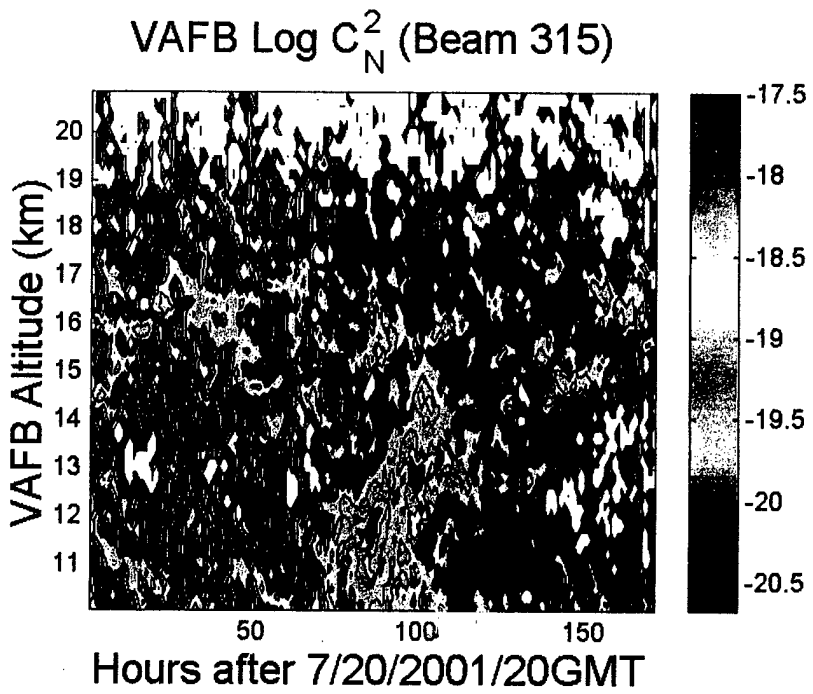
VAFB Log C_N^2 (Beam 315)
VAFB Altitude (km)
20
19
18
17
16
15
14
13
12
11
50
100
150
Hours after 7/20/2001/20GMT
-17.5
-18
-18.5
-19
-19.5
-20
-20.5

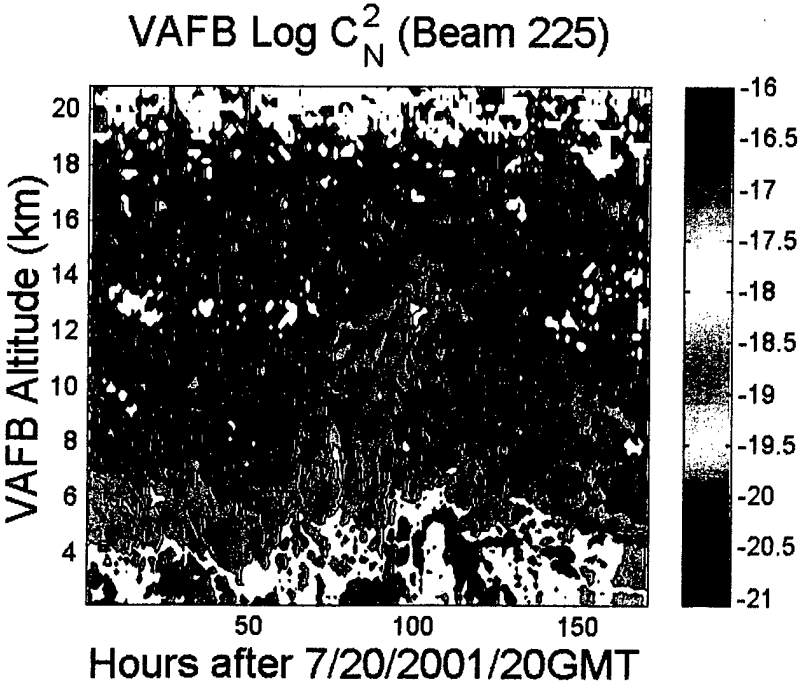
VAFB Log C_N^2 (Beam 225)
VAFB Altitude (km)
20
18
16
14
12
10
8
6
4
50
100
150
Hours after 7/20/2001/20GMT
-16
-16.5
-17
-17.5
-18
-18.5
-19
-19.5
-20
-20.5
-21

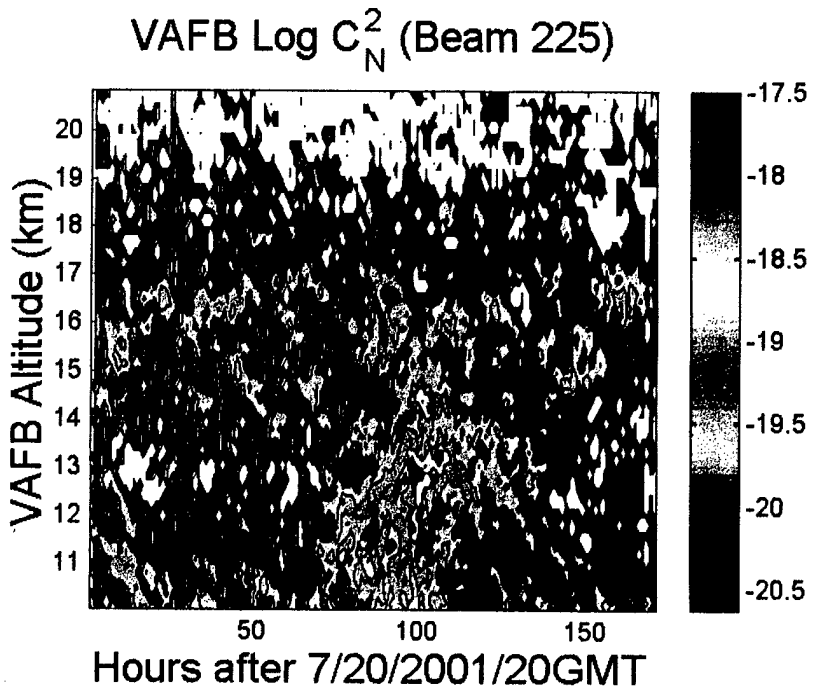
VAFB Log C_N^2 (Beam 225)
VAFB Altitude (km)
20
19
18
17
16
15
14
13
12
11
50
100
150
Hours after 7/20/2001/20GMT
-17.5
-18
-18.5
-19
-19.5
-20
-20.5

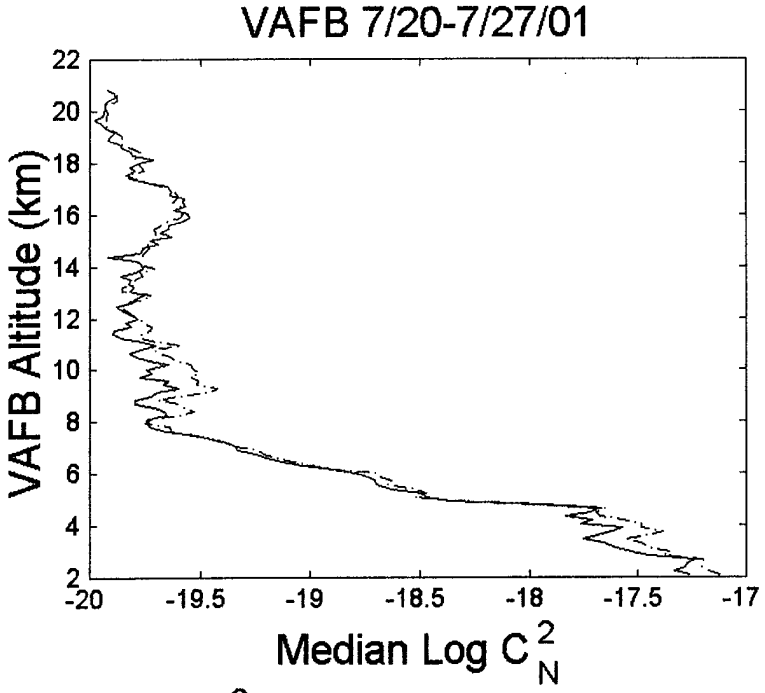
VAFB 7/20-7/27/01
VAFB Altitude (km)
22
20
18
16
14
12
10
8
6
4
2
-20
-19.5
-19
-18.5
-18
-17.5
-17
Median Log C_N^2

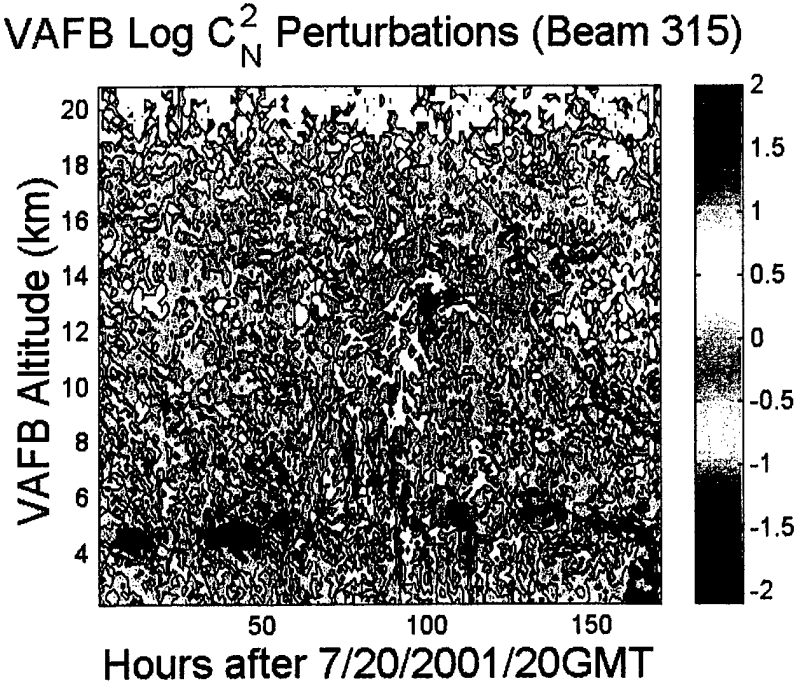
VAFB Log C_N^2 Perturbations (Beam 315)
VAFB Altitude (km)
20
18
16
14
12
10
8
6
4
2
1.5
1
0.5
0
-0.5
-1
-1.5
-2
50
100
150
Hours after 7/20/2001/20GMT

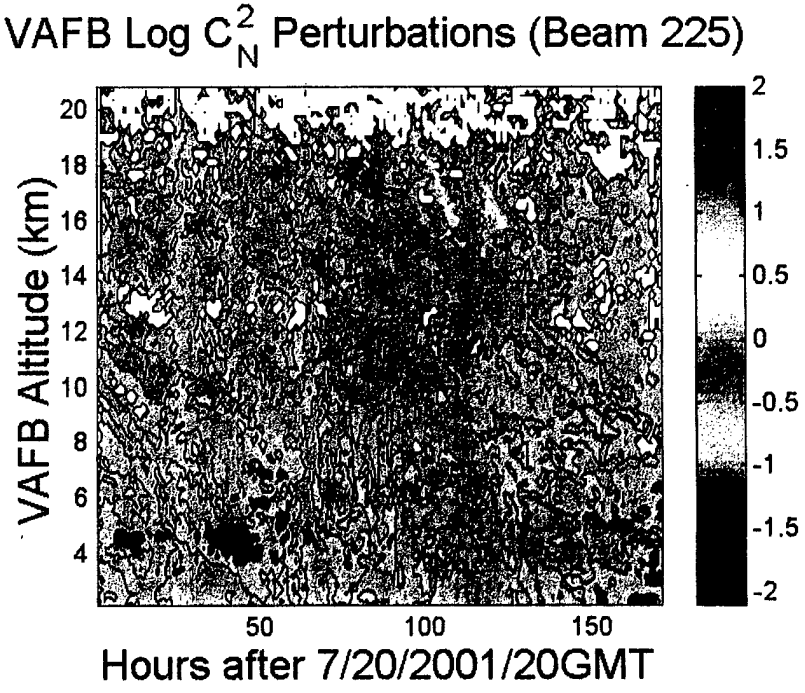
VAFB Log C_N^2 Perturbations (Beam 225)
VAFB Altitude (km)
20
18
16
14
12
10
8
6
4
2
1.5
1
0.5
0
-0.5
-1
-1.5
-2
50
100
150
Hours after 7/20/2001/20GMT

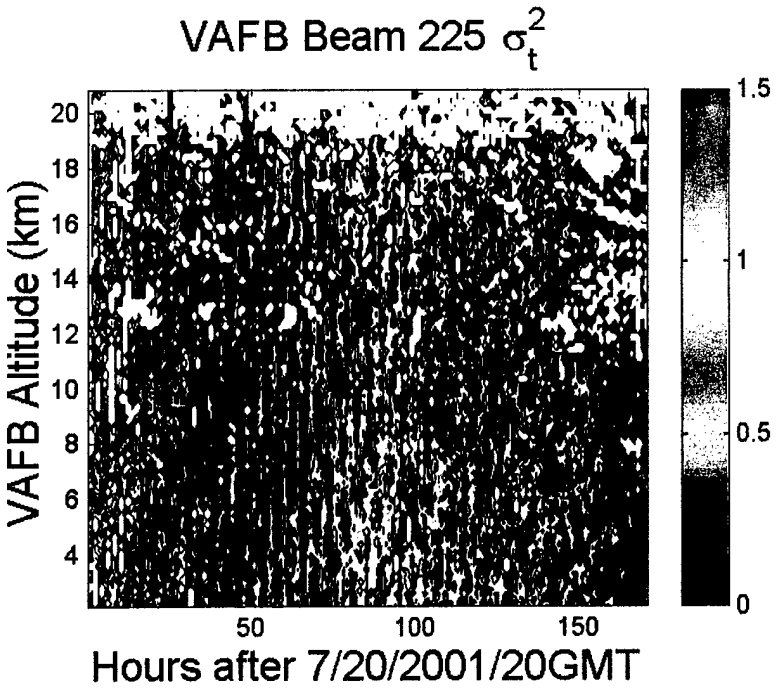
VAFB Beam 225 σ_t^2
VAFB Altitude (km)
20
18
16
14
12
10
8
6
4
50
100
150
Hours after 7/20/2001/20GMT
1.5
1
0.5
0

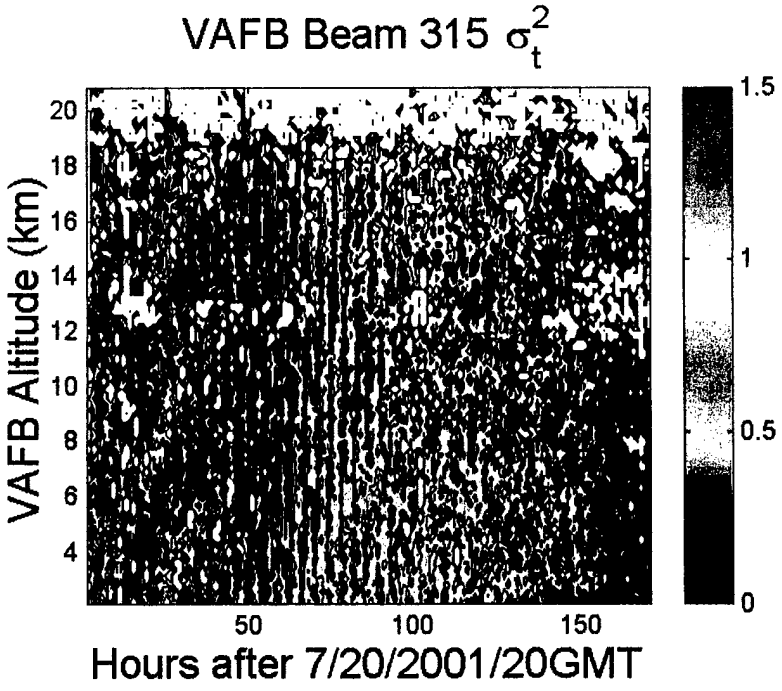
VAFB Beam 315 σ_t^2
VAFB Altitude (km)
20
18
16
14
12
10
8
6
4
50
100
150
Hours after 7/20/2001/20GMT
1.5
1
0.5
0

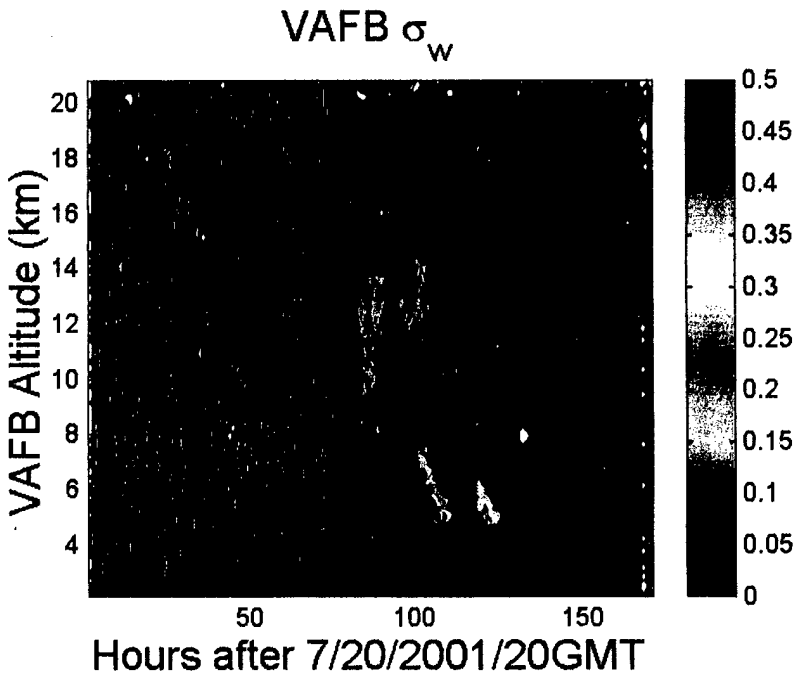
VAFB σ_w
VAFB Altitude (km)
20
18
16
14
12
10
8
6
4
50
100
150
Hours after 7/20/2001/20GMT
0.5
0.45
0.4
0.35
0.3
0.25
0.2
0.15
0.1
0.05
0


LOW
570
564
582
576
588
HIGH
FRIDAY
July 20
2001
500-MILLIBAR HEIGHT CONTOURS
AT 7:00 A.M., E.S.T.

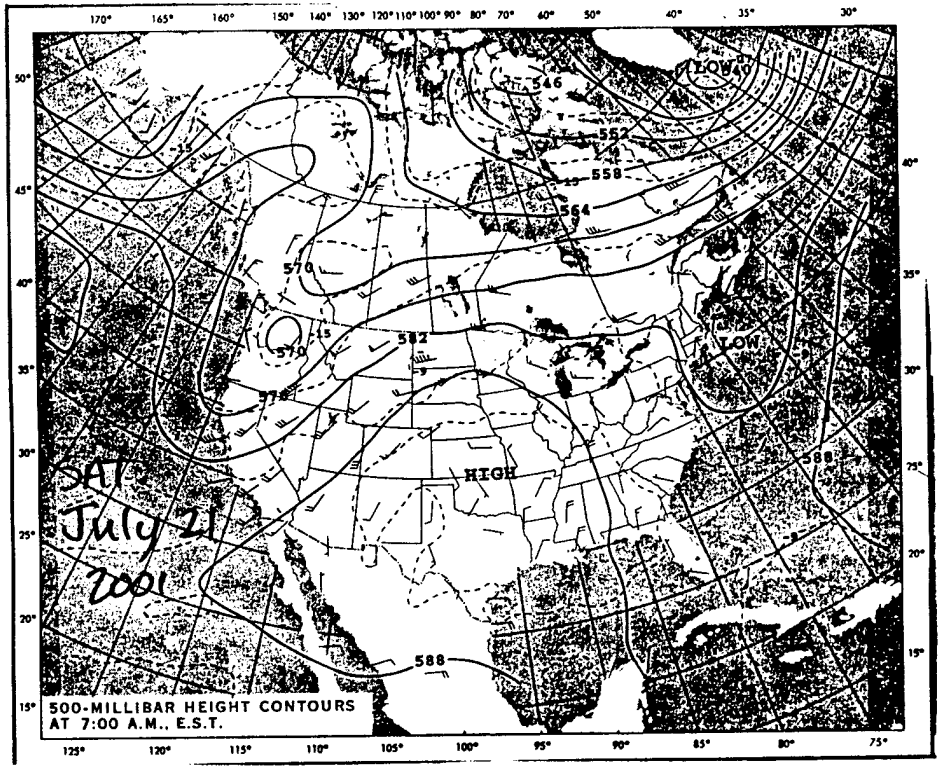
LOW
546
552
558
564
570
576
582
588
HIGH
SAT
July 21
2001
500-MILLIBAR HEIGHT CONTOURS
AT 7:00 A.M., E.S.T.

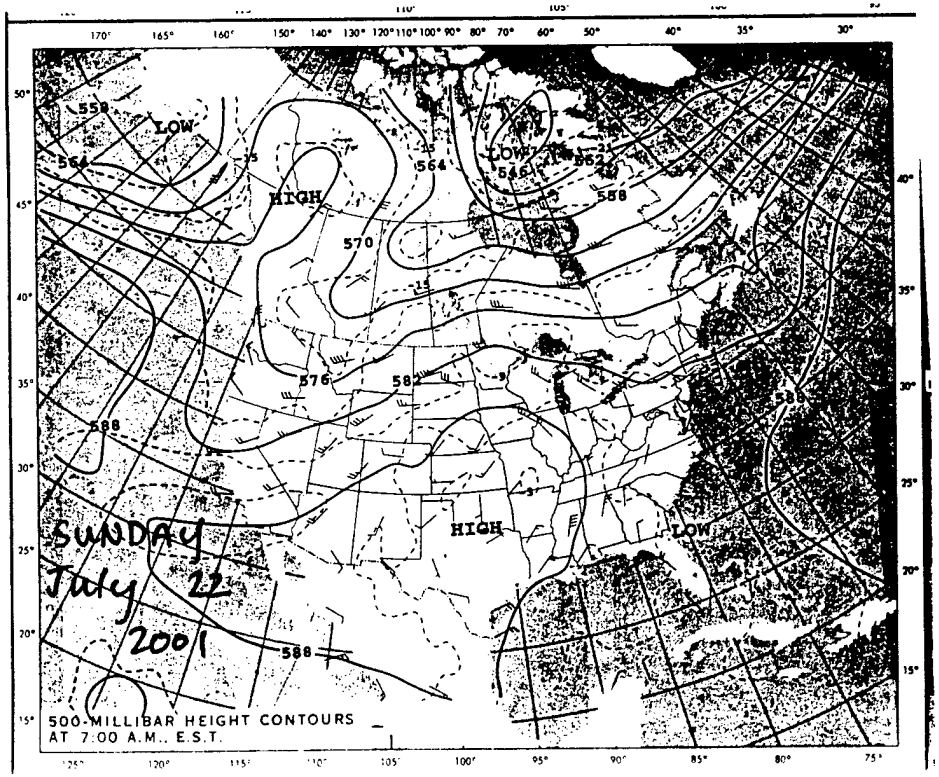
LOW
564
570
576
582
588
HIGH
SUNDAY
July 22
2001
500-MILLIBAR HEIGHT CONTOURS
AT 7:00 A.M., E.S.T.

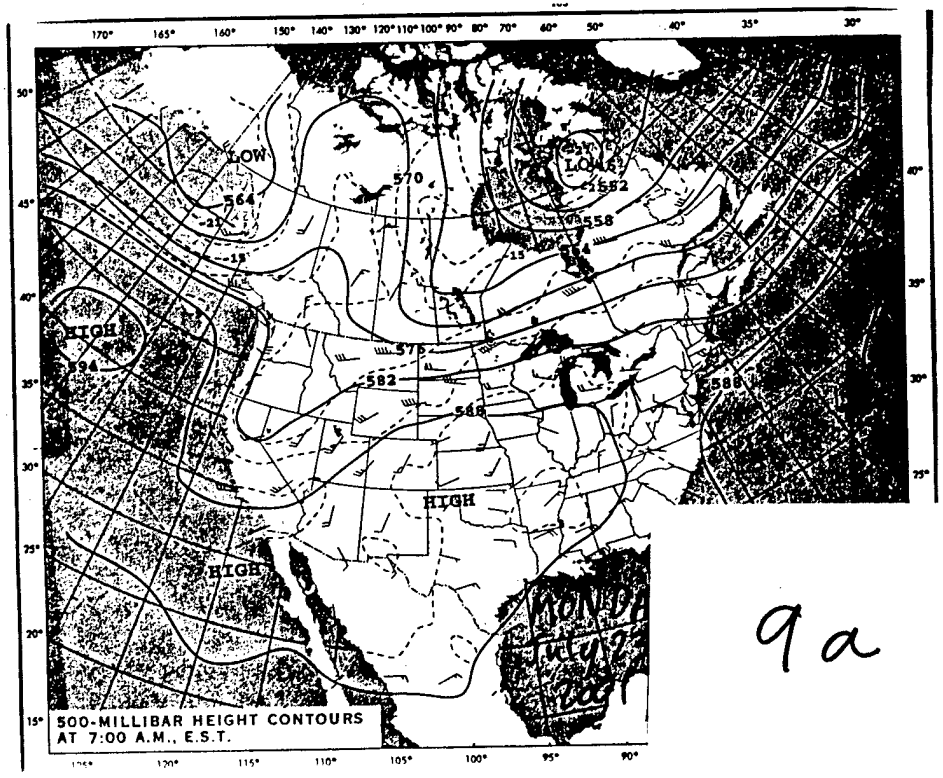
LOW
564
570
582
588
HIGH
MONDAY
July 23
2001
500-MILLIBAR HEIGHT CONTOURS
AT 7:00 A.M., E.S.T.

9a

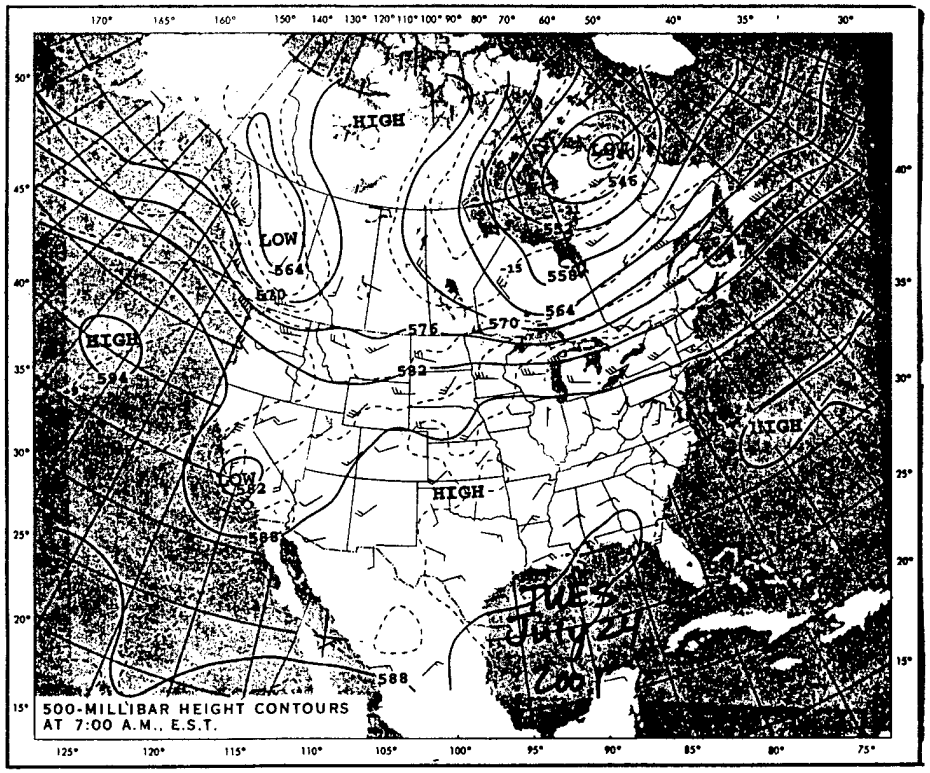
HIGH
LOW
564
546
558
570
576
582
588
HIGH
HIGH
LOW
582
588
TUES
July 24
2001
500-MILLIBAR HEIGHT CONTOURS
AT 7:00 A.M., E.S.T.

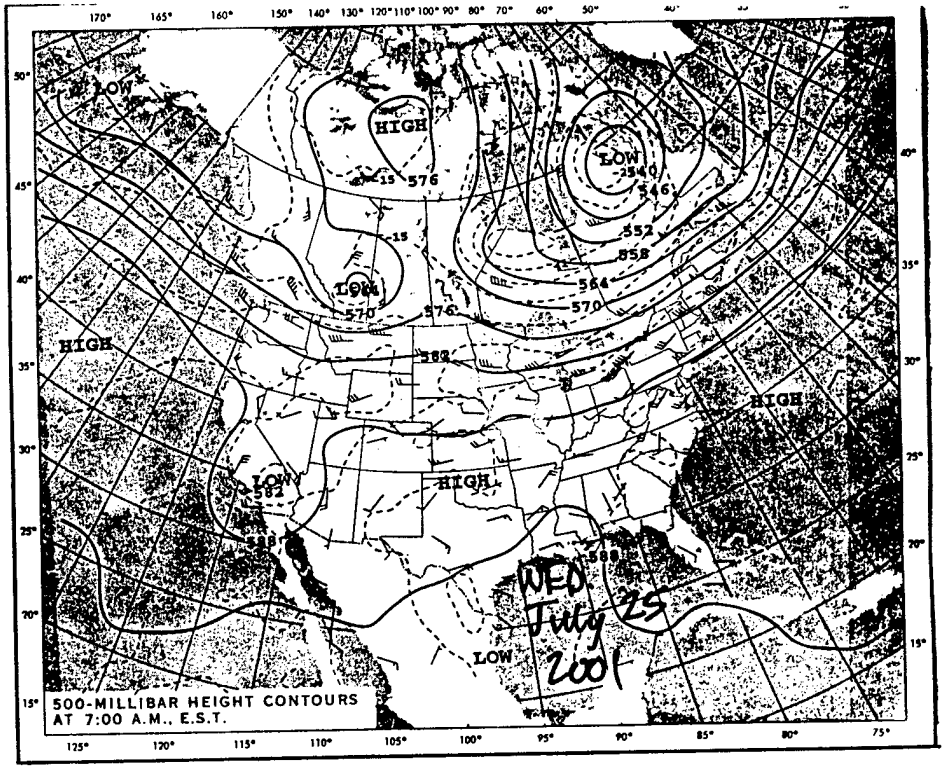
LOW
HIGH
LOW
-2540
546
552
558
564
570
576
582
588
HIGH
HIGH
LOW
582
588
LOW
WED
July 25
2001
500-MILLIBAR HEIGHT CONTOURS
AT 7:00 A.M., E.S.T.

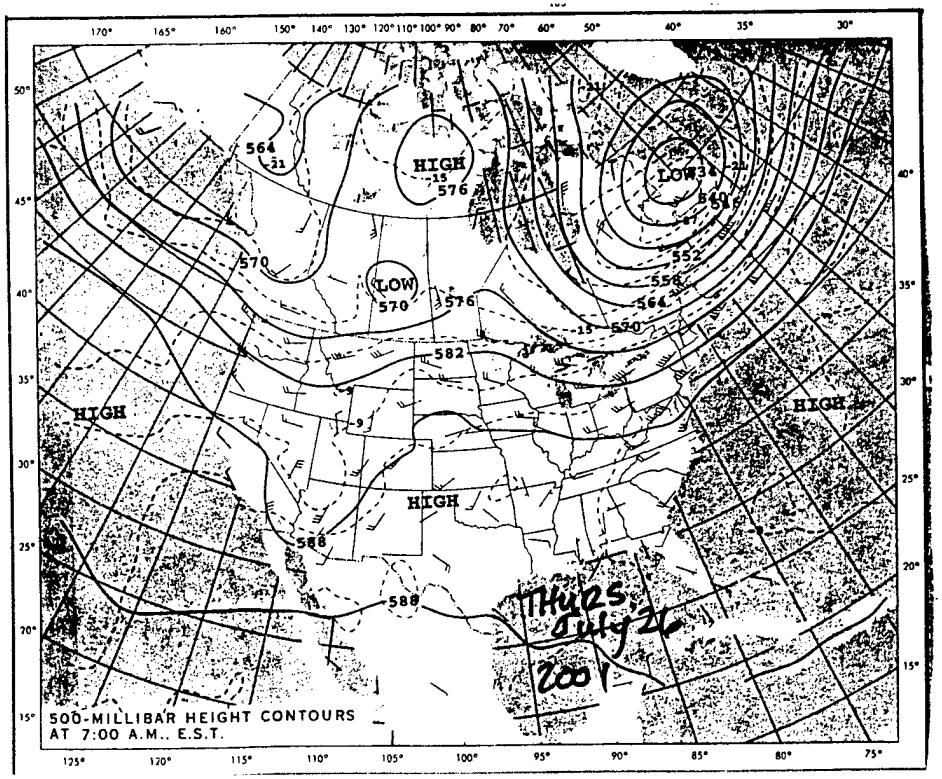
564
HIGH
576
LOW
570
552
558
564
570
576
582
HIGH
HIGH
588
588
THURS
July 26
2001
500-MILLIBAR HEIGHT CONTOURS
AT 7:00 A.M., E.S.T.

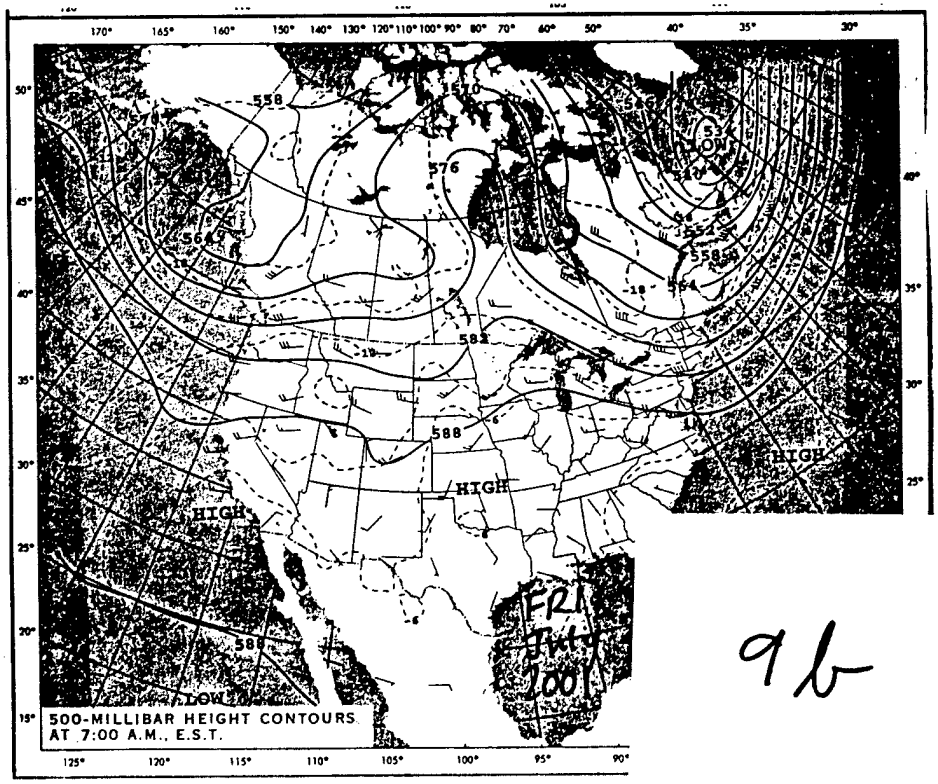
558
570
576
582
588
HIGH
HIGH
HIGH
FRI
July 27
2001
500-MILLIBAR HEIGHT CONTOURS
AT 7:00 A.M., E.S.T.

9b

72393 VBG Vandenberg Afb

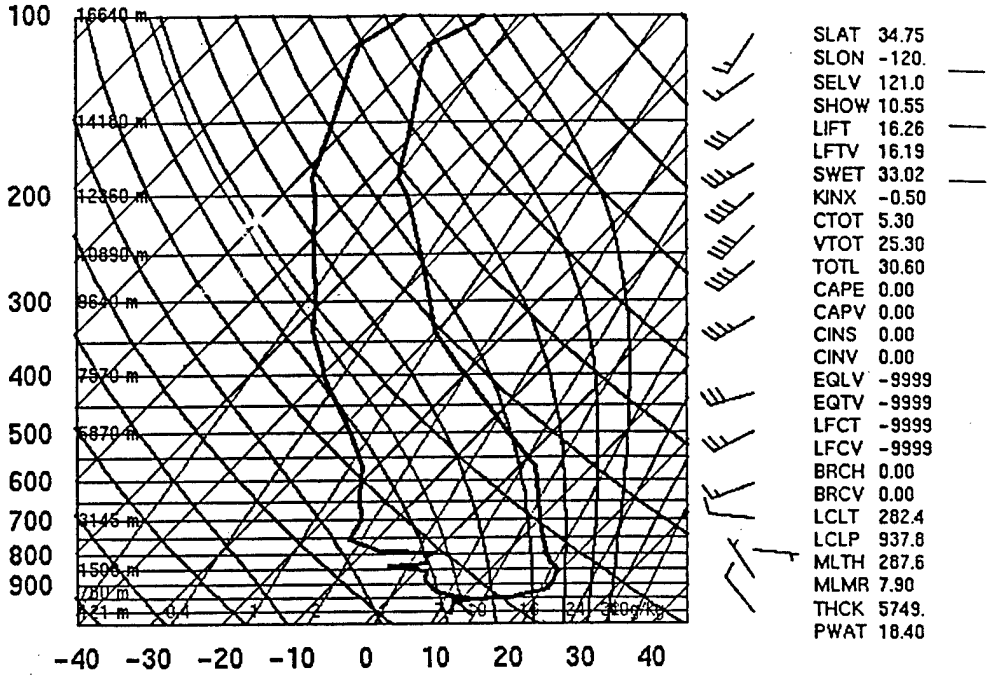

00Z 23 Jul 2001

72393 VBG Vandenberg Afb

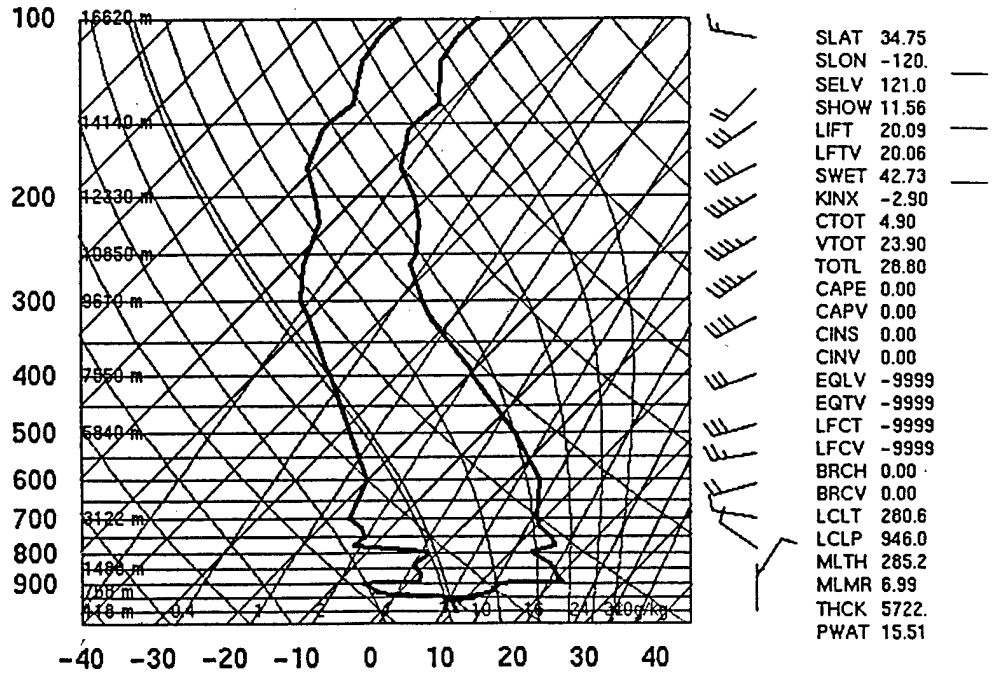

12Z 23 Jul 2001

72393 VBG Vandenberg Afb

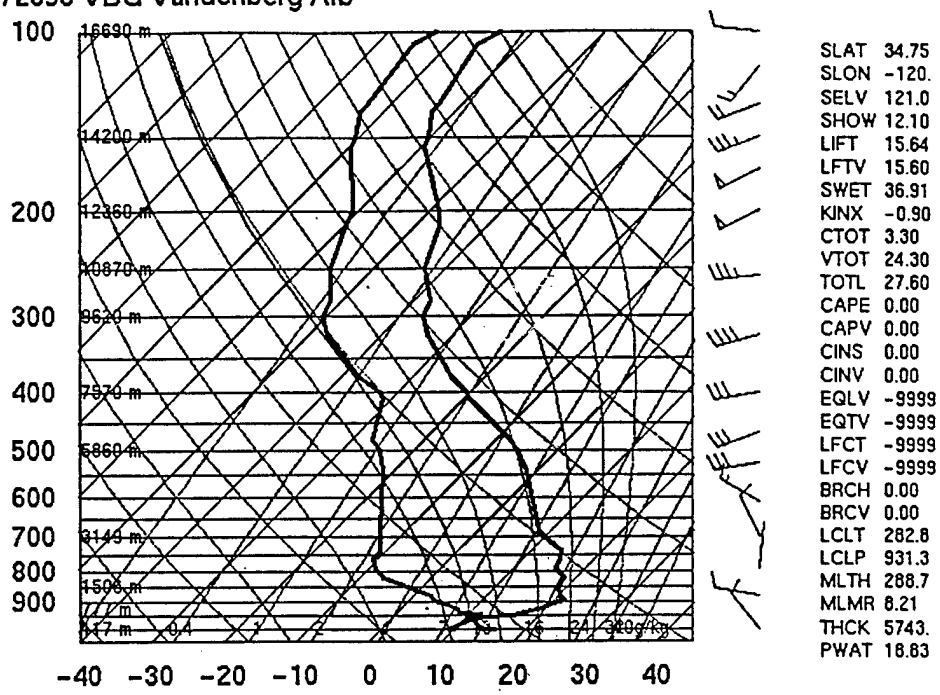

00Z 24 Jul 2001

72393 VBG Vandenberg Afb

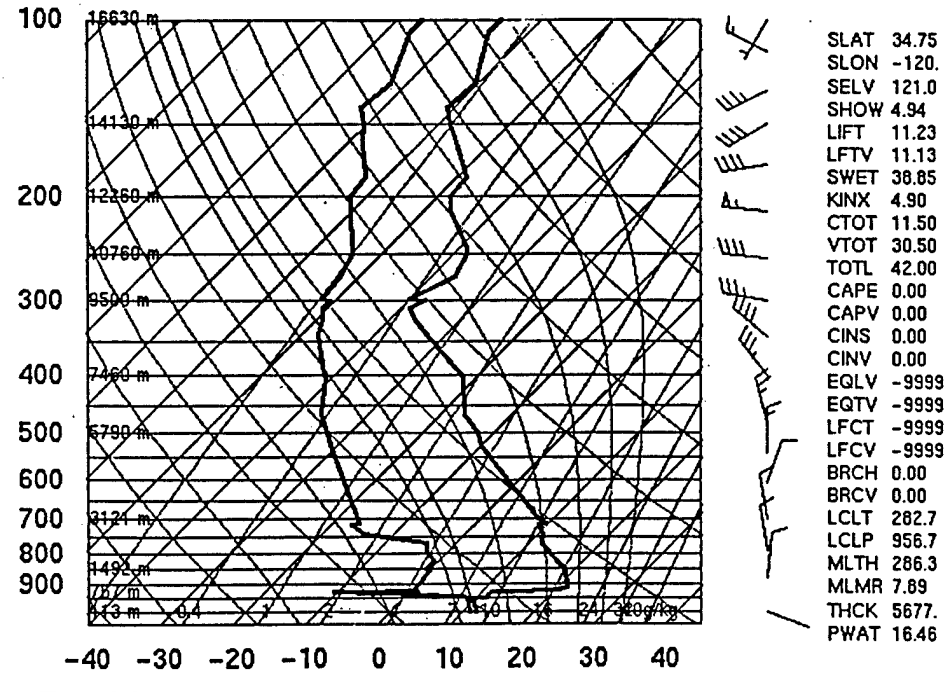

12Z 24 Jul 2001

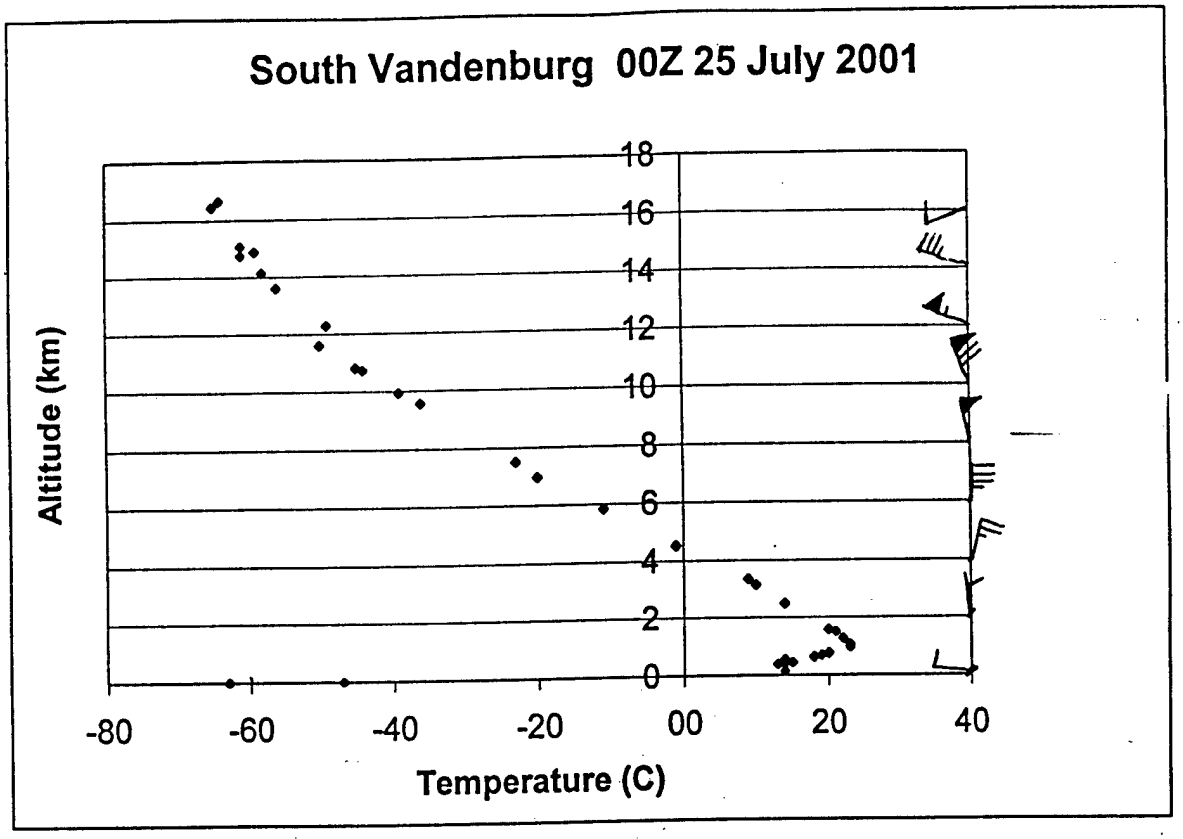
South Vandenburg 00Z 25 July 2001
Altitude (km)
18
16
14
12
10
8
6
4
2
0
-80
-60
-40
-20
00
20
40
Temperature (C)

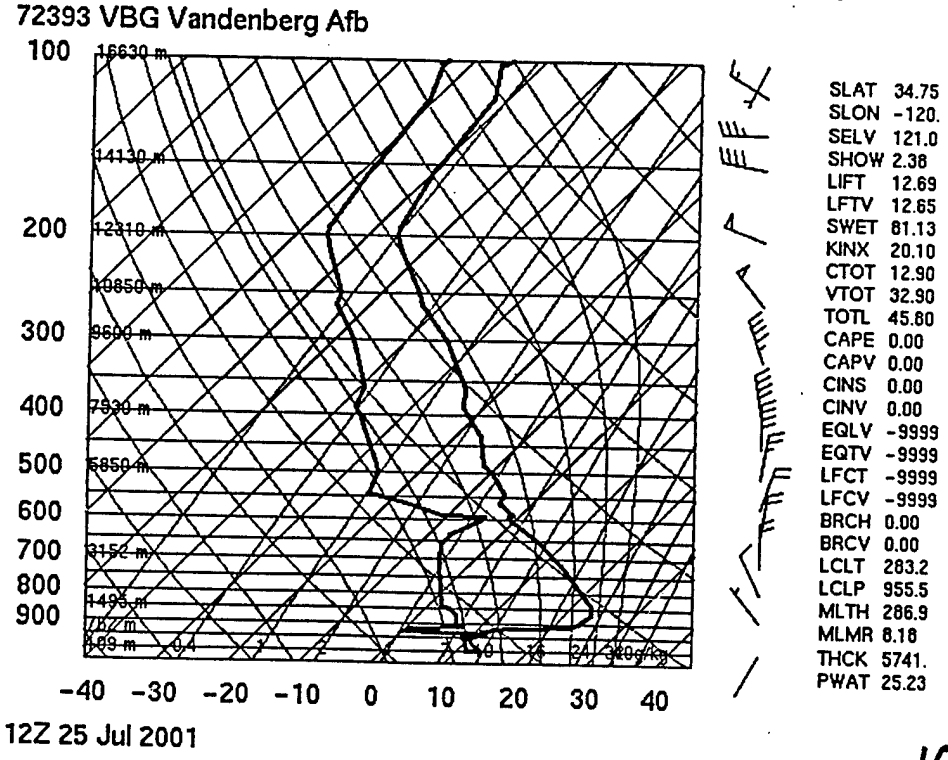
72393 VBG Vandenberg Afb
100
200
300
400
500
600
700
800
900
16630 m
14130 m
12310 m
10850 m
9600 m
7530 m
5850 m
3152 m
1495 m
-40 -30 -20 -10 0 10 20 30 40
12Z 25 Jul 2001
SLAT 34.75
SLON -120.
SELV 121.0
SHOW 2.38
LIFT 12.69
LFTV 12.65
SWET 81.13
KINX 20.10
CTOT 12.90
VTOT 32.90
TOTL 45.80
CAPE 0.00
CAPV 0.00
CINS 0.00
CINV 0.00
EQLV -9999
EQTV -9999
LFCT -9999
LFCV -9999
BRCH 0.00
BRCV 0.00
LCLT 283.2
LCLP 955.5
MLTH 286.9
MLMR 8.18
THCK 5741.
PWAT 25.23

72393 VBG Vandenberg Afb

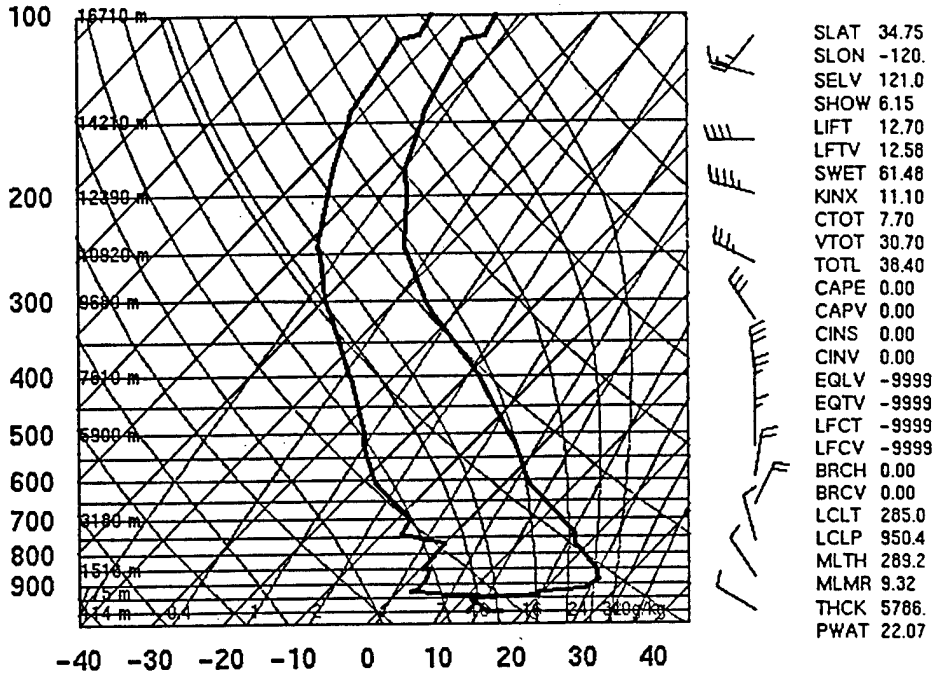

00Z 26 Jul 2001

72393 VBG Vandenberg Afb

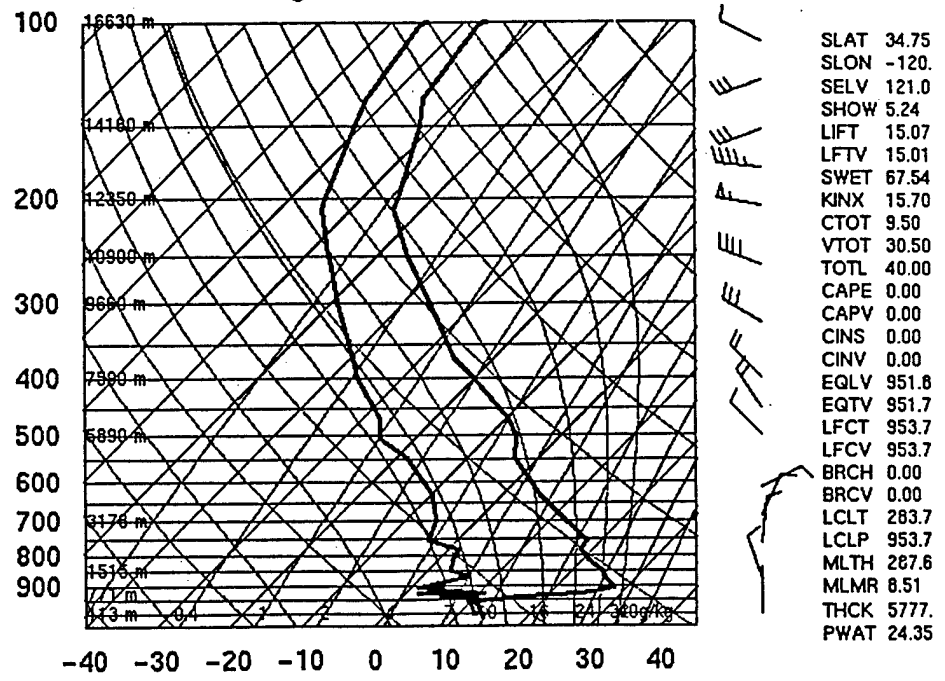

12Z 26 Jul 2001

72393 VBG Vandenberg Afb

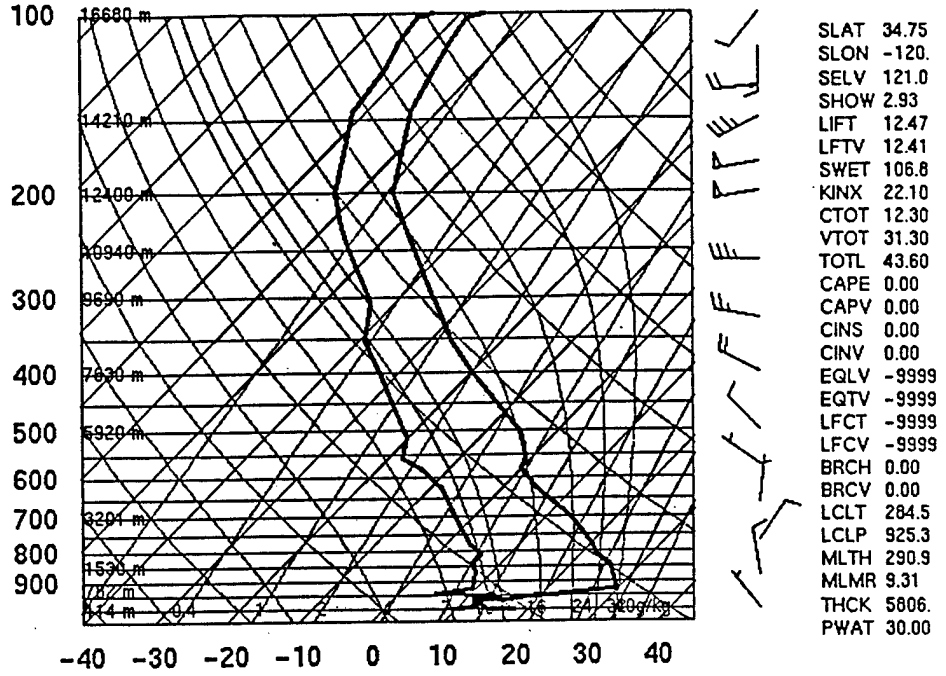

00Z 27 Jul 2001

72393 VBG Vandenberg Afb

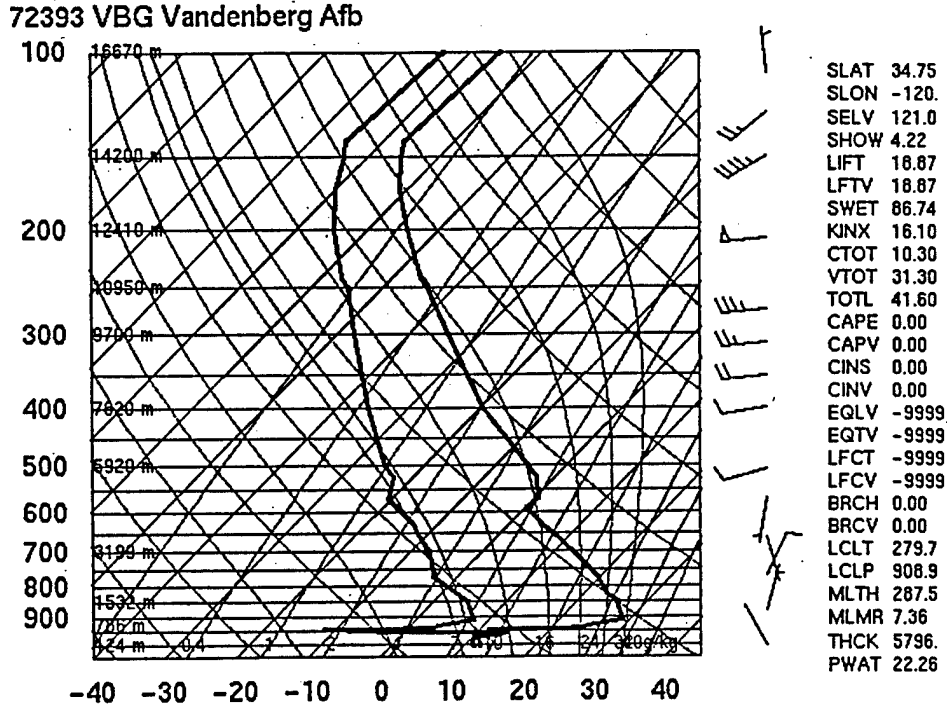

12Z 27 Jul 2001

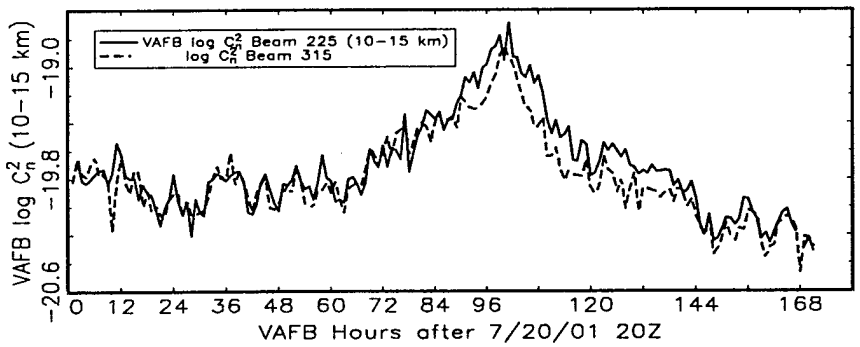
VAFB log C_n^2 Beam 225 (10–15 km)
log C_n^2 Beam 315
VAFB log C_n^2 (10–15 km)
−19.0
−19.8
−20.6
0 12 24 36 48 60 72 84 96 120 144 168
VAFB Hours after 7/20/01 20Z

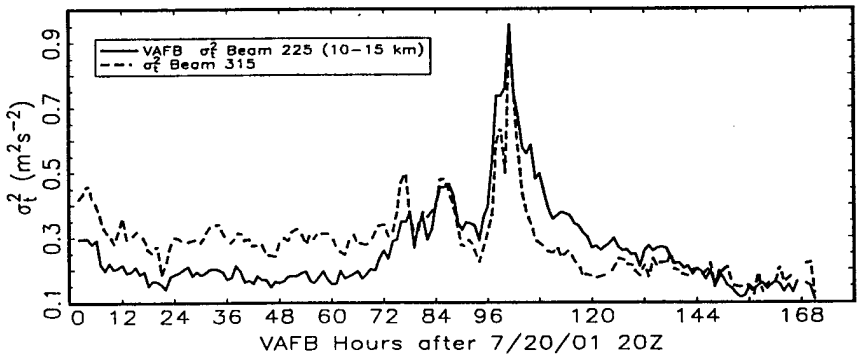
VAFB σ_t^2 Beam 225 (10–15 km)
σ_t^2 Beam 315
σ_t^2 (m^2s^{-2})
0.9
0.7
0.5
0.3
0.1
0 12 24 36 48 60 72 84 96 120 144 168
VAFB Hours after 7/20/01 20Z

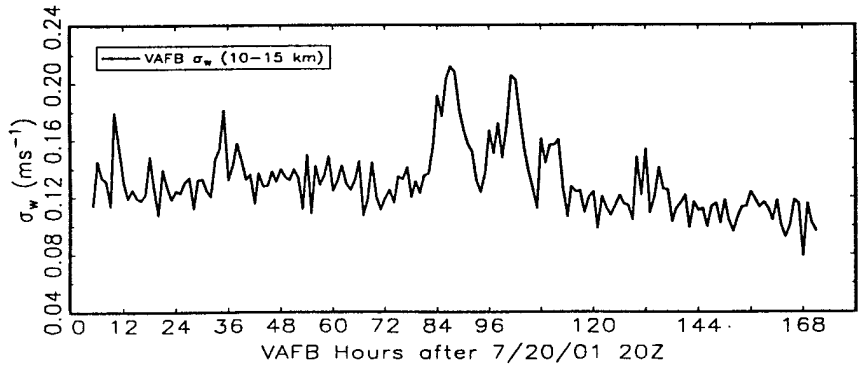
VAFB σ_w (10–15 km)
σ_w (ms^{-1})
0.24
0.20
0.16
0.12
0.08
0.04
0 12 24 36 48 60 72 84 96 120 144 168
VAFB Hours after 7/20/01 20Z

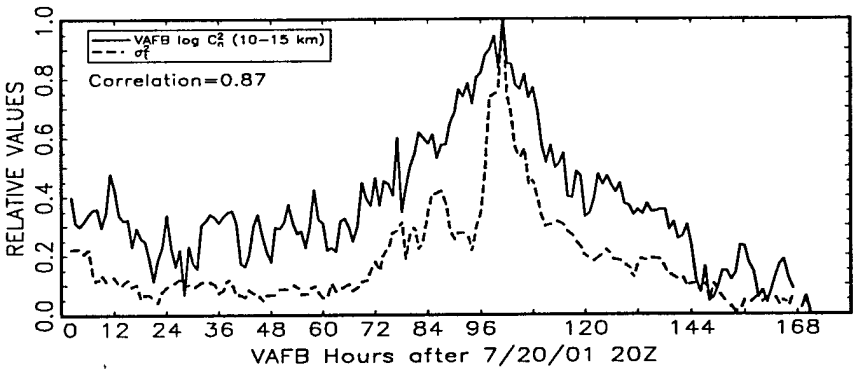
VAFB log C_n^2 (10–15 km)
σ_t^2
Correlation=0.87
RELATIVE VALUES
1.0
0.8
0.6
0.4
0.2
0.0
0 12 24 36 48 60 72 84 96 120 144 168
VAFB Hours after 7/20/01 20Z

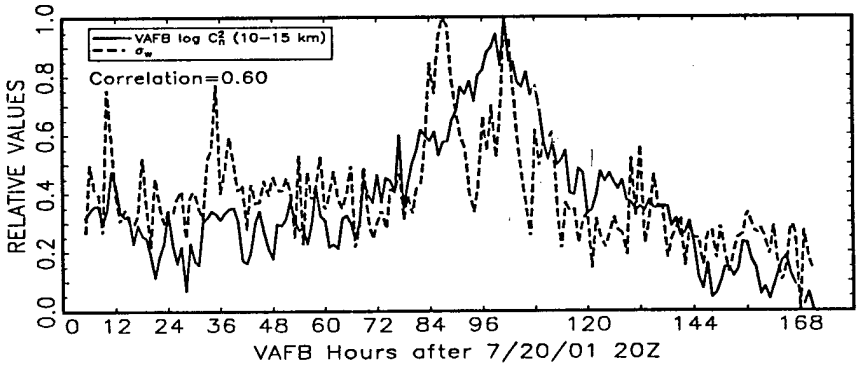
VAFB log C_n^2 (10–15 km)
σ_w
Correlation=0.60
RELATIVE VALUES
1.0
0.8
0.6
0.4
0.2
0.0
0 12 24 36 48 60 72 84 96 120 144 168
VAFB Hours after 7/20/01 20Z

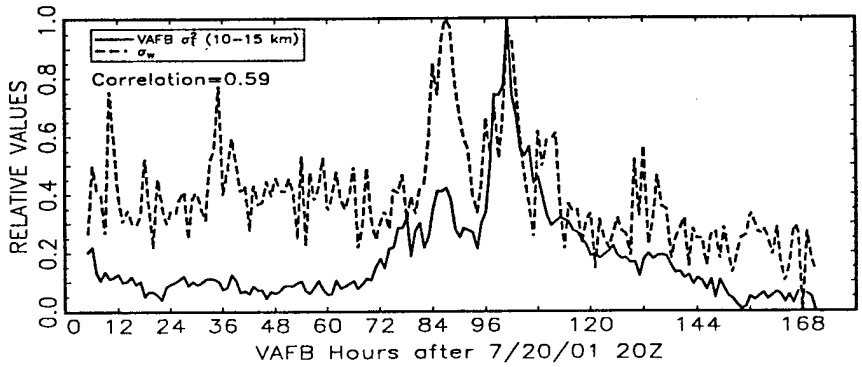
VAFB σ_t^2 (10–15 km)
σ_w
Correlation=0.59
RELATIVE VALUES
1.0
0.8
0.6
0.4
0.2
0.0
0 12 24 36 48 60 72 84 96 120 144 168
VAFB Hours after 7/20/01 20Z

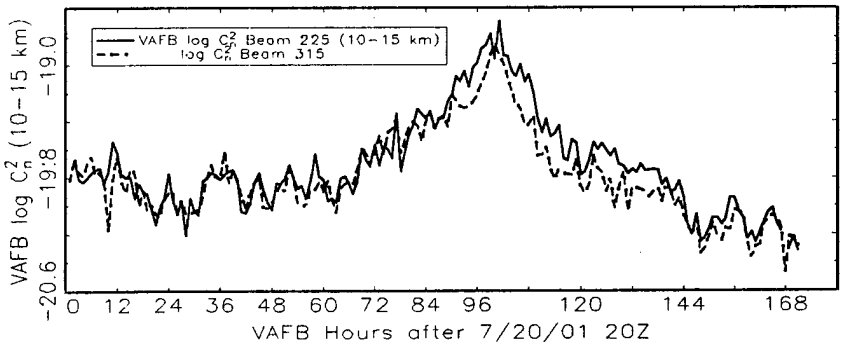
VAFB log C_n^2 Beam 225 (10–15 km)
log C_n^2 Beam 315
VAFB log C_n^2 (10–15 km)
-20.6 -19.8 -19.0
0 12 24 36 48 60 72 84 96 120 144 168
VAFB Hours after 7/20/01 20Z

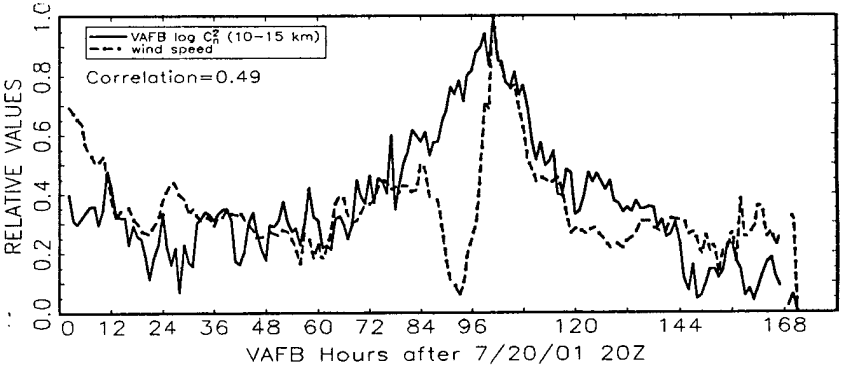
VAFB log C_n^2 (10–15 km)
wind speed
Correlation=0.49
RELATIVE VALUES
0.0 0.2 0.4 0.6 0.8 1.0
0 12 24 36 48 60 72 84 96 120 144 168
VAFB Hours after 7/20/01 20Z

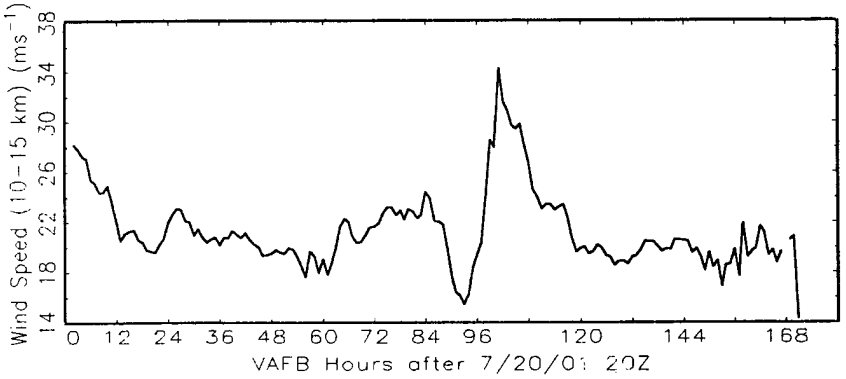
Wind Speed (10–15 km) (ms^{-1})
14 18 22 26 30 34 38
0 12 24 36 48 60 72 84 96 120 144 168
VAFB Hours after 7/20/01 20Z

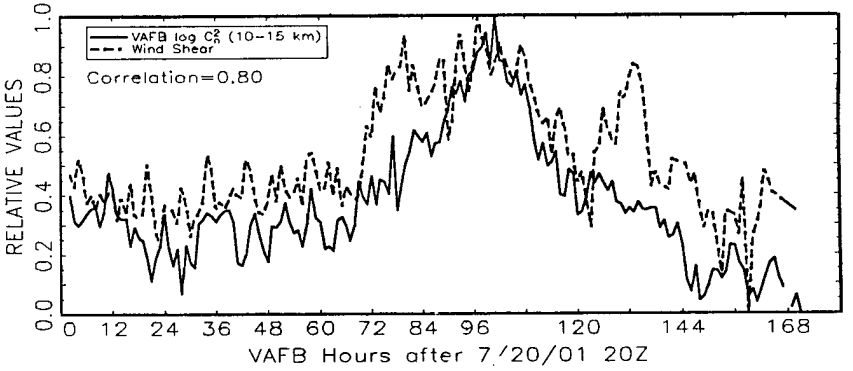
VAFB log C_n^2 (10–15 km)
Wind Shear
Correlation=0.80
RELATIVE VALUES
0.0 0.2 0.4 0.6 0.8 1.0
0 12 24 36 48 60 72 84 96 120 144 168
VAFB Hours after 7/20/01 20Z

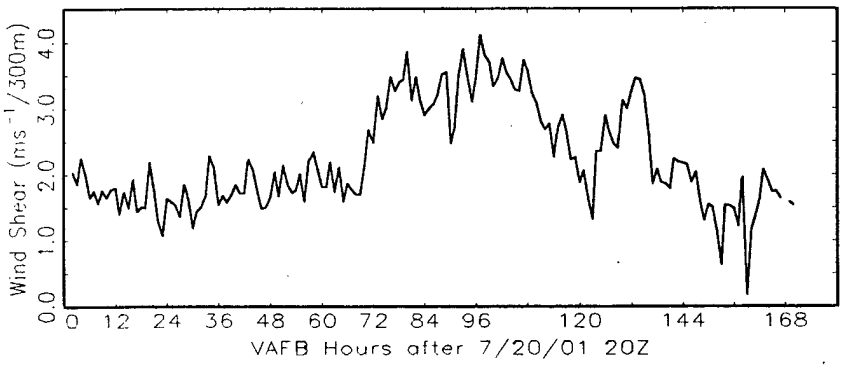
Wind Shear (ms^{-1}/300m)
0.0 1.0 2.0 3.0 4.0
0 12 24 36 48 60 72 84 96 120 144 168
VAFB Hours after 7/20/01 20Z

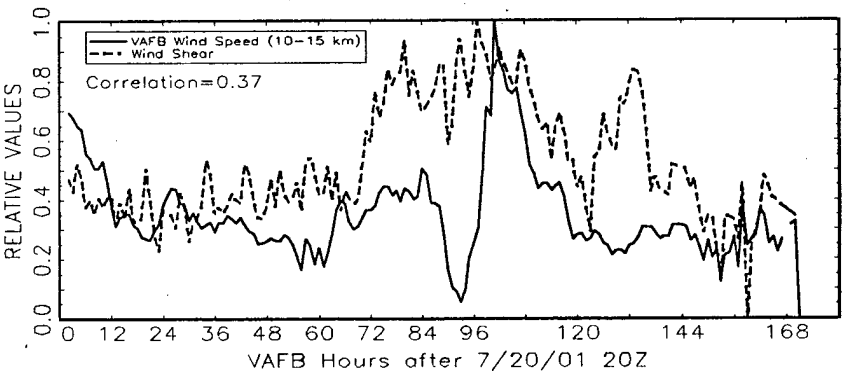
VAFB Wind Speed (10–15 km)
Wind Shear
Correlation=0.37
RELATIVE VALUES
0.0 0.2 0.4 0.6 0.8 1.0
0 12 24 36 48 60 72 84 96 120 144 168
VAFB Hours after 7/20/01 20Z

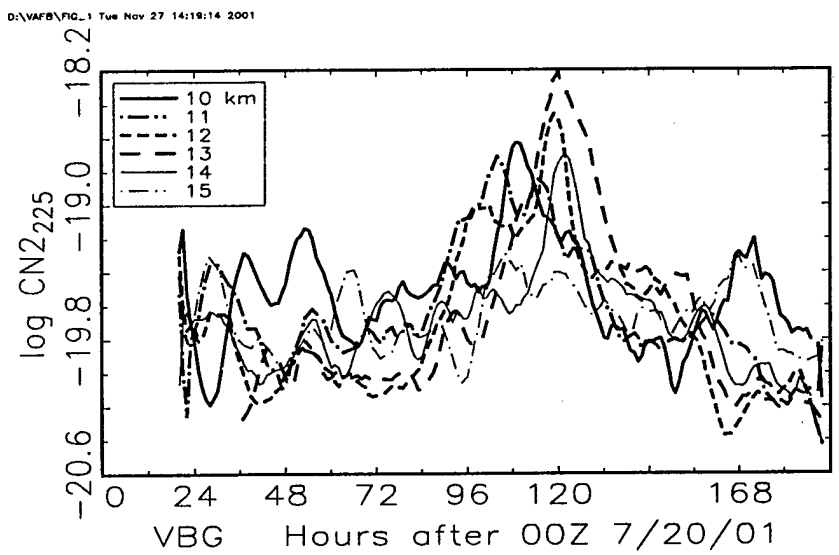
D:\VAFB\FIG_1 Tue Nov 27 14:19:14 2001
log CN2225
-18.2
-19.0
-19.8
-20.6
10 km
11
12
13
14
15
0
24
48
72
96
120
168
VBG Hours after 00Z 7/20/01

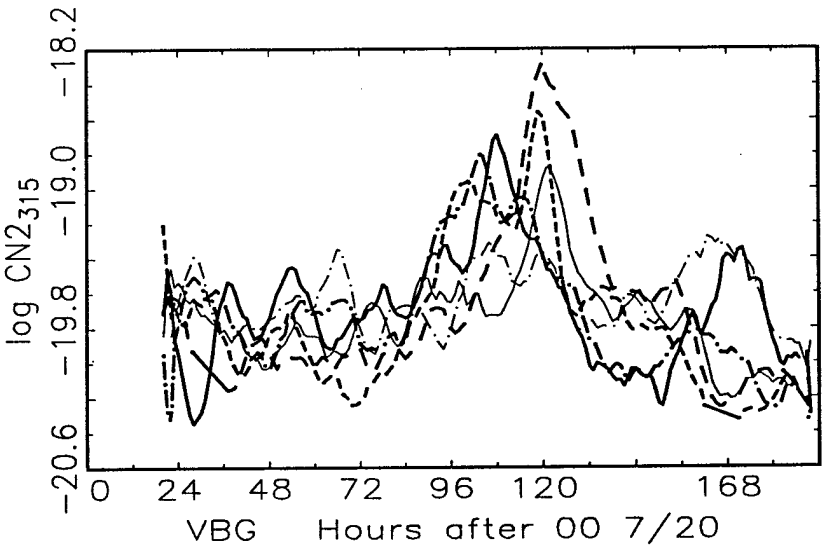
log CN2315
-18.2
-19.0
-19.8
-20.6
0
24
48
72
96
120
168
VBG Hours after 00 7/20

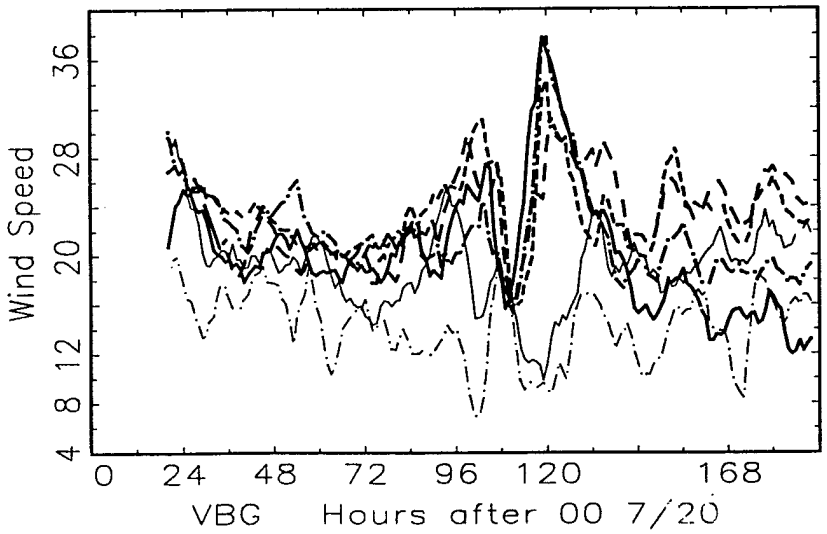
Wind Speed
4
8
12
20
28
36
0
24
48
72
96
120
168
VBG Hours after 00 7/20

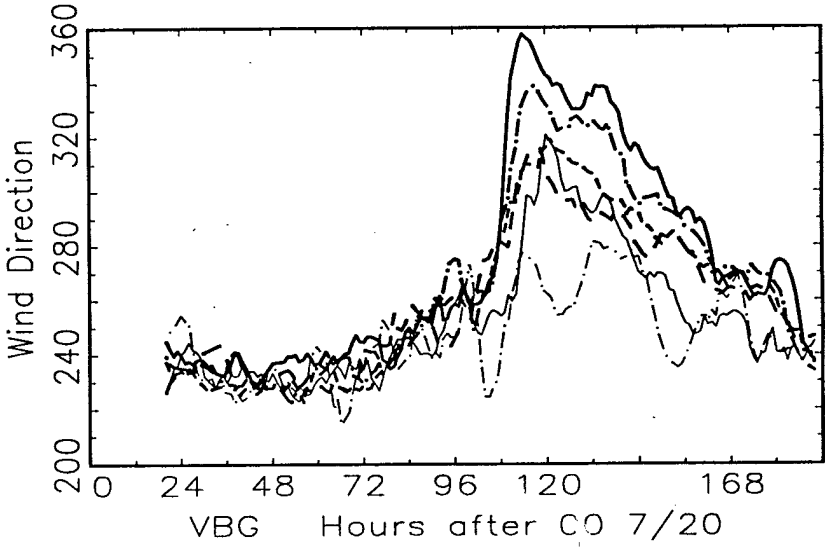
Wind Direction
200
240
280
320
360
0
24
48
72
96
120
168
VBG Hours after CO 7/20

Appendix C. Case studies of waves and turbulence at the MU MST radar.

Observations taken with the Middle and Upper (MU) Atmosphere MST radar located near Shigaraki, Japan, were available for about 100 hours per month during April 1986 through December 1996, as well as for an extended period (422 hours long) during April 1995. The MU radar has five beams, one vertical and one 10 degrees from the vertical toward each of the four cardinal directions. Following quality control checking, the individual 6-minute profiles were used to make hourly medians of the backscattered power on the meridional beams, horizontal wind components, and specific turbulent kinetic energy on the meridional beams, plus the hourly standard deviation of the vertical velocity. Relative backscattered power is used since the MU radar is not calibrated to report C_n^2 and transmitted power records were not available to permit a post-observation calibration, such as comparisons with cosmic noise. The radar data were augmented with rawinsonde ascents from Wajima and Shionomisaki, located north and south of MU, respectively.

Four cases were chosen for presentation here, to illustrate the relationships seen among the radar variables.

April 1995. This segment of observations lasted 422 hours and is the longest one available. Time-height plots of the power and horizontal wind speed are given in Fig. C1. Tropopause heights at Shionomisaki (Wajima) are shown by black dots (diamonds). The abscissa is hours after the first hour of the segment. Note that during relatively quiet periods, such as around hour 210 and hour 325, when the tropopause height shows little change with latitude, there is a sharp increase of power just above the tropopause whereas during other periods the vertical gradient of power is more diffuse. The periods of large tropopause height gradient usually correspond with the passages of jet streaks, i.e., pulses of very strong winds. A relationship between wind speed and power (or C_n^2) was reported by others (e.g., Hufnagel,1974; Gage et al., 1980). The individual hourly profiles of power are given in Fig. C2, along with the median of all hourly values at each level (crosses) and the median of all hourly horizontal wind speeds (dots, shifted by 80 m/s relative to the values on the abscissa). Note that the strongest winds are at about 12 km, this level corresponds roughly to the average tropopause height (compare Fig. C1). Fig. C4 shows a time series of the median of the hourly values of power over all levels from 12 to 18 km (roughly, the lowest 6 km of the stratosphere) in the upper left panel. Corresponding time series of the wind speed and wind shear (defined as $[(du/dz)^2+(dv/dz)^2]^{1/2}$ where dz=300m) are given in the left-center and lower panels, respectively. Pairs of these time series are compared in the right-hand panels, where each is plotted with a range of unity. The correlation coefficient for each pair is given in each panel; they range from 0.20 for the power-shear pair to 0.00 for the speed-shear pair with an intermediate value of 0.17 for power-speed. Fig. C4 is similar to Fig. C3 except the variables are power, specific kinetic energy (σ_t^2, determined using the spectral width corrected for beam, shear, and wave-broadening effects) and the standard deviation of vertical velocity (σ_w) which is taken as an indicator of gravity wave intensity. The largest correlation in Fig. C4 is that for the power-σ_w pair (0.41), the smallest is for σ_t^2-σ_w (0.18), and that for power- σ_t^2 (0.31) is intermediate. The correlation between power and σ_t^2 indicates that strong refractivity turbulence is accompanied by strong mechanical turbulence, as expected. For this case study the closest correlation is that between power and σ_w, implying that the intensity of high-frequency gravity waves is critical for the production of refractivity turbulence. The mean wind speed is seen in this case to be a relatively poor predictor of power, contrary to Hufnagel's model; this poor positive correlation between power and wind speed will be shown more dramatically in two of the following three case studies.

January 1996. Figs. C5-C8 are similar to Figs. C1-C4, except they are for a period of 103 hours beginning on 8 January 1996. Also, Fig. C5 shows time-height plots of the meridional wind speed (an indicator of the passage of troughs and ridges), the vertical shear per 300m, σ_w, and σ_t^2. Fig. C5 shows that the strong winds early in the period were accompanied by strong σ_w , and the weak winds late in the period were accompanied by weak σ_w. In Fig. C7 the correlation between

power and wind speed is seen to be 0.47; while this value is large it is not as great as that for power-shear (0.63), power- σ_t^2 (0.59), or power- σ_w (0.73).

February 1987. Figs. C9-C12 are similar to Figs. C5-C8, except they are for a 79-hour period beginning on 3 February 1987. The strongest winds are late in the period, while strongest σ_w are early in the period. Figs. C11 and C12 show that the power correlates positively with σ_w (0.47) in this case, whereas power correlates negatively with wind speed (-0.26). The correlation of power with vertical wind shear is positive but relatively weak (0.17).

May 1996. Figs. C13-C16 are similar to Figs. C5-C8, except they are for a 103-hour period beginning on 20 May 1996. In Fig. C13, wind speed near 12 km shows two maxima (similar to Fig. C9), but in this case the meridional wind is first strongly positive, then negative, then again positive, implying the passage of a trough-ridge pattern (in contrast to Fig. C9 where the meridional wind speed did not show an oscillating pattern). Figs. C15 and and C16 show that power is most closely correlated with σ_w (0.46) and power is negatively correlated with both wind speed (-0.42) and vertical wind shear (-0.26).

In summary, these cases illustrate that while there is a relationship between wind speed and power (C_n^2) on a large-scale basis, the correlation of power with σ_w (an indicator of gravity wave intensity) is much more robust. The vertical wind shears associated with these gravity waves are superposed on the vertical shears of the prevailing winds and lead to local dynamic instabilities that break down into turbulence. This scenario follows that encapsulated in the model of Warnock and VanZandt (1985) and is similar in concept to that given in Dewan et al. (1993), and follows from the well-known relationship between C_n^2 and L_o plus that between L_o and micro-scale wind shear. In view of this scenario, it is clear that any efforts to predict C_n^2 levels must take into account the strengths of gravity wave source mechanisms, i.e., it is not sufficient to predict the large-scale flow in the region where a forecast of C_n^2 is desired. Warnock et al. (1988) found that the C_n^2 model developed using observations from Colorado (a region rich in terrain-launched gravity waves) had to be modified significantly to match observations taken over the flat terrain of Illinois. Since gravity waves upwelling from the planetary boundary layer, launched by flow over rough terrain or by convection, are often the most important source of vertically propagating gravity waves, prediction schemes must include forecasts of boundary layer winds and stability.

References:

Dewan, E.M., R. E. Good, R. Beland, and J. Brown, 1993: A model for (optical turbulence) profiles using radiosonde data. PL-TR-93-2043 (ERP No. 1121), 42 pp.

Gage, K.S., J.L. Green, and T. E. VanZandt, 1980: Use of Doppler radar for the measurement of atmospheric turbulence parameters from the intensity of clear-air echoes. Radio Sci.,15, 407-416.

Hufnagel, R.E., 1974: Variations of atmospheric turbulence, Digest of technical papers, Topical meeting on Optical Propagation Through Turbulence, pages Wa1-1 to Wa1-4.

Warnock, J.M., R.R. Beland, J.H. Brown, W.L. Clark, F.D. Eaton, L.D. Favier, K.S. Gage, J.L. Green, W.H. Hatch, J.R. Hines, E.A. Murphy, G.D. Nastrom, W. A. Peterson, T.E. VanZandt, 1988: Comparison among clear-air radar, thermosonde and optical measurements and model estimates of Cn2 made in very flat terrrain over Illinois. Presented at the Fourth Workshop on MST Radars, Kyoto, Nov 29-Dec 2. Handbook for MAP, Vol. 28, 432-438.

Warnock, J.M., and T.E. VanZandt, 1985: A statistical model to estimate the refractivity turbulence structure constant C_n^2 in the free atmosphere. NOAA-TM-ERL-AL-10, 175pp.

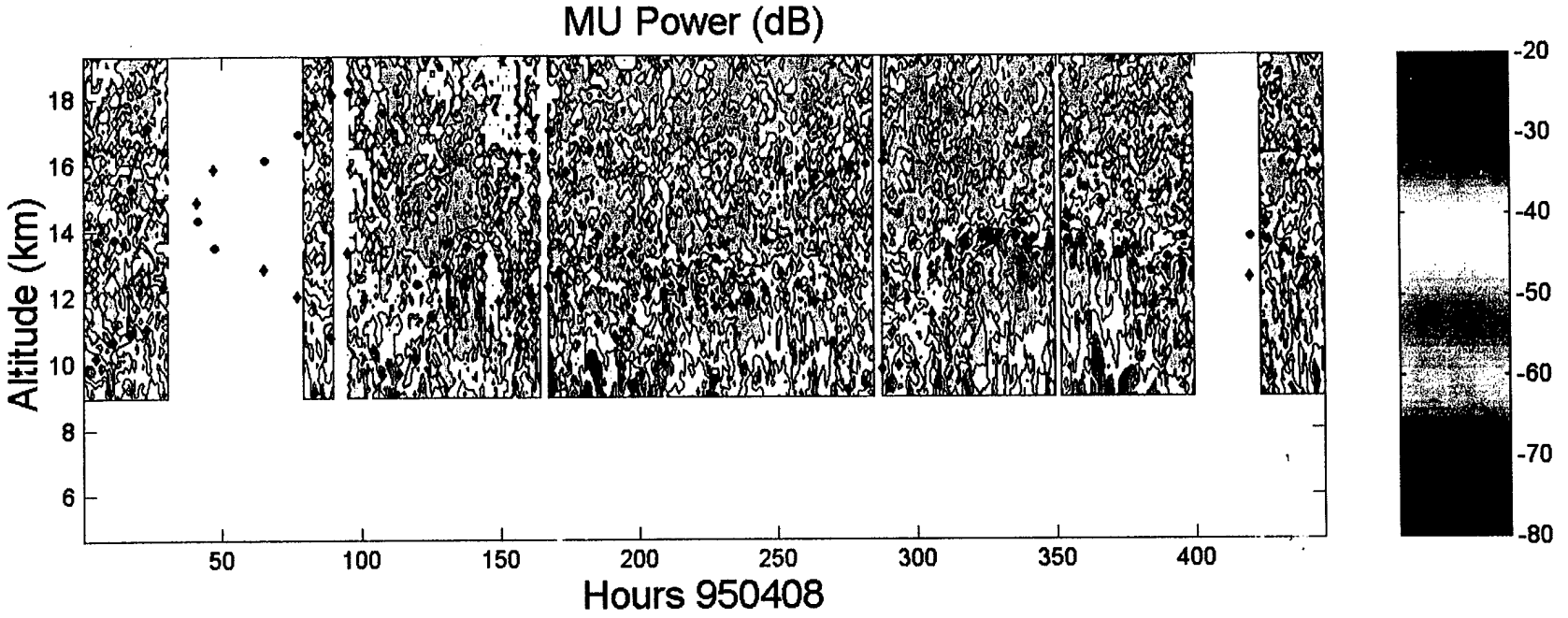
MU Power (dB)
Altitude (km)
18
16
14
12
10
8
6
50
100
150
200
250
300
350
400
Hours 950408
-20
-30
-40
-50
-60
-70
-80

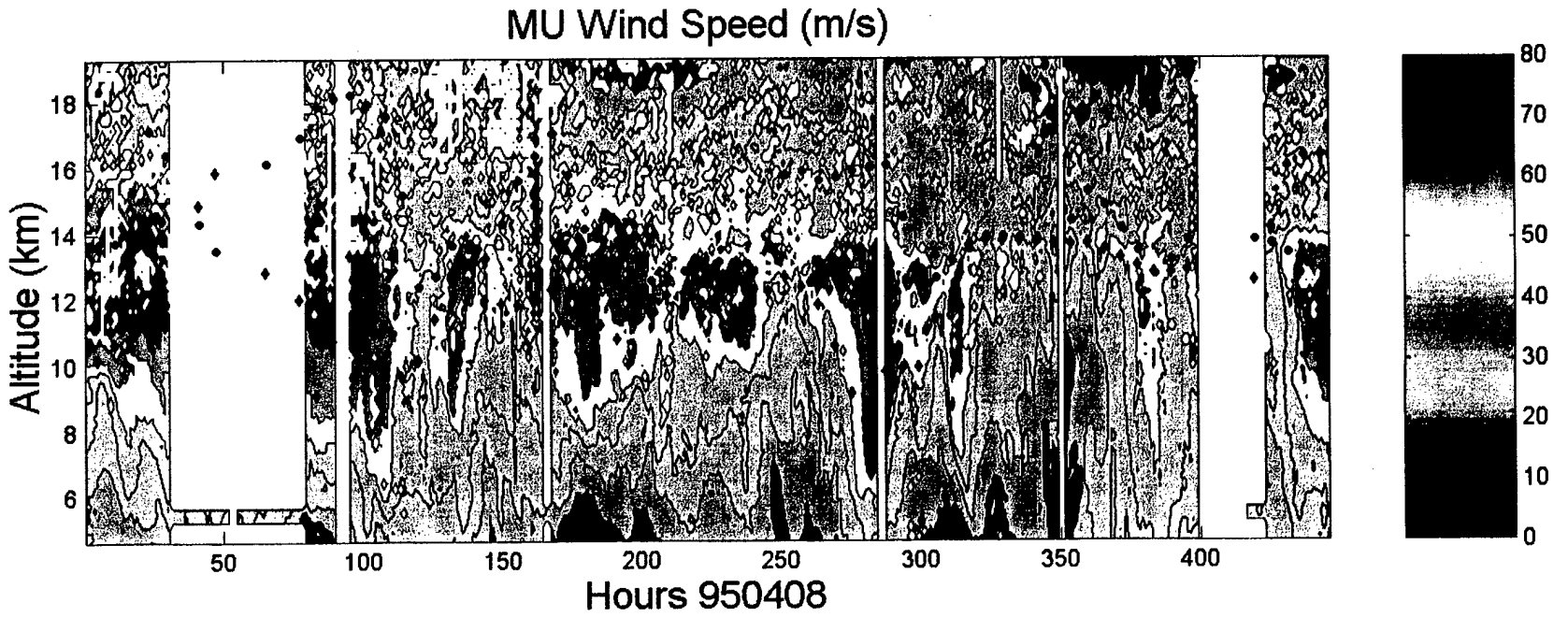
MU Wind Speed (m/s)
Altitude (km)
18
16
14
12
10
8
6
50
100
150
200
250
300
350
400
Hours 950408
80
70
60
50
40
30
20
10
0

C1

mudata01\case_stu\apr95 Tue Jan 08 09:19:48 2002

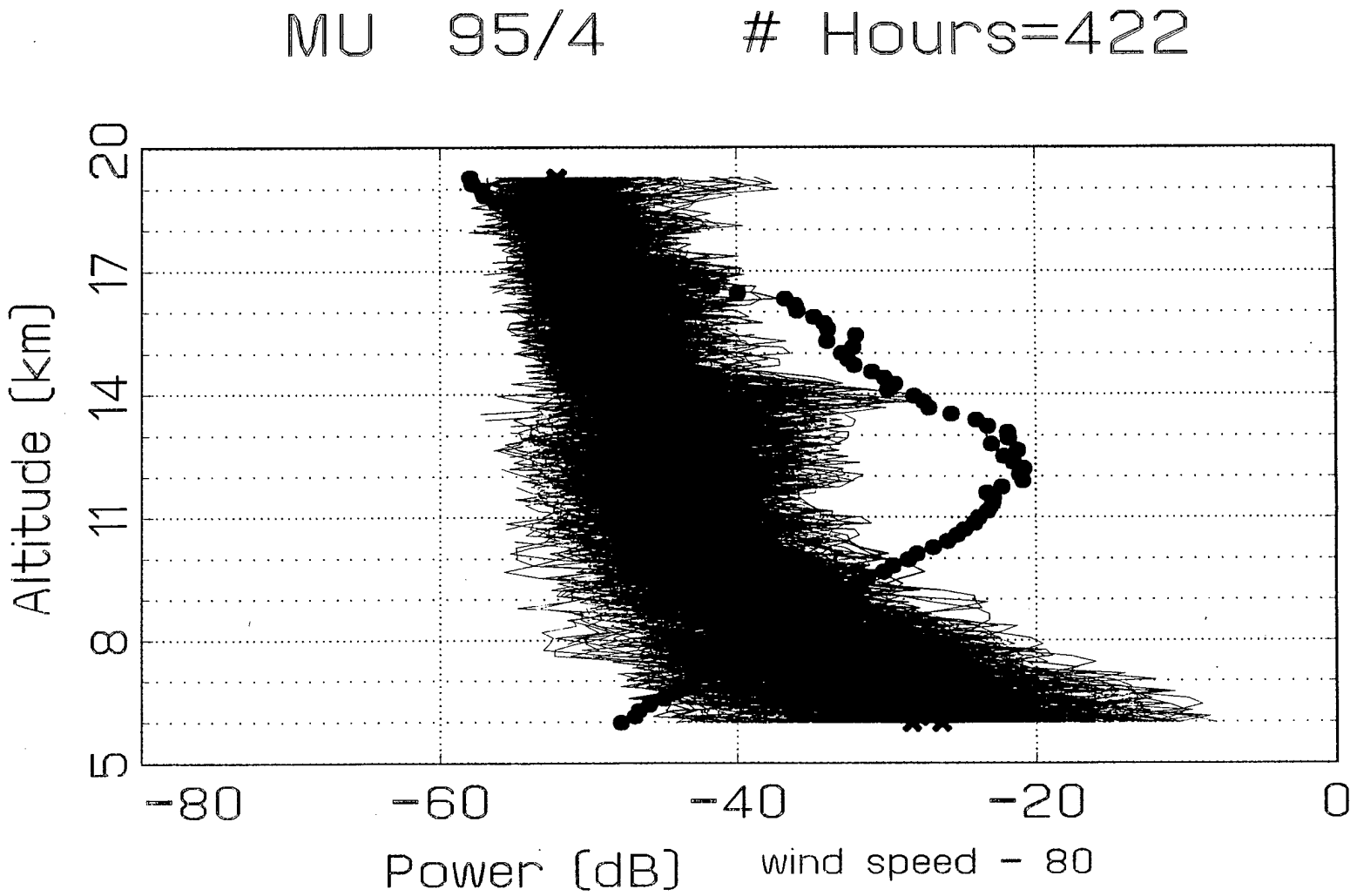

C2

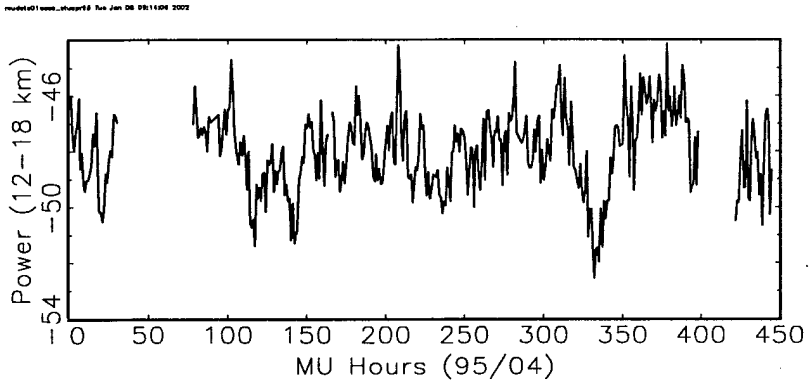
Power (12-18 km)
-54
-50
-46
0
50
100
150
200
250
300
350
400
450
MU Hours (95/04)

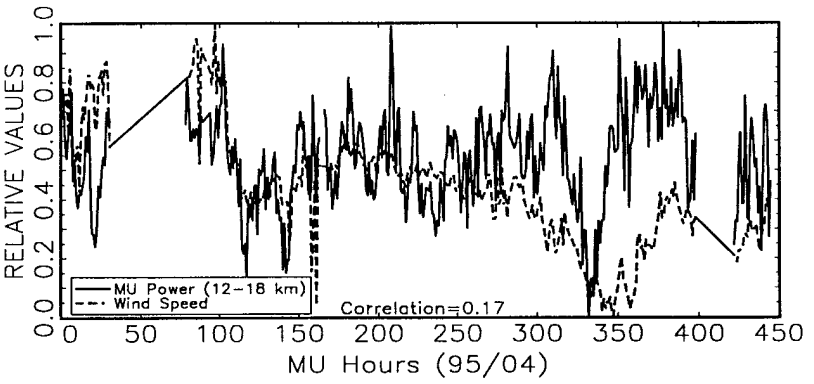
RELATIVE VALUES
0.0
0.2
0.4
0.6
0.8
1.0
MU Power (12-18 km)
Wind Speed
Correlation=0.17
0
50
100
150
200
250
300
350
400
450
MU Hours (95/04)

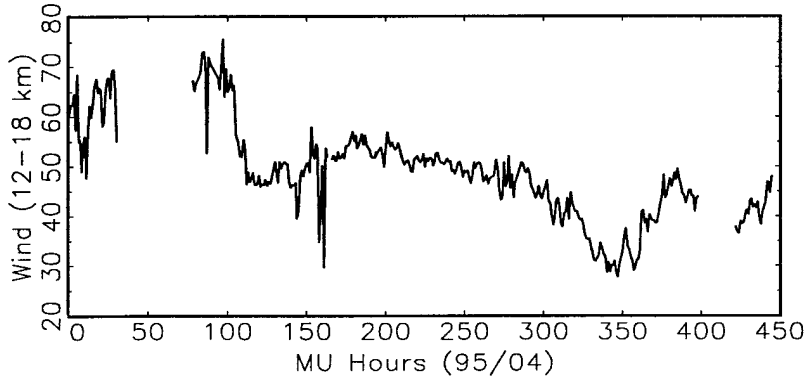
Wind (12-18 km)
20
30
40
50
60
70
80
0
50
100
150
200
250
300
350
400
450
MU Hours (95/04)

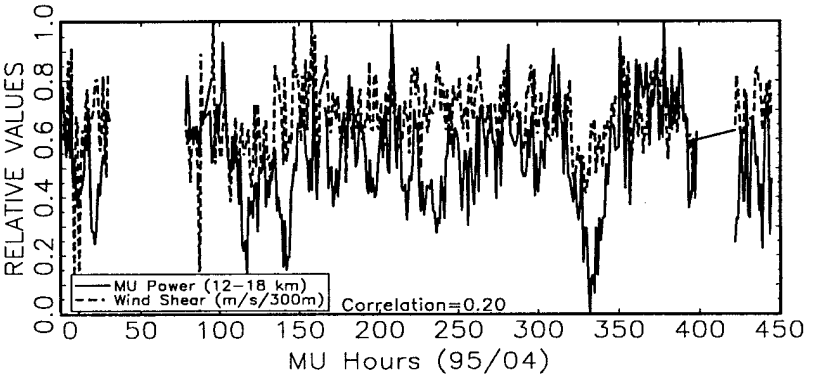
RELATIVE VALUES
0.0
0.2
0.4
0.6
0.8
1.0
MU Power (12-18 km)
Wind Shear (m/s/300m)
Correlation=0.20
0
50
100
150
200
250
300
350
400
450
MU Hours (95/04)

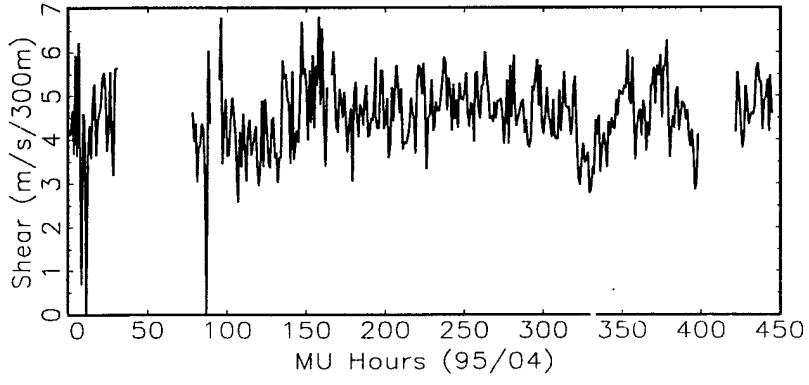
Shear (m/s/300m)
0
1
2
3
4
5
6
7
0
50
100
150
200
250
300
350
400
450
MU Hours (95/04)

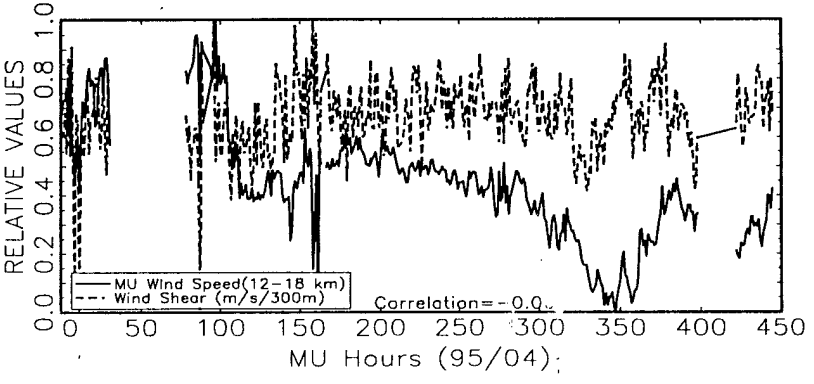
RELATIVE VALUES
0.0
0.2
0.4
0.6
0.8
1.0
MU Wind Speed(12-18 km)
Wind Shear (m/s/300m)
Correlation=-0.0..
0
50
100
150
200
250
300
350
400
450
MU Hours (95/04)

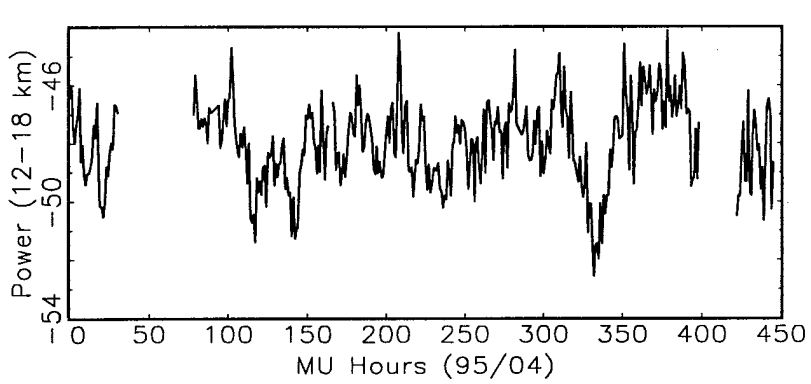
Power (12–18 km)
-54
-50
-46
0
50
100
150
200
250
300
350
400
450
MU Hours (95/04)

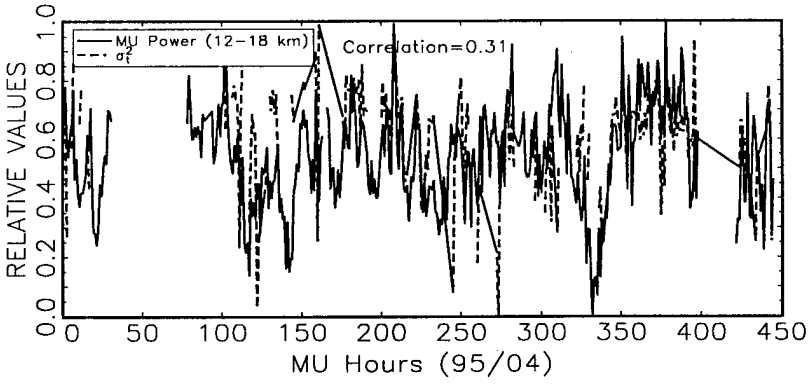
MU Power (12–18 km)
σ_t^2
Correlation=0.31
RELATIVE VALUES
0.0
0.2
0.4
0.6
0.8
1.0
0
50
100
150
200
250
300
350
400
450
MU Hours (95/04)

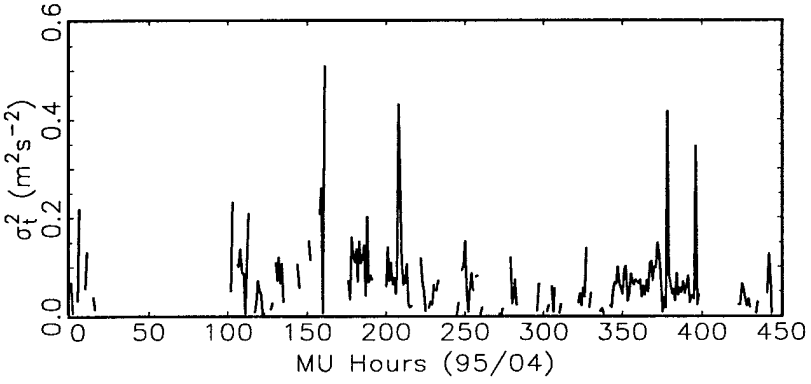
σ_t^2 (m^2s^{-2})
0.0
0.2
0.4
0.6
0
50
100
150
200
250
300
350
400
450
MU Hours (95/04)

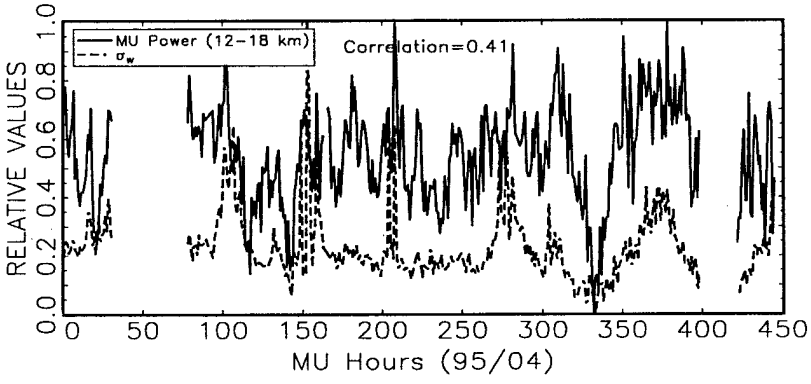
MU Power (12–18 km)
σ_w
Correlation=0.41
RELATIVE VALUES
0.0
0.2
0.4
0.6
0.8
1.0
0
50
100
150
200
250
300
350
400
450
MU Hours (95/04)

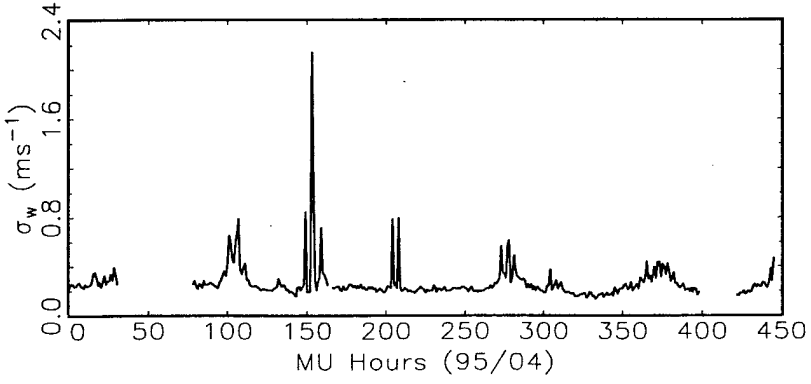
σ_w (ms^{-1})
0.0
0.8
1.6
2.4
0
50
100
150
200
250
300
350
400
450
MU Hours (95/04)

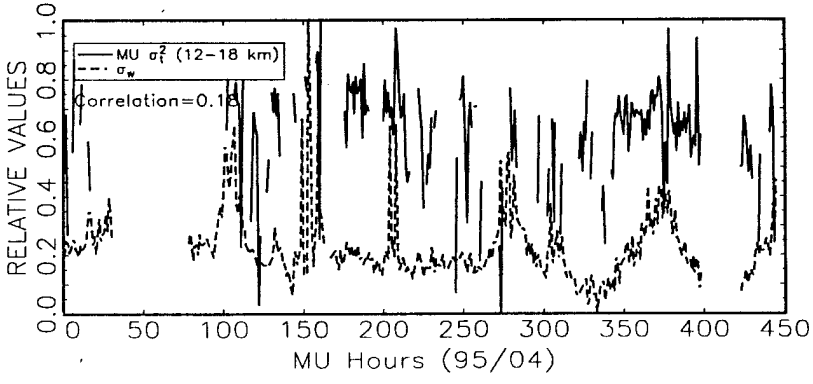
MU σ_t^2 (12–18 km)
σ_w
Correlation=0.18
RELATIVE VALUES
0.0
0.2
0.4
0.6
0.8
1.0
0
50
100
150
200
250
300
350
400
450
MU Hours (95/04)

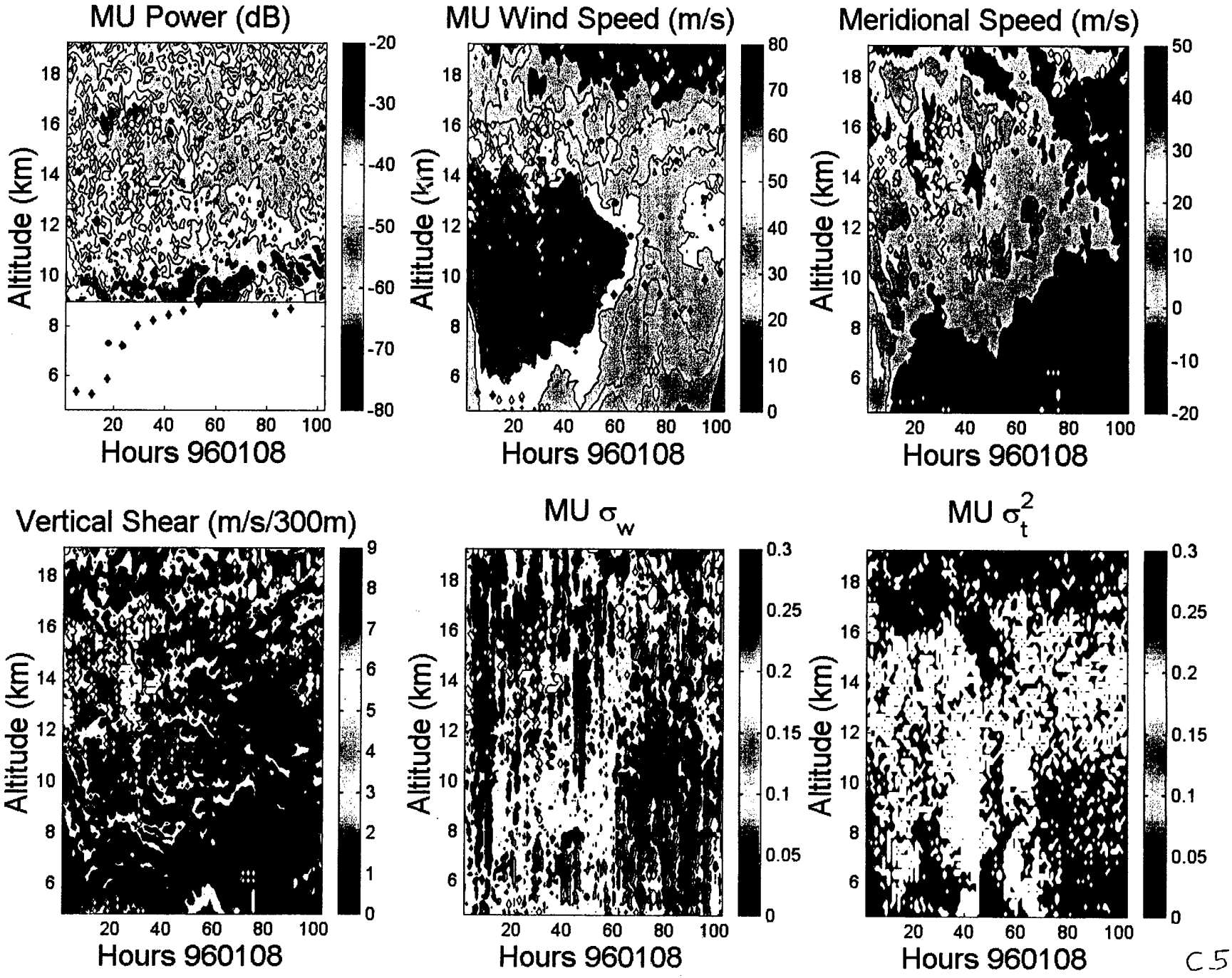
MU Power (dB)
MU Wind Speed (m/s)
Meridional Speed (m/s)
Vertical Shear (m/s/300m)
MU σ_w
MU σ_t^2
Altitude (km)
Hours 960108
18
16
14
12
10
8
6
20
40
60
80
100
-20
-30
-40
-50
-60
-70
-80
70
50
30
0
10
-10
9
7
5
4
3
2
1
0.3
0.25
0.2
0.15
0.1
0.05

C5

mudata01\case_stu\apr95 Tue Jan 08 09:27:09 2002

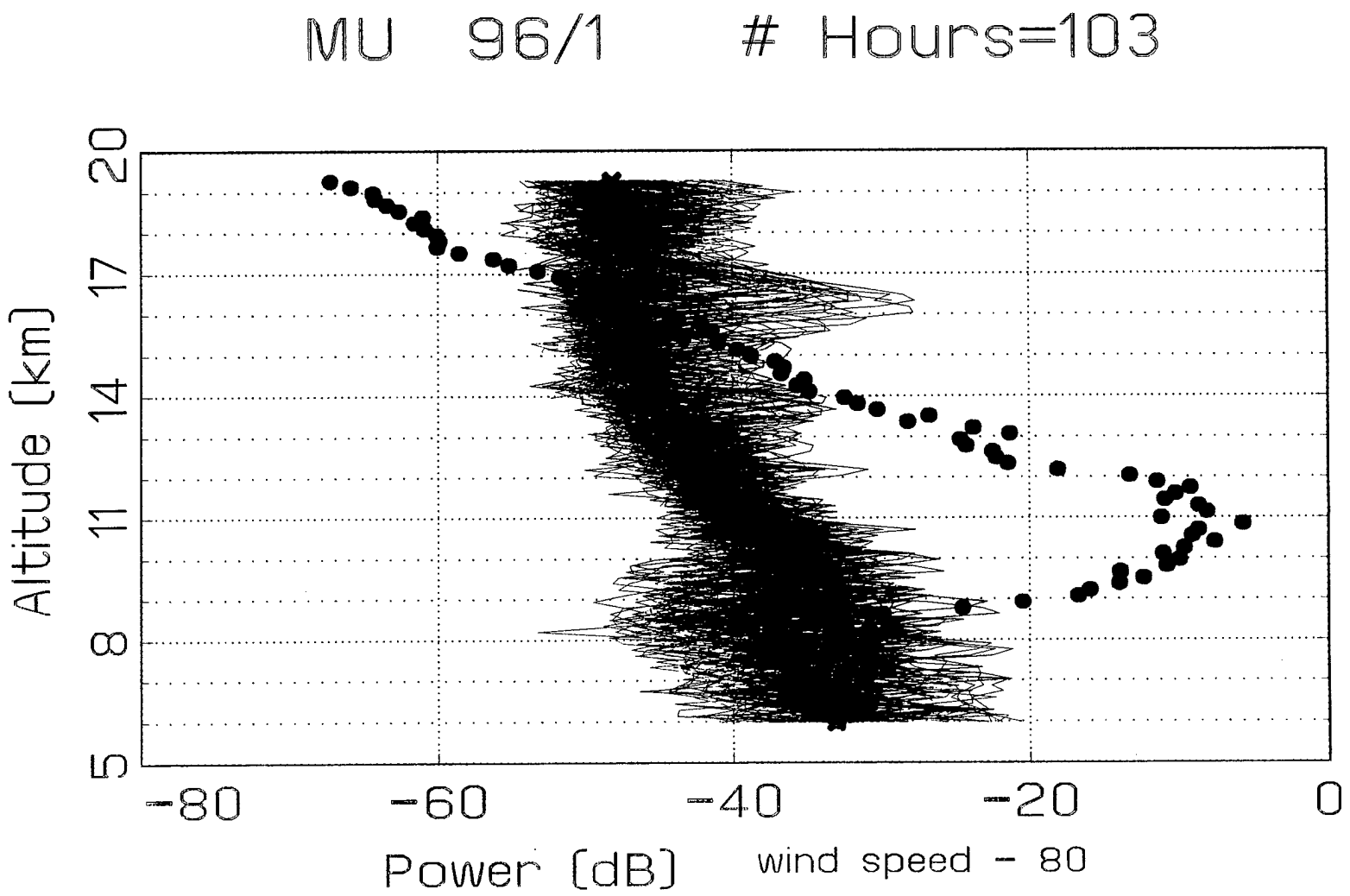

C6

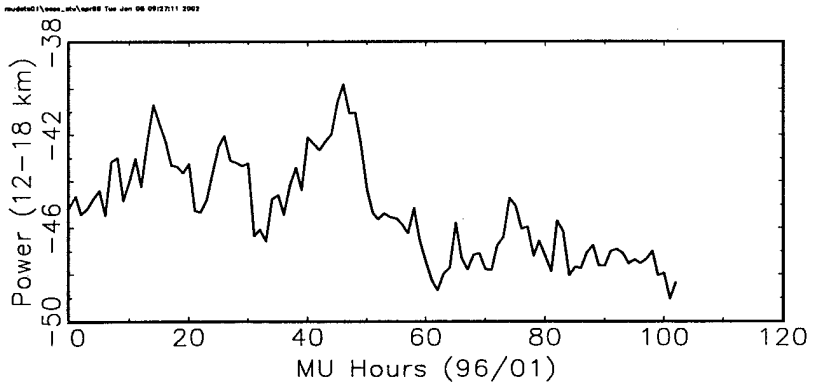
Power (12–18 km)
-38
-42
-46
-50
0
20
40
60
80
100
120
MU Hours (96/01)

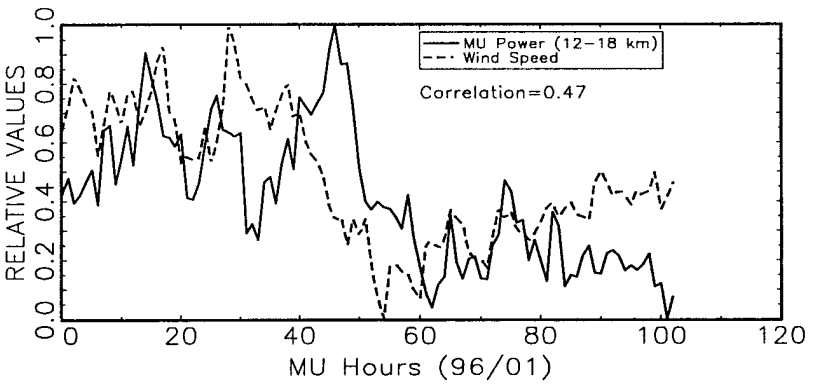
MU Power (12–18 km)
Wind Speed
Correlation=0.47
RELATIVE VALUES
0.0
0.2
0.4
0.6
0.8
1.0
0
20
40
60
80
100
120
MU Hours (96/01)

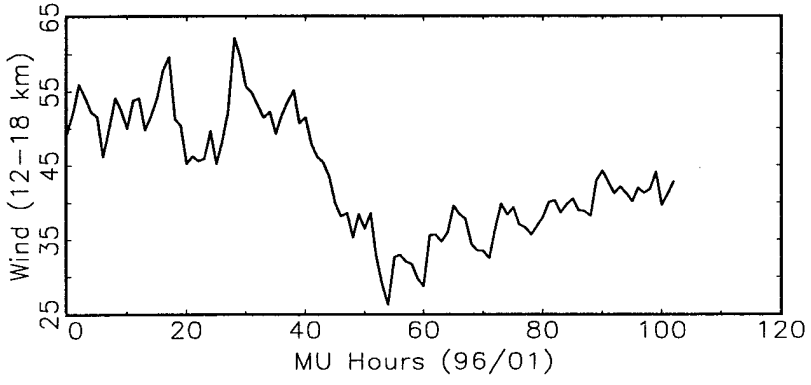
Wind (12–18 km)
65
55
45
35
25
0
20
40
60
80
100
120
MU Hours (96/01)

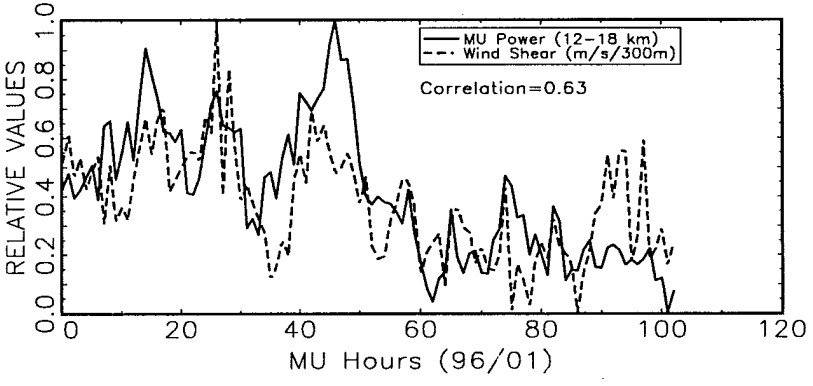
MU Power (12–18 km)
Wind Shear (m/s/300m)
Correlation=0.63
RELATIVE VALUES
0.0
0.2
0.4
0.6
0.8
1.0
0
20
40
60
80
100
120
MU Hours (96/01)

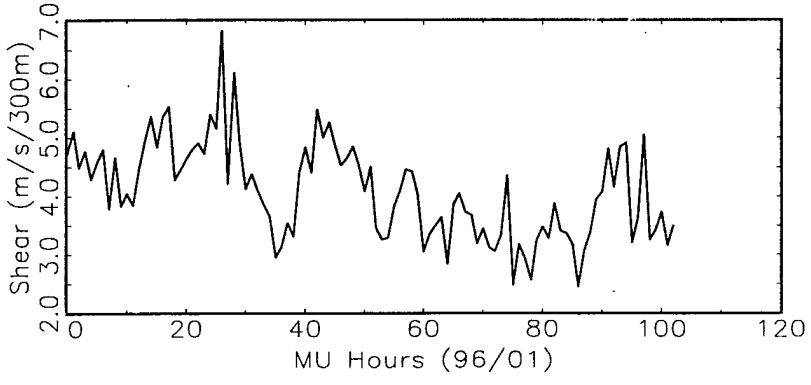
Shear (m/s/300m)
7.0
6.0
5.0
4.0
3.0
2.0
0
20
40
60
80
100
120
MU Hours (96/01)

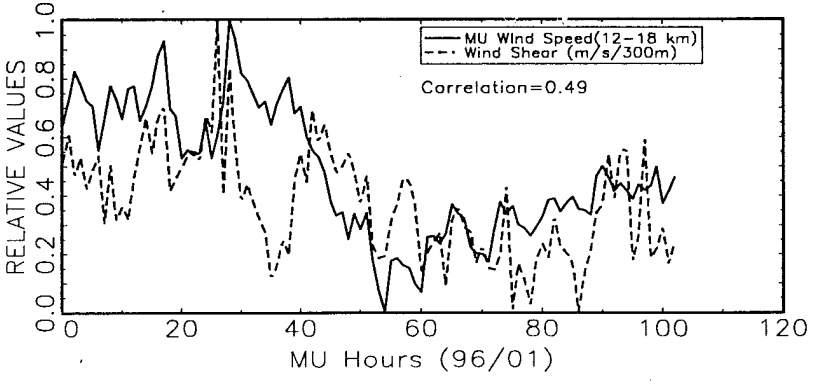
MU Wind Speed(12–18 km)
Wind Shear (m/s/300m)
Correlation=0.49
RELATIVE VALUES
0.0
0.2
0.4
0.6
0.8
1.0
0
20
40
60
80
100
120
MU Hours (96/01)

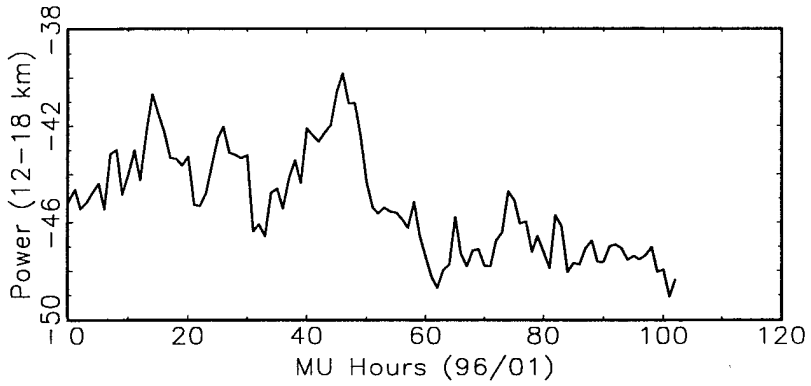
Power (12–18 km)
-38
-42
-46
-50
0
20
40
60
80
100
120
MU Hours (96/01)

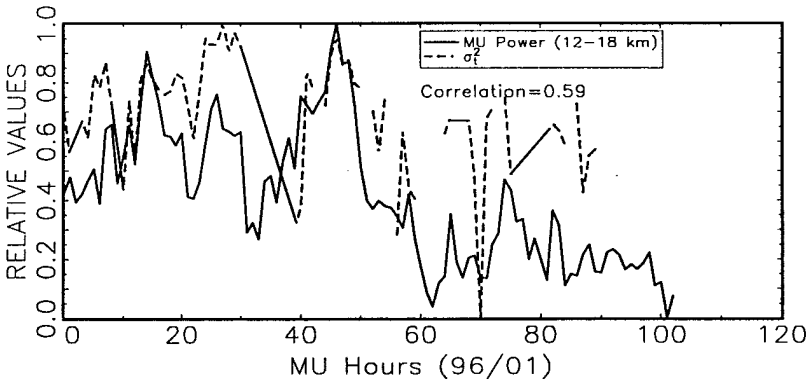
RELATIVE VALUES
0.0
0.2
0.4
0.6
0.8
1.0
MU Power (12–18 km)
σ_t^2
Correlation=0.59
0
20
40
60
80
100
120
MU Hours (96/01)

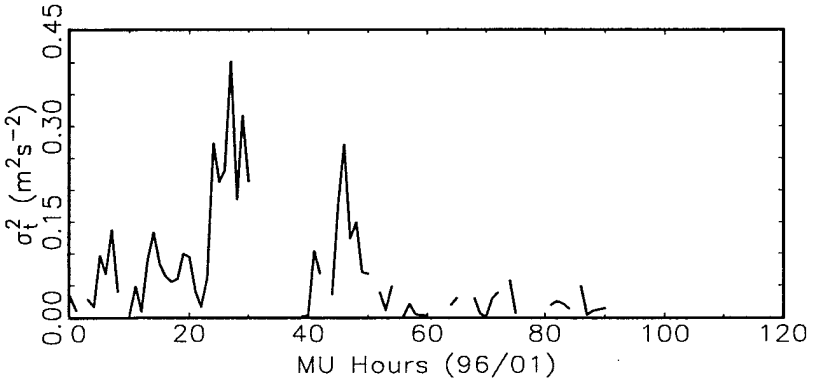
σ_t^2 (m^2s^{-2})
0.45
0.30
0.15
0.00
0
20
40
60
80
100
120
MU Hours (96/01)

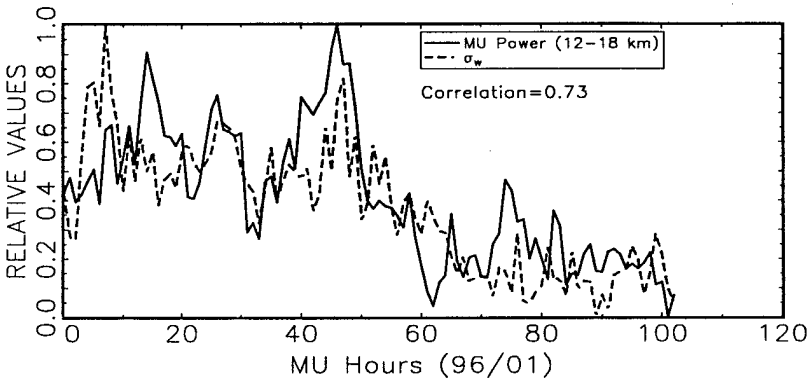
RELATIVE VALUES
0.0
0.2
0.4
0.6
0.8
1.0
MU Power (12–18 km)
σ_w
Correlation=0.73
0
20
40
60
80
100
120
MU Hours (96/01)

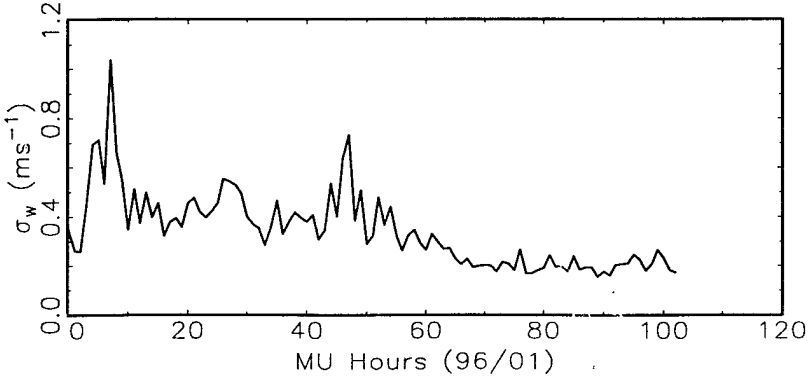
σ_w (ms^{-1})
1.2
0.8
0.4
0.0
0
20
40
60
80
100
120
MU Hours (96/01)

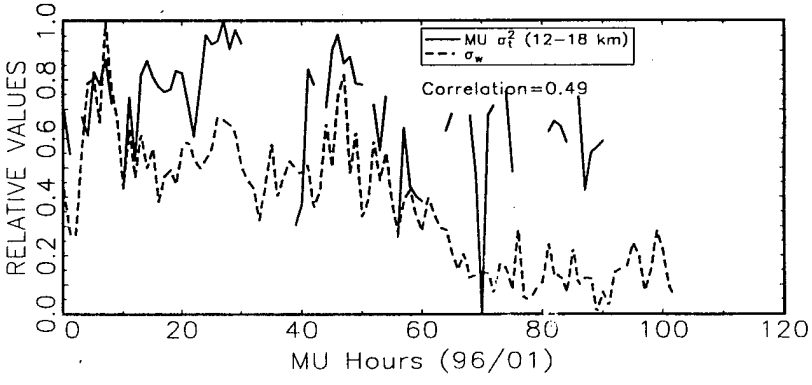
RELATIVE VALUES
0.0
0.2
0.4
0.6
0.8
1.0
MU σ_t^2 (12–18 km)
σ_w
Correlation=0.49
0
20
40
60
80
100
120
MU Hours (96/01)

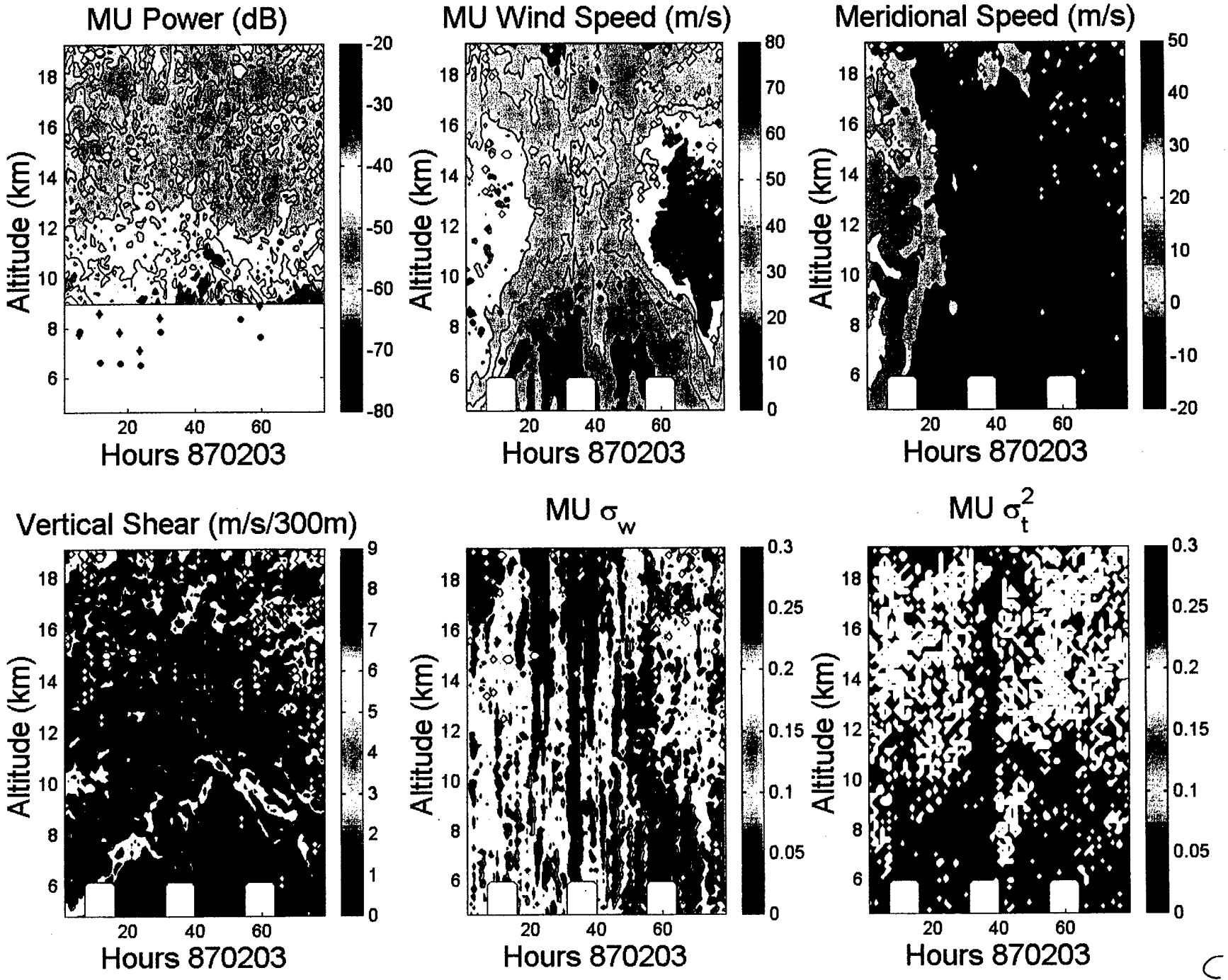
MU Power (dB)
MU Wind Speed (m/s)
Meridional Speed (m/s)
Vertical Shear (m/s/300m)
MU σ_w
MU σ_t^2
Altitude (km)
Hours 870203
18
16
14
12
10
8
6
20
40
60
-20
-30
-40
-50
-60
-70
-80
80
70
60
50
40
30
20
10
0
50
40
30
20
10
0
-10
-20
9
8
7
6
5
4
3
2
1
0
0.3
0.25
0.2
0.15
0.1
0.05
0

C9

mudata01\case_stu\dec96 Tue Jan 08 11:04:54 2002

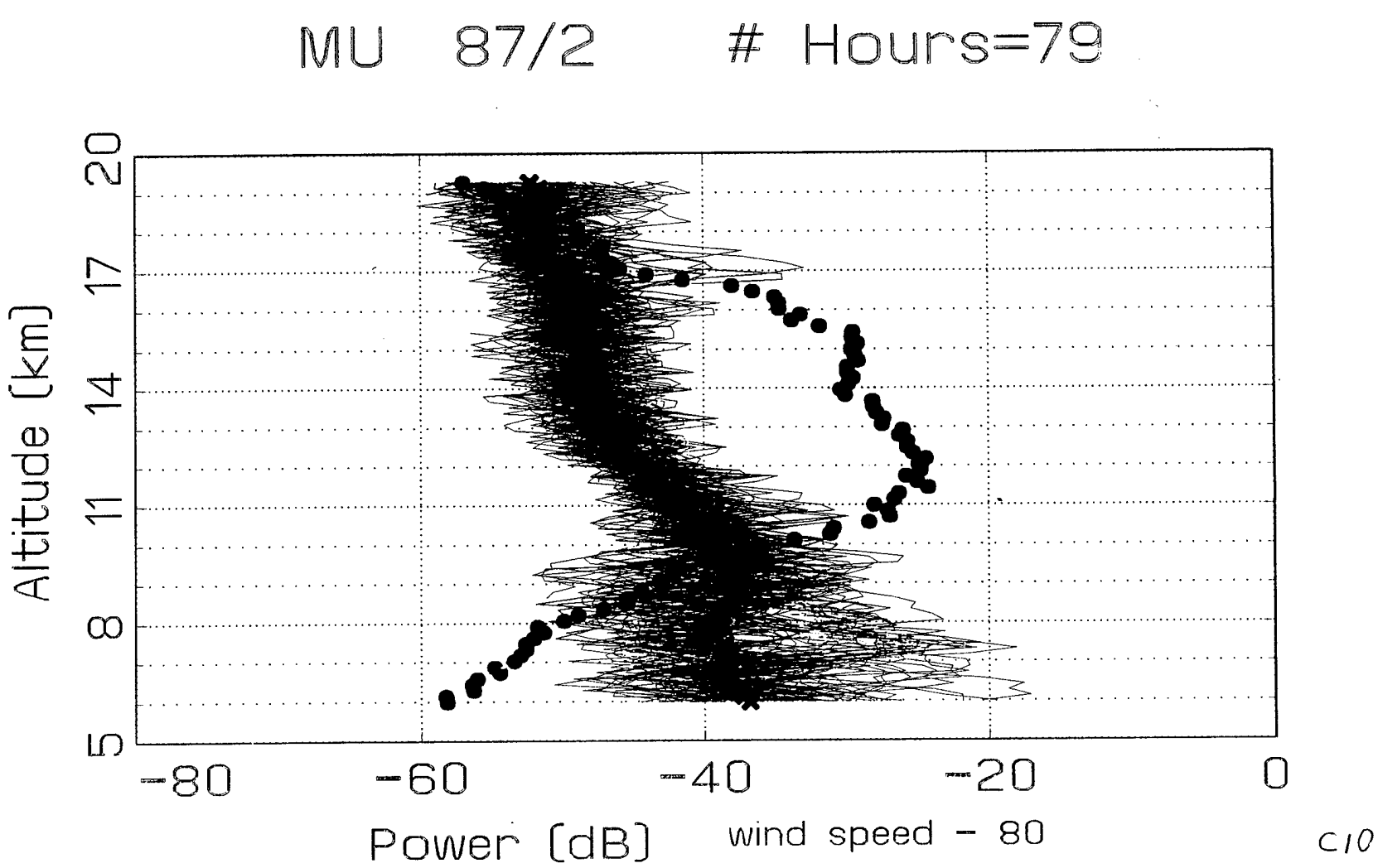

C10

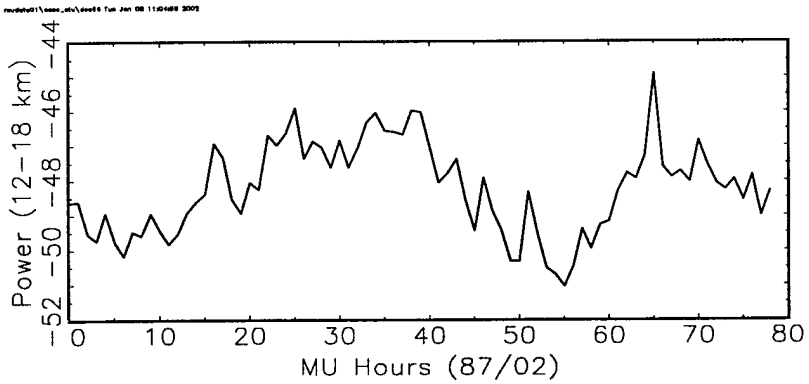
Power (12–18 km)
-52 -50 -48 -46 -44
0 10 20 30 40 50 60 70 80
MU Hours (87/02)

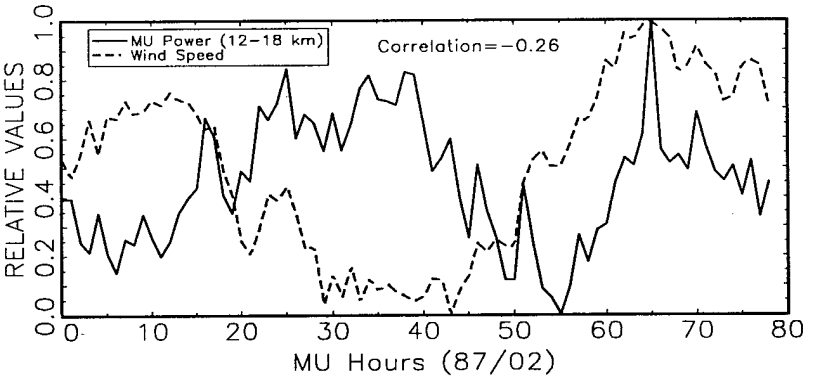
MU Power (12–18 km)
Wind Speed
Correlation=−0.26
RELATIVE VALUES
0.0 0.2 0.4 0.6 0.8 1.0
0 10 20 30 40 50 60 70 80
MU Hours (87/02)

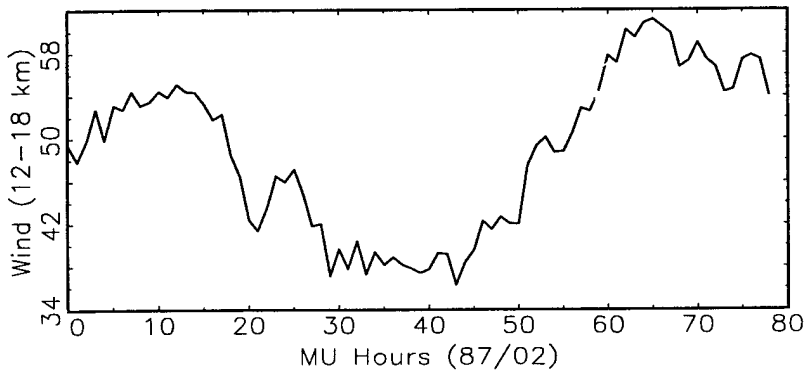
Wind (12–18 km)
34 42 50 58
0 10 20 30 40 50 60 70 80
MU Hours (87/02)

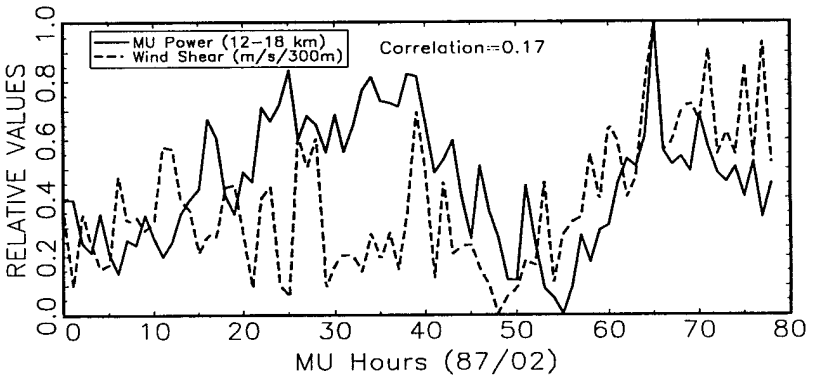
MU Power (12–18 km)
Wind Shear (m/s/300m)
Correlation=0.17
RELATIVE VALUES
0.0 0.2 0.4 0.6 0.8 1.0
0 10 20 30 40 50 60 70 80
MU Hours (87/02)

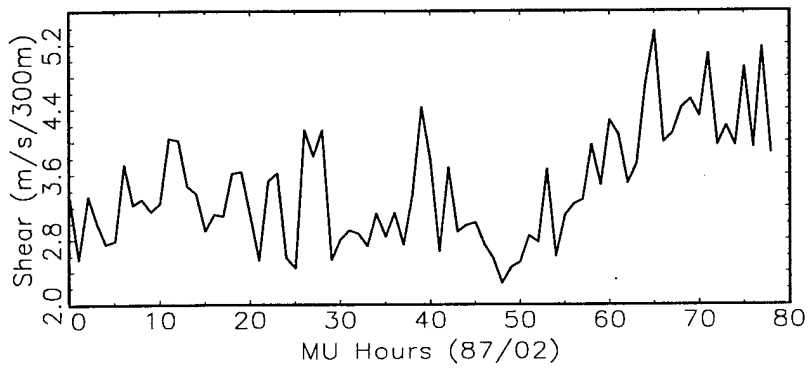
Shear (m/s/300m)
2.0 2.8 3.6 4.4 5.2
0 10 20 30 40 50 60 70 80
MU Hours (87/02)

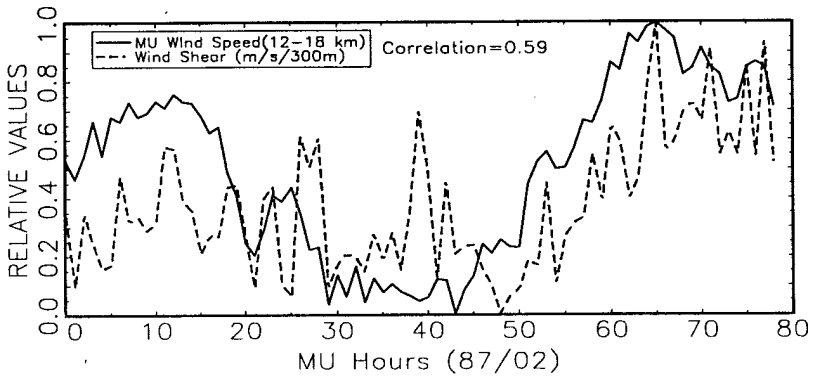
MU Wind Speed(12–18 km)
Wind Shear (m/s/300m)
Correlation=0.59
RELATIVE VALUES
0.0 0.2 0.4 0.6 0.8 1.0
0 10 20 30 40 50 60 70 80
MU Hours (87/02)

C11

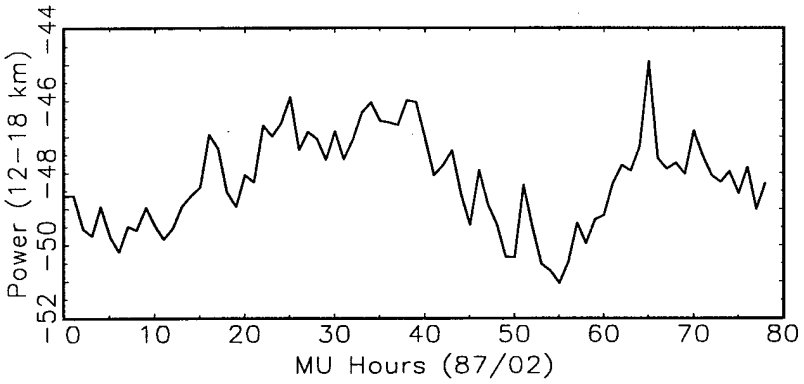
Power (12–18 km)
−52 −50 −48 −46 −44
0 10 20 30 40 50 60 70 80
MU Hours (87/02)

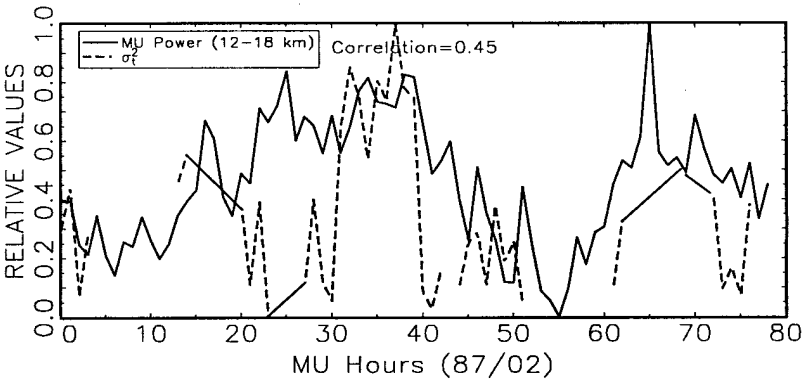
MU Power (12–18 km)
σ_t^2
Correlation=0.45
RELATIVE VALUES
0.0 0.2 0.4 0.6 0.8 1.0
0 10 20 30 40 50 60 70 80
MU Hours (87/02)

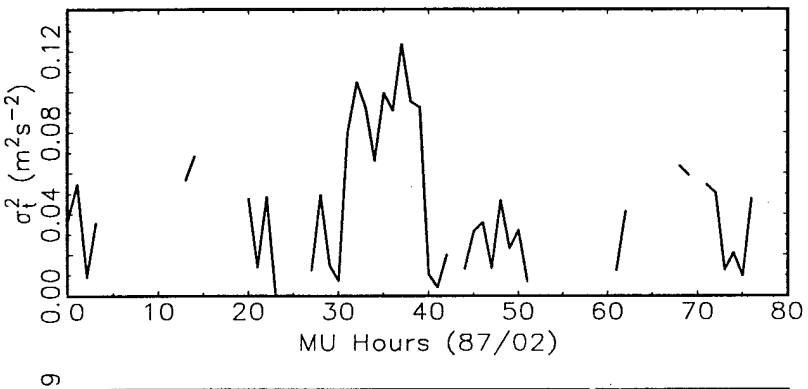
σ_t^2 (m^2s^{-2})
0.00 0.04 0.08 0.12
0 10 20 30 40 50 60 70 80
MU Hours (87/02)

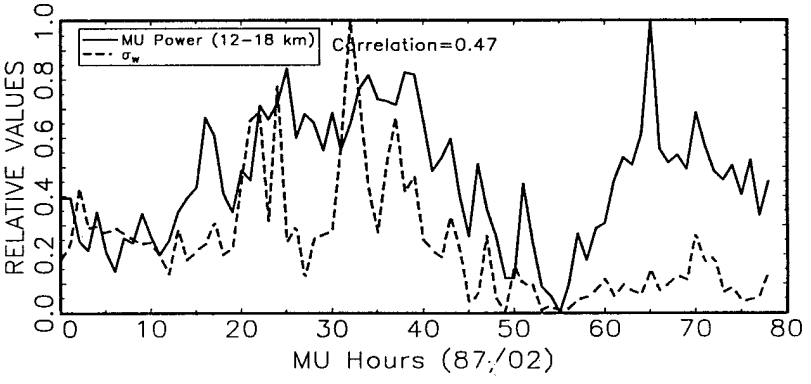
MU Power (12–18 km)
σ_w
Correlation=0.47
RELATIVE VALUES
0.0 0.2 0.4 0.6 0.8 1.0
0 10 20 30 40 50 60 70 80
MU Hours (87/02)

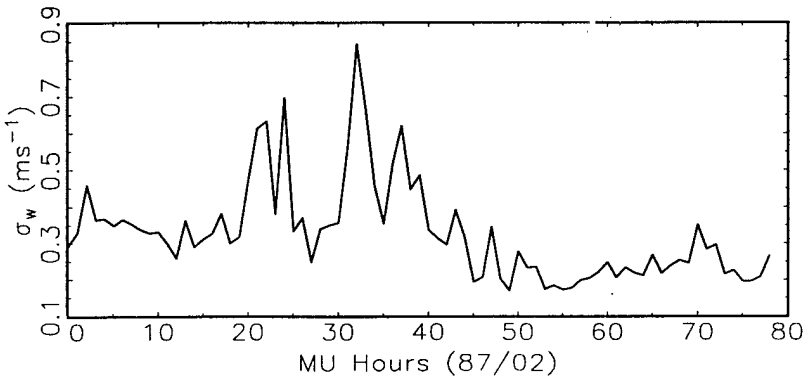
σ_w (ms^{-1})
0.1 0.3 0.5 0.7 0.9
0 10 20 30 40 50 60 70 80
MU Hours (87/02)

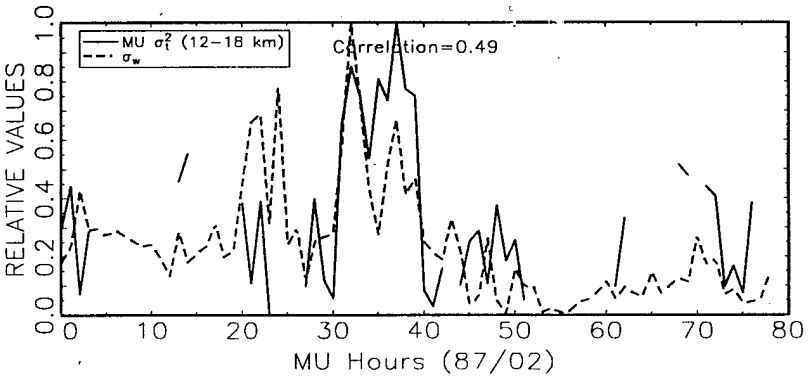
MU σ_t^2 (12–18 km)
σ_w
Correlation=0.49
RELATIVE VALUES
0.0 0.2 0.4 0.6 0.8 1.0
0 10 20 30 40 50 60 70 80
MU Hours (87/02)

C12

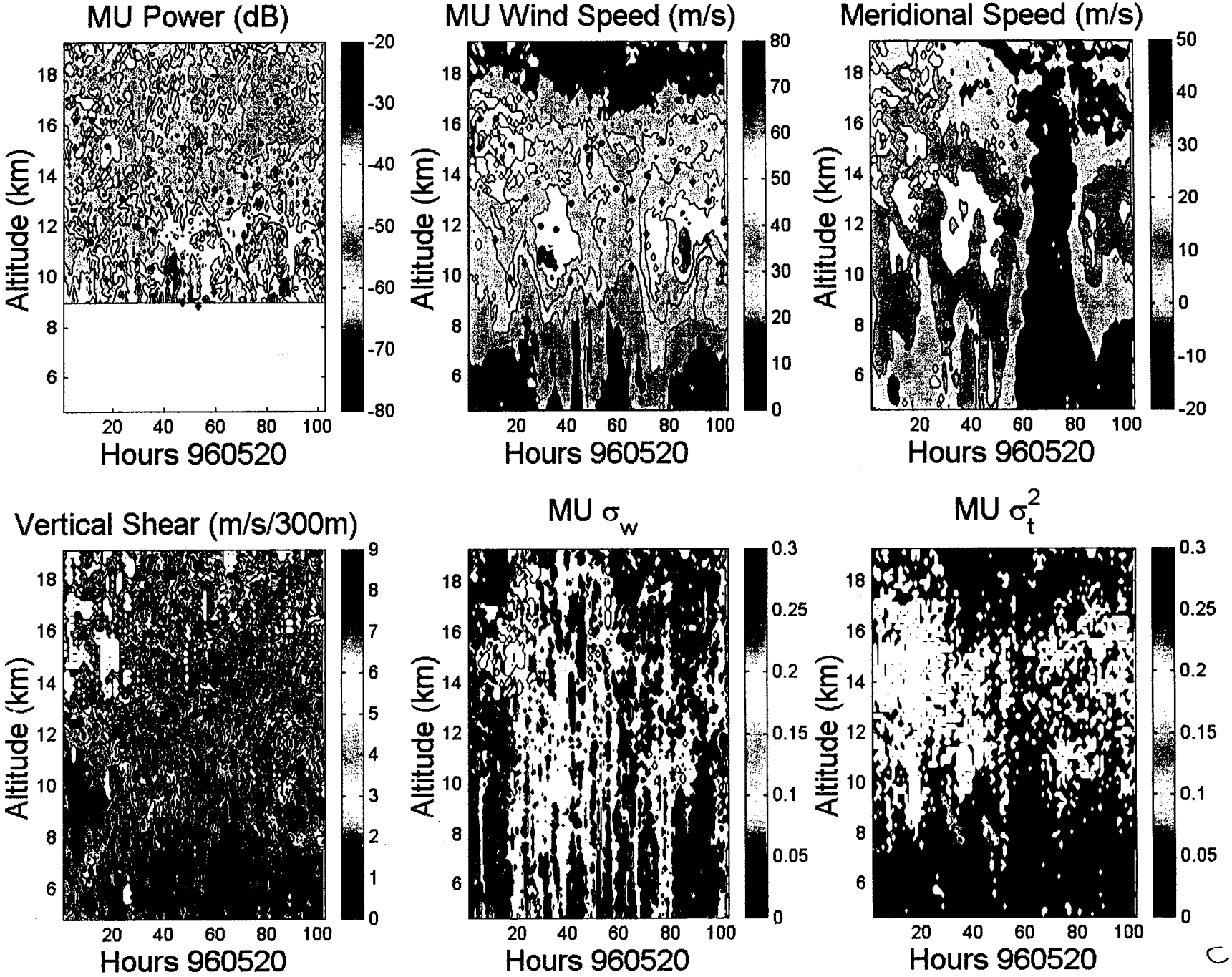
MU Power (dB)
MU Wind Speed (m/s)
Meridional Speed (m/s)
Vertical Shear (m/s/300m)
MU σ_w
MU σ_t^2
Altitude (km)
Hours 960520
6
8
10
12
14
16
18
20
40
60
80
100
-20
-30
-40
-50
-60
-70
-80
0
10
20
30
40
50
60
70
80
-10
0
1
2
3
4
5
6
7
8
9
0.05
0.1
0.15
0.2
0.25
0.3

C13

mudata01\case_stu\dec96 Tue Jan 08 10:22:24 2002

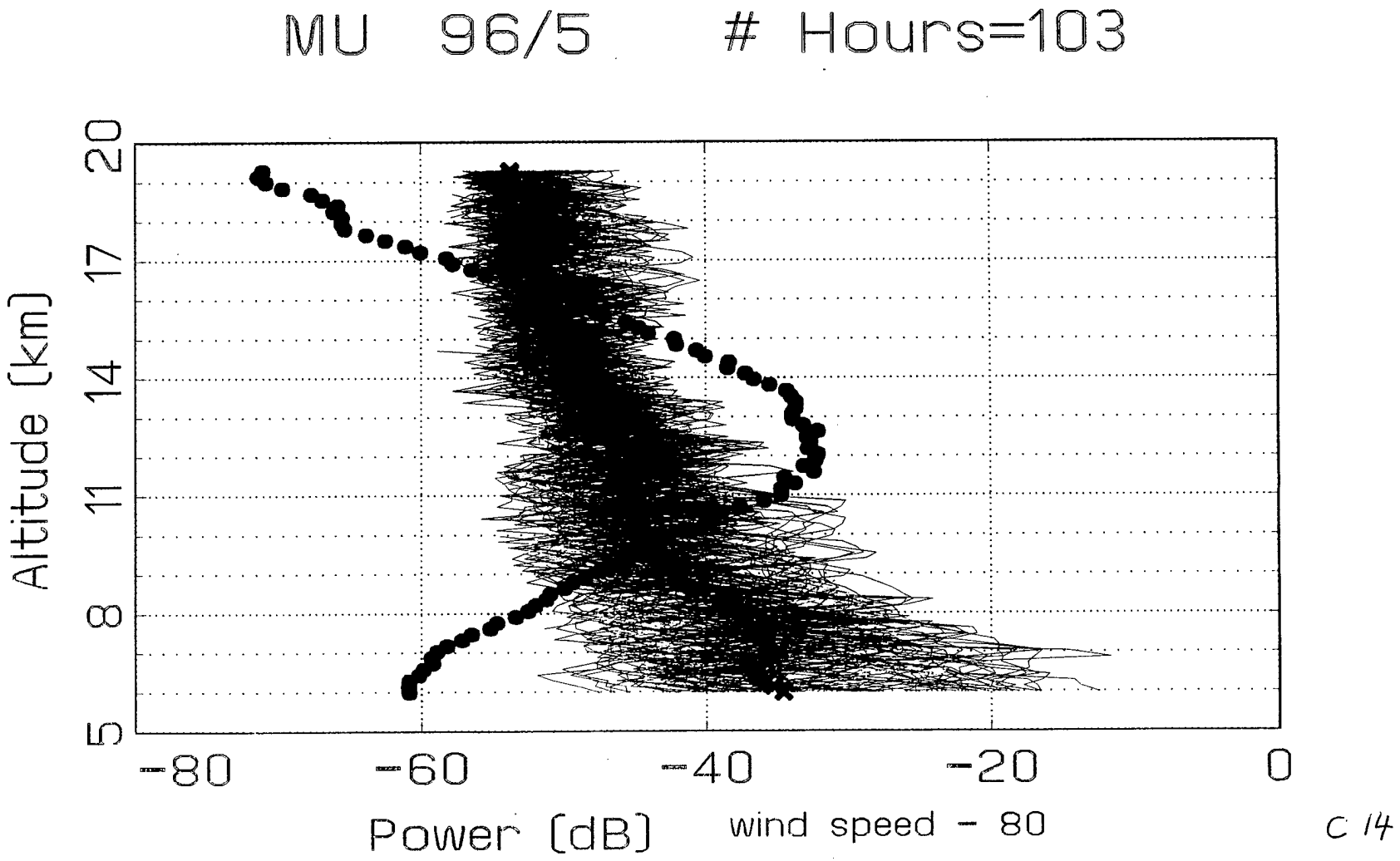

C 14

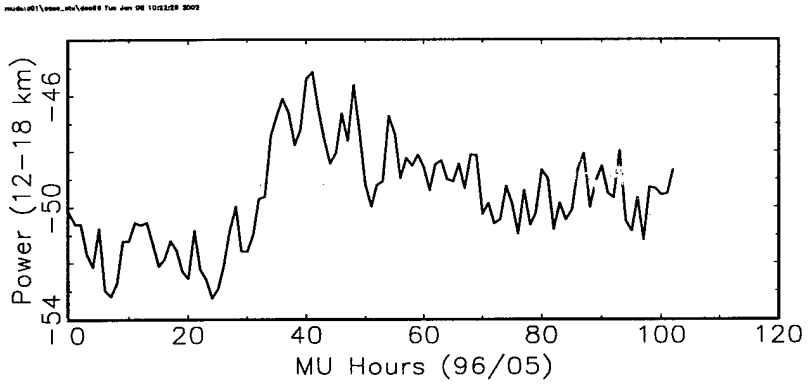
Power (12–18 km)
-54
-50
-46
0
20
40
60
80
100
120
MU Hours (96/05)

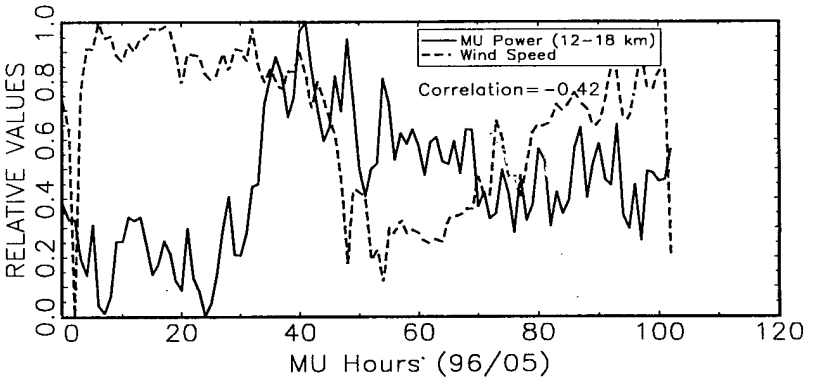
MU Power (12–18 km)
Wind Speed
Correlation= -0.42
RELATIVE VALUES
0.0
0.2
0.4
0.6
0.8
1.0
0
20
40
60
80
100
120
MU Hours (96/05)

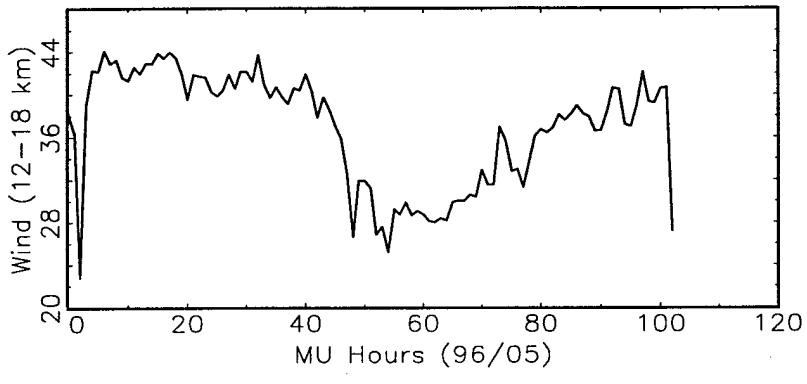
Wind (12–18 km)
20
28
36
44
0
20
40
60
80
100
120
MU Hours (96/05)

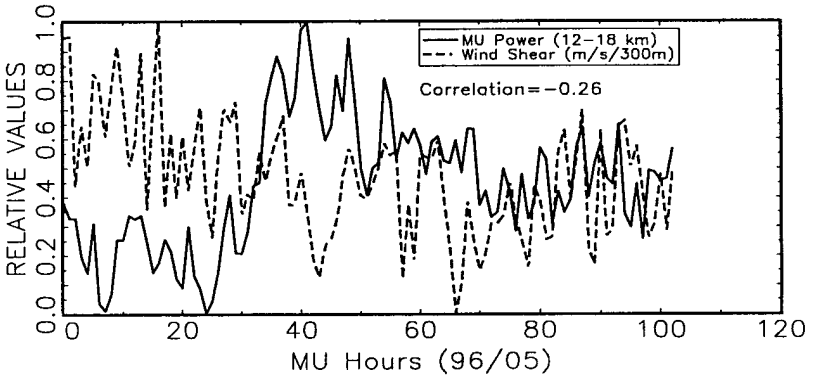
MU Power (12–18 km)
Wind Shear (m/s/300m)
Correlation= -0.26
RELATIVE VALUES
0.0
0.2
0.4
0.6
0.8
1.0
0
20
40
60
80
100
120
MU Hours (96/05)

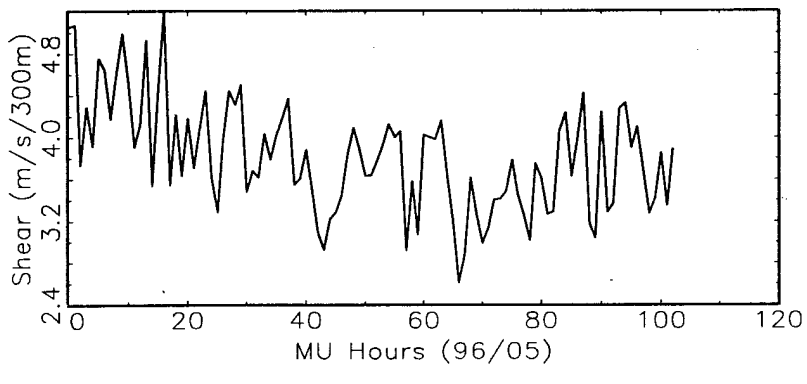
Shear (m/s/300m)
2.4
3.2
4.0
4.8
0
20
40
60
80
100
120
MU Hours (96/05)

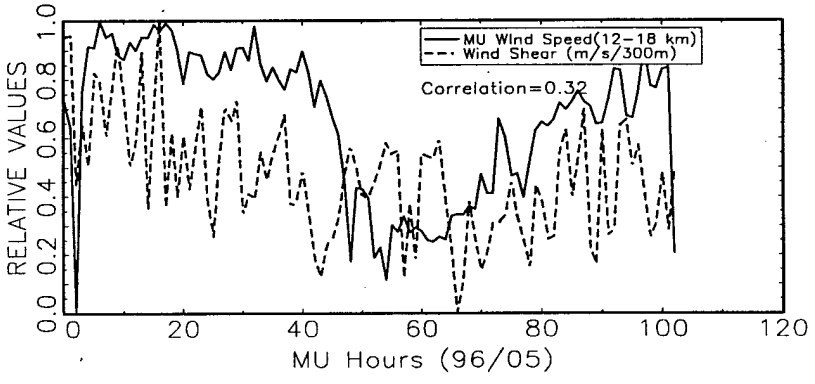
MU Wind Speed(12–18 km)
Wind Shear (m/s/300m)
Correlation=0.32
RELATIVE VALUES
0.0
0.2
0.4
0.6
0.8
1.0
0
20
40
60
80
100
120
MU Hours (96/05)

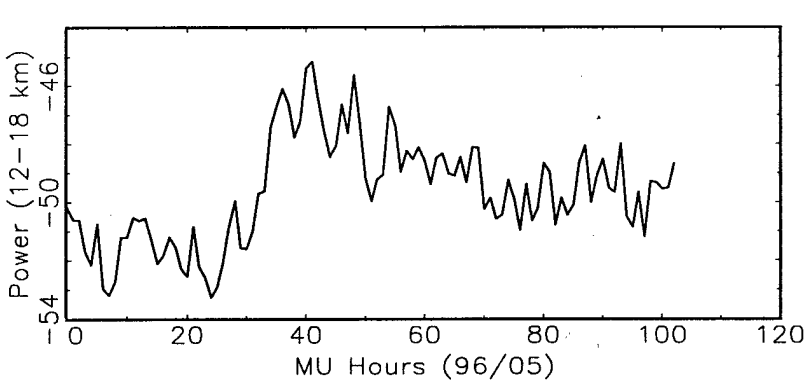
Power (12–18 km)
-54
-50
-46
0
20
40
60
80
100
120
MU Hours (96/05)

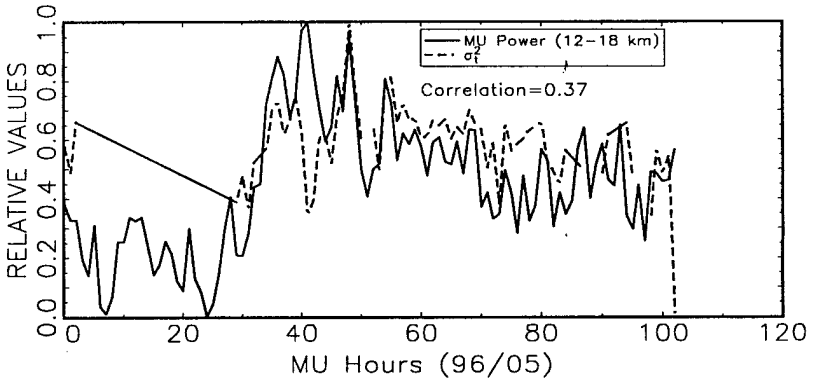
MU Power (12–18 km)
Correlation=0.37
RELATIVE VALUES
0.0
0.2
0.4
0.6
0.8
1.0
0
20
40
60
80
100
120
MU Hours (96/05)

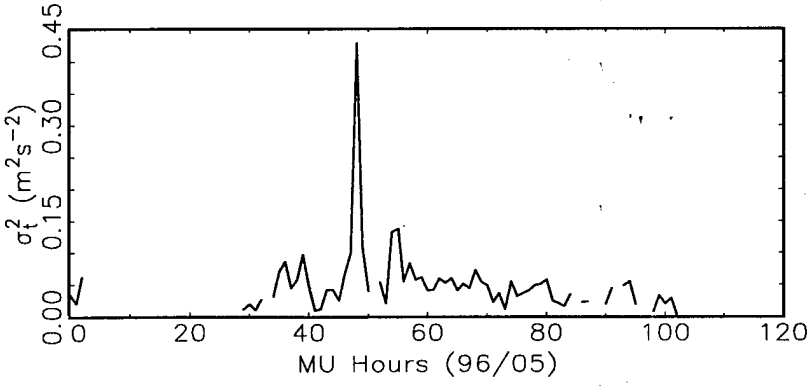
σ_t^2 (m^2s^{-2})
0.00
0.15
0.30
0.45
0
20
40
60
80
100
120
MU Hours (96/05)

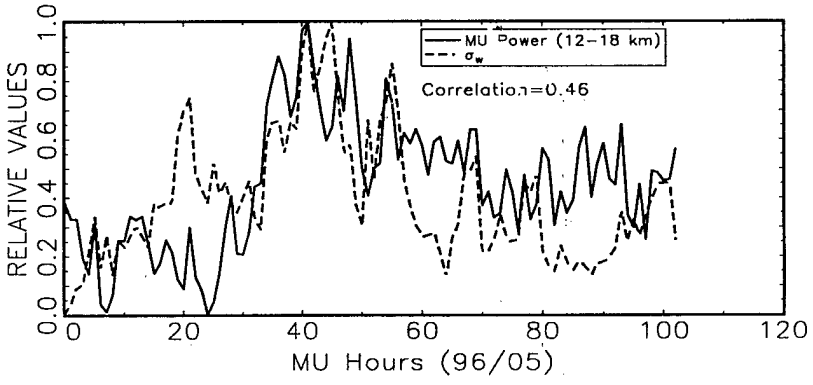
MU Power (12–18 km)
σ_w
Correlation=0.46
RELATIVE VALUES
0.0
0.2
0.4
0.6
0.8
1.0
0
20
40
60
80
100
120
MU Hours (96/05)

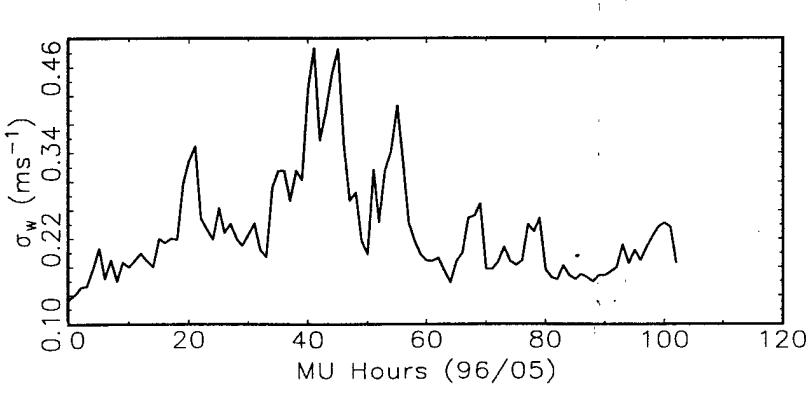
σ_w (ms^{-1})
0.10
0.22
0.34
0.46
0
20
40
60
80
100
120
MU Hours (96/05)

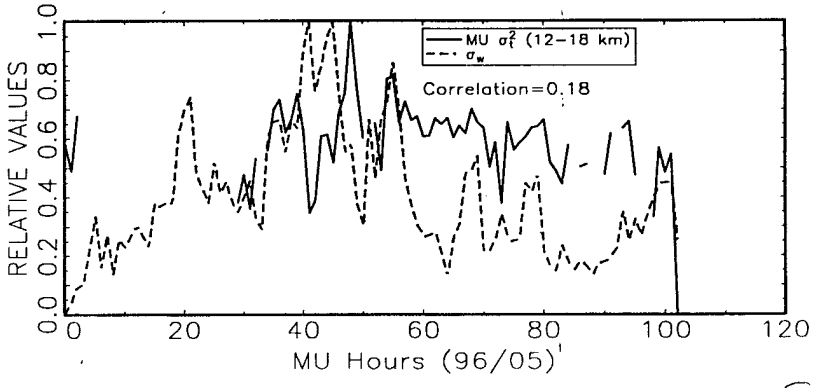
MU σ_t^2 (12–18 km)
σ_w
Correlation=0.18
RELATIVE VALUES
0.0
0.2
0.4
0.6
0.8
1.0
0
20
40
60
80
100
120
MU Hours (96/05)